# The importance of high discharge events on the export of Carbon and Phosphorus in the Wüstebach Catchment

Special focus on nanoparticulate and fine colloidal P transport during events

Author: J.D. Vogel (Forschungzentrum Jülich & University of Amsterdam)
Supervisor: Prof. Dr. Roland Bol (Forschungzentrum Jülich & University of Amsterdam)
Daily Supervisor: Dr. Nina Gottselig (University of Bonn)
Second Supervisor: Dr. Annemieke Kooijman (University of Amsterdam)

Thesis MSc Earth Sciences University of Amsterdam, 42 ECTS
31-08-2018, student number: 10683836

# Contents

s

# Abbreviations and Glossary

µm (micrometer): unit for scale, 1 * $10^{-6}$ m. 1 µm = 100 nm

AF4 (Asymmetric Flow Field Flow Fractionation): A type of Field Flow Fractionation (section 3.3.4)

AS (Autosampler): used in this thesis to label samples.

Colloids or colloidal material: organic or inorganic insoluble substances with a diameter of 1 nm – 1000 nm suspended in a liquid (see also fine colloids and nanoparticles).

DOC (Dissolved Organic Carbon): Organic Carbon smaller than 0.45 µm. DOC **always** refers to filtered samples.

DOP (Dissolved Organic Phosphorus): Organic Phosphorus smaller than 0.45 µm. DOP **always** refers to filtered samples.

DWD (Deutscher Wetterdienst): German Weather Service

FFF (Field Flow Fractionation): Group of separation techniques which separate particles on basis of their size without destructing or interacting with the sample (section 3.3.4).

Fine colloids: organic or inorganic insoluble substances with a diameter of 100 nm – 450 nm suspended in a liquid

FZJ (Forschungzentrum Jülich): institute where the research was conducted.

ICP-MS (Inductively Coupled Plasma- Mass Spectrometry): A method to quantify elemental concentrations (section 3.3.3).

kDa (Kilodalton): atomic mass unit. Particles smaller than 1 kDa do not enter the FFF (exit via membrane). 1 kDa is considered to be equal to particles smaller than 0.66 nm.

Milli-Q: Ultrapure water (Type 1) 18.2 MΩ $cm^{-1}$ at 25 °C (Millipore Cooperation, Burlington, USA)

Mt (Megatonne): unit for mass, 1*$10^{9}$ kg

Nanoparticles or nanoparticulate material: organic or inorganic insoluble substances with a diameter of 1 nm – 100 nm suspended in a liquid. FeO and AlO complexes, humic and fluvic acids and clays

Nm (nanometer): unit for scale, 1×$10^{-9}$ m, 0.01 µm

OC (Organic Carbon): Total Organic Carbon in a sample. OC can refer to both POC and DOC depending on the fraction or filtration.

PES (Polyethersulfone): Filter material used in this Thesis

POC (Particulate Organic Carbon): Organic Carbon larger than 0.45 µm in diameter. Including clay colloids, silt particles, sand particles and larger plant debris.

TERENO (Terrestrial Observatories Network): A German network of terrestrial observatories of which the Wüstebach Catchment is a part.

# Abstract

Events are important for the export of C and P. This thesis researched the role of events for the export of C and P in the Wüstebach Catchment. DOC losses were evaluated for 12 historical events. P losses were evaluated for 2 events sampled in 2018. It was found that sampling with a higher temporal resolution (10 minutes – 1 hour) improved the estimation of DOC losses during events. On average DOC export was underestimated with 33% without high-resolution sampling on a weekly basis. The exact loss per event was in 5 out of 12 cases clearly underestimated because the falling limb of the hydrograph was not fully covered. It was not possible to quantify the importance of events on annual DOC fluxes in a reasonable way. Winter events can dominate the annual DOC export (discharge * concentration) because discharge can remain high for several weeks during winter events. During summer events maximum DOC concentrations are much higher, but event duration is often limited to <1 day. The total DOC export during a single large snowmelt event equaled the total export of 170 extreme summer storm events.

P, Fe and Al concentrations were highest during peak discharge for the 2 events sampled in 2018. The largest part of Fe and Al during peak flow is truly dissolved (<1 kDa). It was found that smaller nanoparticles (1 nm – 20 nm) reacted stronger to precipitation and snowmelt events than larger nanoparticles (20 nm – 60 nm). Smaller nanoparticles also seem to reach the stream earlier than larger nanoparticles. Nanoparticulate Al and Fe was strongly correlated with nanoparticulate P suggesting associated transport. During events the mobilization and transportation of nanoparticles is therefore an important pathway of P losses. The May event showed better results due to a higher resolution sampling and a larger spread in the obtained values. Our results provided more insight in the transport dynamics of the 'dissolved' (<0.45 um) fractions of P, Fe and Al. A part of these 'dissolved' fractions is actually not dissolved, but colloidal. Our results show that transportation time of colloids is size dependent with larger colloids responding later than smaller colloids. Since only two events are discussed in this thesis, more research is necessary to control whether our observations are observed as well in other storms or other catchment conditions.

# 1. Introduction

Transport by streams is one of the most important pathways of Carbon (C) and Phosphorus (P) losses from catchments (Haygarth et al. 1999; Cole et al. 2007; Stacy et al. 2015). Especially high discharge events caused by precipitation or snowmelt play an important role in the loss of C and P (Haygarth et al. 1999; Stutter et al. 2008; Raymond & Saiers, 2010; Inamdar et al. 2011; Julich et al. 2017). This thesis focusses on the impact of high discharge events on the loss of C and P from a forested headwater catchment in the Eifel Mountains (Germany).

On a global scale, 210 Mt DOC (OC < 0.45 µm) and 170 Mt POC (OC > 0.45 µm) is exported by rivers each year (Bolan et al. 2011). Although DOC is only a relatively small fraction of the Soil Organic Carbon (SOC) pool, DOC is more mobile and is actively cycled in the soil (Kalbitz & Kaiser, 2003; Bolan et al. 2011). Transport and deposition of OC is a fundamental part of the terrestrial carbon cycle (Stallard et al. 1998; Cole et al. 2007). DOC also affects food web structures in aquatic systems (Jansson et al. 2007). Too high DOC concentrations can however have adverse effects. High DOC concentrations increase the Chemical Oxygen Demand reducing oxygen availability in streams (Jones, 1992). High DOC concentrations are also a problem for water treatment processes as DOC can be transformed into unwanted substances during drinking water production (Regan et al. 2017). The deposition of POC on ocean floors impacts the global C cycle on longer timescales (Leipe et al. 2011).

High Phosphorus (P) concentrations in aquatic systems can induce eutrophication which is one of the major environmental problems we are facing (Rockström et al. 2009). Currently diffuse P sources from agriculture receive a lot of scientific attention (Bol et al. 2018). Much less is attention is given to natural ecosystems were soil P concentrations are much lower (Sharpley et al. 2013). The lack of knowledge in natural ecosystems limits our understanding on natural background P levels which are nonetheless used for policy making in the Water Framework Directive (Phillips & Pitt, 2015; Bol et al. 2018). Better understanding the forest P cycle would improve our knowledge on what drives P losses under natural conditions. In most forest ecosystems, P is a limiting nutrient (Lang et al. 2016). The primary source of P in ecosystems is weatherable P which can be found in fresh sediments or bedrock (Walker & Syers, 1976; Hedin et al. 2003). Over time, weatherable P becomes depleted while soil P becomes occulated in stable associations with Fe, Al or clays reducing the bioavailability of P (Crews et al. 1995). In many ecosystems, atmospheric P deposition is the only source of fresh P (Hedin et al. 2003). When less P is available, the P cycle becomes tighter reducing P losses to a minimum (Lang et al. 2016). P fluxes in forest ecosystems deal therefore typically with low concentrations making quantifications of these fluxes a challenge (Kruse et al. 2015; Bol et al. 2016).

This MSc thesis focuses on extreme discharge events induced by precipitation and snowmelt on the export of C and P. Special attention is given to Aluminum (Al) and Iron (Fe) which are important binding partners of nanoparticulate and fine colloidal P. This thesis contains three main parts. The first part aims to find out when storms occur in the region and how the catchment responds to storms. As no information was available on this topic, a small research was conducted combining meteorological data and discharge data. The second part deals with DOC dynamics during historical events. 12 events in the period 2011-2015 were sampled with a high temporal resolution and DOC concentrations were determined for these samples. The value and quality of these additional samples will be assessed by estimating weekly DOC losses with and without additional samples. Attention is also given to maximum rainfall intensity and catchment dryness as predictor variables for peak DOC concentrations. The third part deals with two events sampled in 2018 which are analyzed for OC, P, Fe and Al. For these events

an innovative combination between Asymmetric Flow Field Fraction (AF4) and Inductively Coupled Plasma – Mass Spectrometry (ICP-MS) is used to gain in-depth insight in the transportation forms of P during events.

## 1.1. The importance of events for C export

The importance of precipitation events for the export of POC and DOC has been acknowledged by various authors (e.g. Raymond & Saiers, 2010; Inamdar et al., 2011). Raymond & Saiers (2010) concluded that 86% of total DOC is exported during events and 70% of this export takes place on the rising limb of the hydrograph. Other papers however suggest that high DOC concentrations are typically found after peak flow (Inamdar et al. 2011; Tunaley et al. 2016). Within catchments, several processes are related to OC transport. This can also explain large differences between studies. One process is overland flow when precipitation amounts exceed the infiltration capacity of soils (Morgan, 2009). Overland flow can be of importance in forested catchments (Dhillon & Inamdar, 2014). During such occasions, POC is generally found in high amounts close to peak discharge (Dhillon & Inamdar, 2014). Subsurface processes form an alternative pathway of OC transport (Laudon et al. 2011; Grabs et al. 2012). During rainfall events, new precipitation can create a pressure wave which pushes older water in soils towards the stream (Stockinger et al. 2014). The pressure wave can mobilize DOC and transport DOC to streams (Grabs et al. 2012). Especially when water is pushed through the riparian zone, water can become highly enriched in DOC (Laudon et al. 2011; Grabs et al. 2012). The activation of preferential flow paths might simulate the quick transport of new precipitation towards the riparian zone inducing a larger pressure wave pressure wave (Bogena et al. 2013; Stockinger et al. 2014; Wiekenkamp et al. 2016).

The timing of precipitation events is important for stream water DOC concentrations. Tunaley et al. (2016) found a pattern between catchment dryness and DOC concentrations. During dry and warm conditions, DOC accumulates in soil water which is unconnected to the stream. During events, the DOC rich soil water can be transported by subsurface flow processes described earlier. When the catchment is wet, soil water and stream water are constantly connected. Therefore, DOC doesn't accumulate in soil water. If an event occurs during the winter, maximum DOC concentrations are therefore much lower. DOC production is much lower as well during the winter period (Dawson et al. 2008).

Special occasions of high DOC losses are reported during annual snowmelt (Boyer et al. 1997. DOC concentrations during such events are only slightly elevated (Boyer et al. 1997). Because discharge can be very high for several weeks during snowmelt the DOC flux (discharge * concentration) can be impressive. Snowmelt events can contribute up to 49% of annual DOC losses (Sebestyen et al., 2009). High DOC losses after snowmelt are caused by DOC accumulation under the snow cover due to continuing microbial activity (Hornberger et al. 1994; Boyer et al. 1997). When the snow melts, water can infiltrate the soil enabling the transport of DOC. The entire catchment is washed out due to the very wet catchment conditions in combination with a high amount of meltwater.

## 1.2. The importance of events for P export

The importance of precipitation events for P transport from soils to water has been acknowledged in several studies on agricultural fields (Haygarth et al. 1999; Haithwaite & Dils, 2000; Preedy et al., 2001; Withers et al., 2003 Evans & Johnes, 2004; Stutter et al. 2008). Especially the link between soil erosion and transport of Particulate P (>0.45 µm) has been made clear (Haithwaite & Dils, 2000; Sharpley et al. 2013). In natural ecosystems, research on P fluxes is often limited by low P concentrations (Bol et al. 2016). Very few papers have been published on P losses during high discharge events in natural forest

ecosystems. Julich et al. (2017) show that P concentrations can increase up to a factor 20 during high discharge events. However, Verheyen et al. (2015) showed that for a forested catchment that during peak flow, lower P concentrations can be measured due to P dilution

An interesting feature of P is that P is typically found in an occulated form. Stutter et al. (2008) showed that P export of various forms of P (DOP, PP, FeO-P) during events strongly correlated with the export of suspended solids. P adsorbs to colloids such as humic acids, Fe-oxides, Al-oxides, clays and $CaCO_3$ (Crews et al. 1995; Reddy et al. 1995; Domagalski & Johnson, 2011; Sharpley et al. 2013). Many of these colloids are highly mobile and therefore interesting for the transport of associated elements (Martin et al. 1995; Meyer & Jarrell, 1995; Philliphe & Schaumann, 2014; Trostle et al. 2016). Occasionally samples are filtered with a 0.45 µm filter and everything which passes the filter is defined as D(O)P (Stutter et al. 2008; Verheyen et al. 2015). Although most researchers acknowledge that D(O)P is to a large extent bound to colloids, the analytical power is lacking to study colloidal-P transport into depth. Using the term dissolved for 0.45 µm filtered samples is however misleading and can cause misunderstanding. For instance McMillan et al. (2018) suggest that loosely sorbed P is dissolved during precipitation events if soils become temporarily anoxic while tightly absorbed P is only transported during prolonged flooding. Researchers using a combination between FFF-ICP-MS showed that even during baseflow the majority of P transport can be bound to colloids (Meyer & Jarrell, 1995; Stolpe et al. 2010; Gottselig et al. 2014; Baken et al. 2016, section 1.3). Hedin et al. (2003) found that DOP losses were independent of several ecosystem parameters (age of bedrock, forest age, N:P status), the explanation that DOP is actually composed of nanoparticles and fine colloids would imply that DOP losses are governed by hydrological and geological controls (subsurface flow, erosion, soil type etc.) rather than ecological controls (vegetation type, nutrient status). More research on colloidal P (1 nm – 1000 nm) transport during events would be helpful to understand better when, how and why P is lost from ecosystems.

## 1.3. The importance of nanoparticles and colloids

Colloids are organic or inorganic insoluble substances suspended in a liquid. Colloids differ from particles mainly by their size (<1000 nm in at least one direction) (Delay & Frimmel, 2012). Nanoparticles (<100 nm in at least one direction) are a subfraction of colloids (Delay & Frimmel, 2012). In the size range 1 nm to 1000 nm, a broad range of organic and inorganic particles can be found including clays, cellular debris, bacteria, humic and fluvic acids and metal-oxides (Lead & Wilkinson, 2006). Only hydrated ions of elements are smaller than 1 nm (Lead & Wilkinson, 2006). Nanoparticles and fine colloids are from a biogeochemical point of view interesting as they are highly reactive because they divide their charge over a small surface area (Philliphe & Schaumann, 2014). Smaller nanoparticles are therefore often more reactive although certain exceptions can be found (Wigginton et al. 2009). The mobility and reactivity of nanoparticles make nanoparticles vectors for transport of elements (Martin et al. 1995; Meyer & Jarrell; Philliphe & Schaumann, 2014; Trostle et al. 2016).

Gottselig et al. (2014) presented a method separate colloids in natural streams on basis of their size and to identify the chemical composition of colloidal fractions. Gottselig et al. (2014) separated two fractions. In the 1$^{st}$ fraction (0.66 nm – 20 nm) DOM is the main carrier of Fe, Al and P. In the 2$^{nd}$ fraction (20 nm – 60 nm), DOM is the matrix material meaning that FeO(H) aggregates into complexes under influence of DOM. Gottselig et al. (2017a) later identified a 3$^{rd}$ fraction (clays, 60 nm – 300 nm) containing a mixture between Si, Al, Fe and Mn (see also Regelink et al. 2013). Other researchers found slightly different particle size classes. Stolpe et al. (2013) and Baken et al. (2016) identified two classes. A first fraction (0.5 nm – 3 nm) particles identified as humic-rich colloids and a second fraction (3 nm

– 40 nm) particles identified as iron complexes (FeOH). The fractions of Stolpe et al. (2013) and Baken et al. (2016) and the fractions of Gottselig et al. (2014; 2017a) partially overlap. In this research the particle size fractions of Gottselig et al. (2017a) are used. P was found to be associated to all three fractions described by Gottselig et al. (2017a) and the two fractions of Stolpe et al. (2013) and Baken et al. (2016). Regelink et al. (2013) showed that on an agricultural clay soil P transport was dominated by clay particles (3rd fraction of Gottselig et al. 2017a). Most studies so far have focused nanoparticulate and fine colloidal P associations during baseflow conditions. In this Master Thesis, changes in nanoparticle and fine colloidal fractions and associated P transport will be research during two high discharge events.

## 1.4. Aim, Hypotheses and thesis set-up

The primary research aim is to quantify the loss of C and P during events. The thesis has also several secondary aims. In this section the aims and hypotheses are introduced and explained. The thesis set-up is as follows. The catchment is introduced in Chapter 2. The methodology is presented for historical events and new events in Chapter 3. Results are presented for historical events In Chapter 4 and for new events in Chapter 5. Results from historical events are discussed in Chapter 6 followed by a discussion on new events in Chapter 7. A summary of the most important findings can be found in Chapter 8.

### 1.4.1. Hydrological responses to precipitation

The aim of this section is to describe how the Wüstebach responds to high-intensity rainfall and high rainfall amounts and at which time of the year such events are likely to occur. This information is useful to define the difference between a severe event and a weak event. Meteorological data from nearby weather stations is studied in combination with discharge data from the Wüstebach (section 3.2). The hypothesis is that a clear difference exists between winter storms and summer storms. Winter storms are expected to last longer with higher total precipitation amounts of a low intensity. Summer storms are expected to last for short periods with short precipitation events with a high intensity. Storms are expected to be most frequent in autumn and winter. Results are presented in section 4.1 and discussed in section 6.1.

### 1.4.2. POC and DOC during events

For 12 historical events (2011-2015) additional samples have been taken with an autosampler. For these additional samples, DOC concentrations were determined. So far, the DOC data was not investigated into detail. In this Master Thesis, weekly DOC export is calculated with and without additional samples. Baseflow (indicator for catchment dryness) and maximum rainfall intensity (indictor for event severity) are assessed in their potential to explain Maximum DOC concentrations during events. Catchment dryness and event severity are expected to be positively correlated with high DOC maximum concentrations. The largest DOC export is however expected during the winter when high discharge levels are reached for longer periods. Results are presented in section 4.3 and discussed in section 6.2.

Two new events sampled in 2018 will be filtered with 5.00 µm, 1.00 µm, 0.45 µm and 0.10 µm filters to separate DOC from POC (section 3.3.5). The hypothesis is that POC becomes more important during peak flow conditions due to erosional processes. Higher POC concentrations are expected during events with a higher maximum precipitation intensity. DOC is expected to respond slower reflecting the travel time of water through the soil (Stockinger et al. 2014). DOC is also expected to be more

dominant after long periods of drought due to the accumulation of DOC in soil water during hydrological disconnection. Results are presented in section 5.1 and 5.2 and discussed in section 7.1.

### 1.4.3. P and its binding partners Al and Fe

For new events, Al, Fe and P are quantified for their total concentrations using ICP-MS (section 3.3.3). FFF-ICP-MS is applied to the event samples to separate three size classes and to quantify the elemental concentrations in these size classes (section 3.3.4). The expectation is that smaller nanoparticles respond faster and more strongly to events than larger nanoparticles or clays. The hypothesis is that P is associated to these transported nanoparticles leading to high P losses during events. The expectation is that the P export during events is mostly linked to the lateral passage of water (pressure wave) through the soil as expected for DOC transported nanoparticle P fractions (see section 1.1.). Clay mobilization is expected to be rare during events and might only occur temporally during high discharge conditions. Results are presented in section 5.1 and 5.2 and results are discussed in section 7.2, 7.3, 7.4 and 7.5.

# 2. Research Location

## 2.1. Geographical setting and research site

The TERENO Wüstebach research catchment is located near Wahlerscheid (50°30'12.7"N 6°19'33.3"E) close to the federal highway B258 connecting Monschau and Schleiden. The research site is situated in the Eifel Mountains at an altitude of approximately 600 meter above sea level (section 2.4). The Wüstebach research catchment compromises the headwaters of a second-order stream contributing to the Rur River. The research catchment area is 38.5 hectares (Graf et al. 2014). The dominant vegetation is Norway spruce (*Picea abies*) with inclusions of Sitka Spruce (*Picea sitchensis*) (see section 2.6 for more information on vegetation). The climate is wet and cool for regional standards (see section 2.3). A variety of soils have developed on periglacial material due to variations in groundwater levels (see section 2.5 and figure 1). Stream water is sampled on a weekly basis at 14 different locations. Station WU14 (Q14 in figure 1) is the catchment outlet and this station is equipped with an autosampler (section 3.1). The Wüstebach catchment was subjected to deforestation around the stream in 2013 and currently undergoes natural revegetation (figure 1). Because the catchment has been monitored before and after deforestation, the impact of deforestation on energy and matter fluxes can be researched (Bogena et al. 2015). Within the catchment a climate station is present, two eddy-covariance tower and an extensive network of wireless soil moisture monitoring devices (Bogena et al. 2015, figure 1 and section 3.3).

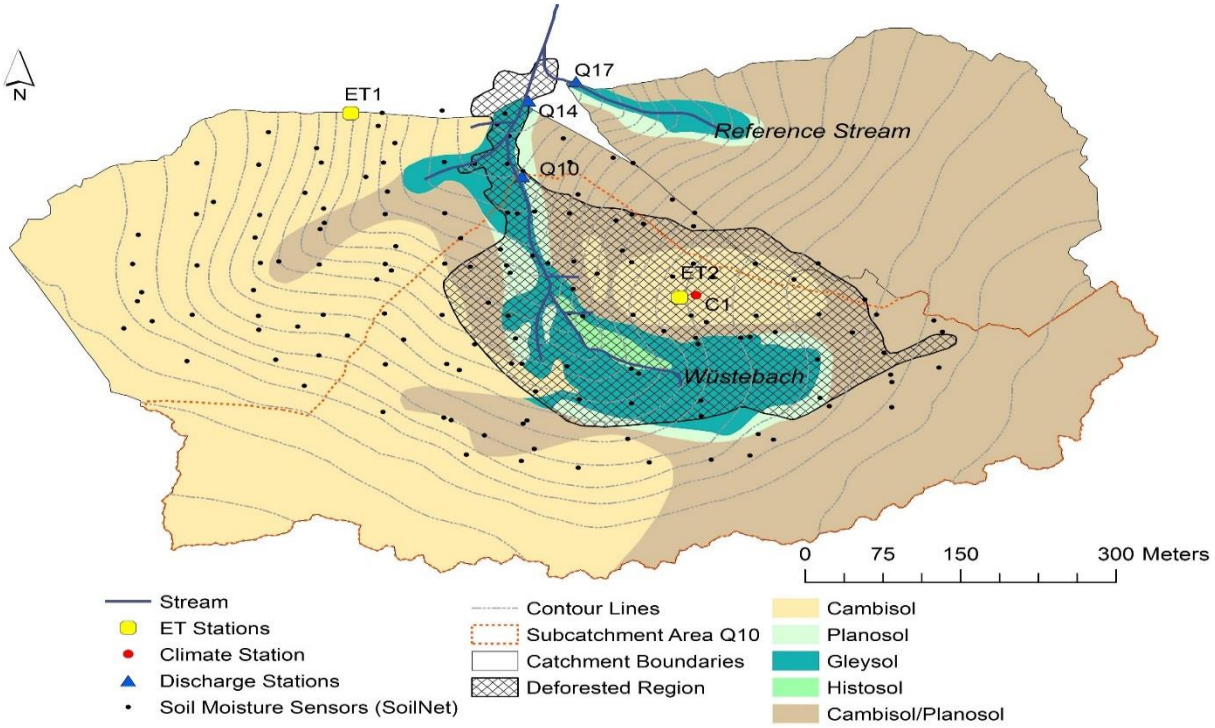


*figure 1. Overview of the Wüstebach catchment and its main properties. Original figure by Wiekenkamp et al. (2016).*

## 2.2. Meteorological stations

In this thesis, several references will be made to specific meteorological stations. These stations are: Monschau-Kalterherberg, Kall-Sistig, TERENO Wüstebach and TERENO Schöneseiffen. In table 1 the

altitude, geographical distance, direction from Wüstebach and data provider are summarized. The German Weather Service (*Deutscher Wetterdienst, DWD)* maintains Monschau-Kalterherberg and Kall-Sistig. FZJ maintains Wüstebach and Schöneseiffen within the TERENO project. The weather stations are complementary because each station has specific limitations. Monschau-Kalterherberg provides historical and recent weather data on nearly all meteorological parameters besides temperature. Kall-Sistig provides historical and recent temperature data. However, Monschau-Kalterherberg and Kall-Sistig are located several kilometers from the Wüstebach while weather phenomena can be very local. TERENO Wüstebach is located in the deforested part of the catchment and would therefore be the ideal information source for local meteorological data. Unfortunately, this station has been operational since 2014. Data can therefore only be used for recent events. TERENO Schöneseiffen is mainly used on occasions when data from TERENO Wüstebach is not available and for cross-reference. In Appendix B Monschau-Kalterherberg is compared with TERENO Wüstebach to discuss how well data from Monschau-Kalterherberg can substitute data from TERENO Wüstebach on basis of 4 years of measurements.

| **Station Name** | **Altitude (m a.s.l.)** | **Distance from Wüstebach (km)** | **Direction from Wüstebach (º)** | **Data source** |
|---|---|---|---|---|
| Monschau-Kalterherberg | 535 | 9.2 | 281.2 (W) | DWD |
| Kall-Sistig | 505 | 13.6 | 90.5 (E) | DWD |
| Wüstebach | 610 | 0 | - | TERENO |
| Schöneseiffen | 608 | 3.5 | 63.2 (ENE) | TERENO |

*Table 1. Overview of meteorological stations nearby the Wüstebach Catchment*

## 2.3. Climate of the Eifel-Ardennes Region and the occurrence of storms

Western winds originating from the Atlantic Ocean are the prevailing winds in The Eifel-Ardennes region (Meersman et al., 2016). These Atlantic western winds are generally moist and relatively warm causing winters to be mild and summers to be cool. The climate of the Eifel-Ardennes is however considerably cooler and moister than the climate further towards the sea. This difference is caused by the relatively high altitude of the Eifel compared to surrounding lowlands. Meersman et al. (2016) showed that the altitude of the Ardennes and Eifel leads to high precipitation amounts in the western part of the Eifel (High Fens) and a rain shadow further to the east. Annual rainfall is highest 15 km west of the Wüstebach catchment at Mont Rigi (1450 mm/year). At Monschau-Kalterherberg, average annual precipitation is 1220 mm/year (1979-1999). The amount of annual precipitation has slightly increased to 1306 mm/year (1986-2016). Rainfall is generally well distributed throughout the year. November, December and January are the wettest months (140 – 160 mm rainfall) whereas April, May and August are the driest months (94 – 96 mm rainfall). Snow is on average present for 77 days per year in the High Fens (Mormal & Tricot, 2004). The snow cover is not always consistent during winter and might partially or completely melt on several occasions (personal observation). The Wüstebach is located at a slightly lower altitude and further to the east making it likely that the average amount of snow days is slightly less for the Wüstebach. The region is well-known for severe rainfall events (Lowinski, 2014). Mormal & Tricot (2004) report that the three strongest regional precipitation events in the 20$^{th}$ century were 156 mm/day, 129 mm/day and 128 mm/day. Thunderstorms are observed 20

days per year on average and are most likely in July followed by May, June and August (Mormal & Tricot, 2004).

## 2.4. Geology

The Wüstebach catchment is located in the Eifel Mountains which is a part of the Rhenish Massif. The Rhenish Massif is an old mountain range formed during the Variscan Orogeny (+/- 330 Million years ago). During the Varsican Orogeny (mainly) marine sediments of Devonian and Carboniferous were subjected to compressional stress. In the Wüstebach dark-blue to black-grey slightly silty Devonian slates with very local sandstone inclusions make up the bedrock. Older remnants of quartzite can occasionally be found at the highest ridges of the Eifel or lower when transported during periods with periglacial activity (section 2.5). The age of the bedrock and the bedrock type makes the soil poor in nutrients. The Eifel has been subjected to strong erosion after its initial uplift 300 million years ago. After the start of the Alpine orogeny, the Eifel region has been uplifted which has also been associated with volcanic activity in the past (Meyer & Stets, 2007). Over the last 800.000 years the Eifel was uplifted with 200 meters giving the Eifel a second life as a mountain range (Meyer & Stets, 2007). Rivers responded to this uplift with strong incision leading to the typical Eifel landscape of today with relatively flat high plateaus incised deeply by several small streams.

## 2.5. Soils

In the Wüstebach catchment several soil types can be found depending on the groundwater table (figure 1). Near the stream, histosols and gleysols can be found. These soils typically have a high organic matter content. Due to high groundwater levels, biodegradation of organic matter is hampered in these soils allowing organic matter to accumulate. Further upslope, planosols can be found where groundwater tables are periodically high. Cambisols are found on the hillslopes where groundwater rarely reach the topsoil. All soils have been formed on periglacial material parent material. Periglacial material is a well-mixed soil matrix with a high amount of stone fragments. Periglacial processes occur when the topsoil thaws and the subsoil remain frozen. On the frozen subsoil water accumulates causing oversaturation. This allows the soil to flow whenever a slight angle is present (Borchardt, 2012). Since the catchment is located near a ridge in the landscape, all soil material comes from local sources.

Soils around the Wüstebach are generally dominated by silt (50%-70%) with smaller fractions of sand (7%-20%) and clay (<20%) (Borchardt, 2012). The contribution of sand, silt and clay however depends on the location of the soil. Clay content is higher (37%) for upland soils especially in the upper soil horizons while soils near the stream are poor in clay (15%). Soils near the stream are relatively enriched in sands compared to the upland soils. Soils are acidic in general (pH 4) and have a C/N ratio varying between 10.2 and 18.5 with higher C/N ratios in upland areas and lower C/N ratios near the stream.

## 2.6. Vegetation and Forest management

Norway spruce (*Picea abies)* planted after WO II is the main tree species in the catchment (Bogena et al. 2015). Intercalations of Sitka Spruce (*Picea sitchensis*) can be found at some places. Near to the stream, black alder (*Alnus glutinosa*) and Birch (*Betula pendula*) can be found. The deforested part is mainly covered with grasses (mostly *Molinia caerulea*) and mosses near the stream and various types of grasses, brambles and raspberry in the higher parts. Historical data shows that Beech (*Fagus sylvatica)* is the native dominant tree species in the research area. The Eifel National Park aims to restore the original forest type (Beech) (Lennartz & Röös, 2006). Röös & Mauerhof (2014) describe the

forest management in the research catchment consisting mainly of forest thinning, planting of beech trees and deforesting riparian zones to restore natural hydrological processes.

### 2.7. Hydrology and water chemistry

Discharge peaks up to 220 L/s have been recorded for summer events and up to 160 L/s for winter events. During winter events, discharge peaks last long and large volumes of water are exported of several days or week. During summer events, discharge peaks often only last for a few hours. The total water volume transported is much less. Baseflow is generally higher in winter than in summer. Stockinger et al. (2014) found that an average soil moisture content of 35% separates the hydrological winter from the hydrological summer. When the average soil moisture content is higher than 35%, the hillslopes are hydrologically connected to the riparian zone allowing water to transit from hillslopes to the stream. When the soil moisture content falls below 35%, the hillslopes are not connected to the riparian zone. Falling precipitation on hillslopes is either stored on the hillslopes or transferred via preferential flow paths to the stream (Wiekenkamp et al. 2016a). Mean stream water pH is 6.3 (SD: 0.5) and the mean Electrical Conductivity is 250 µs per cm suggesting a moderate nutrient and salt load (Bol et al. 2015).

The Wüstebach catchment has groundwater dominated, surface water dominated springs and springs being a combination between groundwater and surface water sources. The groundwater dominated springs have a low DOC concentrations and show little seasonal variability in terms of DOC concentrations (Weigand et al. 2016). Surface water dominated springs have a strong seasonal DOC variation with DOC maxima during late summer and autumn. DOC concentrations vary much more also on shorter time scales (events) (Weigand et al. 2016). The sample location used in this Thesis is the catchment outlet (WU14) meaning that groundwater springs and surface water springs are mixed. Bol et al. (2015) found that at the catchment outlet, 65% of all water stems from surficial springs and 35% from groundwater sources on average. Especially during events, high DOC concentrations are measured at the catchment outlet. Since groundwater DOC concentrations show very little variability, peak DOC concentrations during events are likely to stem from surficial sources.

On P fluxes and sources in the Wüstebach, much less is known. Due to low P concentrations, P is not measured on a weekly basis. Gottselig et al. (2014) described that total P concentrations where different between water sources in the Wüstebach catchment. Higher P concentrations were measured for overland flow locations (riparian zone) than for mixed streamwater at the catchment outlet. In general, higher P concentrations are expected within the riparian zone where P can accumulate (Klapproth, 2009). From a dataset paper by Gottselig et al. (2017b) it can be seen that in the Wüstebach catchment, P concentrations in the litter/organic soil horizons layer are low in the riparian zone compared to upland soils. In the A-horizon P is enriched in the riparian zone compared to the upslope soils.

## 3. Methodology

### 3.1. Research equipment in the catchment

Discharge is continuously measured at WU14 with a V-notch weir during low water levels (<5 cm) and a Parshall flume during normal to high water levels (>10 cm). Water levels between 5 cm and 10 cm are calculated as an average between the V-notch and Parshall flume. Water level is automatically recalculated to discharge (L/s). In addition to discharge, water temperature, pH, turbidity, $NO_3^-$ and electrical conductivity are continuously measured with a 10-minute resolution. Manual samples are

taken every Monday and analyzed for several chemical parameters including Total P, Total Al and Total Fe. The chemical data from these samples is available in the TEODOOR open data portal. A programmable autosampler (AS) is present at WU14. This autosampler can be set on a certain trigger level (cm). When the water level exceeds the trigger level, the autosampler program is started. The compartment where taken samples are stored is constantly refrigerated (4 °C) ensuring minimal changes in water chemistry. In total 24 sample locations are available

Rainfall data is collected by a pluviometer measuring with a 10-minute resolution. Temperature, wind direction, air pressure and other meteorological measurements are also obtained in the catchment and stored in the TEODOOR open data portal. A wireless soil moisture measurement network (SOILNET) provides real-time data on soil moisture status at three different depths in the catchment (Bogena et al. 2015). SOILNET was not used in this thesis, but the presence of SOILNET might be useful for follow-up research.

## 3.2. Past events

### 3.2.1. Analysis of meteorological data

So far, no research has been done on the seasonality of events specifically for the Wüstebach catchment. Two tests were conducted in this thesis using data from DWD weather station Monschau-Kalterherberg. One test focused on daily precipitation sums (1986-2016) and another test on 10 minute rainfall intensity (2007-2017).

For daily precipitation, the 95$^{th}$ percentile was used as a borderline between extreme values and non-extreme values. The 95$^{th}$ percentile was found on 16.5 mm/day. 533 days over the last 30 years passed this criterion. From these 533 events, 100 random numbers were selected using the datasample function in MATLAB. For these 100 events, the dates were manually divided into months (results: 4.1.1).

In order to decrease computation time, only 10 years of 10 minute rainfall intensity data was evaluated (2007-2017). This provided 300000 data points of which 94.75% equaled 0. All zeroes were removed and from the remaining datapoints (15600), the 99$^{th}$ percentile was calculated. The 99$^{th}$ percentile was 2.0 mm/10 minutes which was considered to be a good border between extreme rainfall and non-extreme rainfall. Only 193 occasions of such heavy rainfall were recorded in 10 years. From these 193 occasions, 100 numbers were randomly selected. The dates were manually divided into months (results: 4.1.1).

### 3.2.2. Creating an event database

From the TERENO data portal, discharge data between 2010 and 2017 was investigated to construct an event database. The decision was made to define a hydrological event as a situation where peak discharge was 3 times higher than baseflow conditions. Applying this condition yielded 98 events in 7 years. For all events in the event database, total rainfall, maximum rainfall intensity and average rainfall intensity were collected from either the DWD open data portal or the TEODOOR data portal. For events between 2014 and 2017 the Wüstebach climate station was used. For other events, Monschau-Kalterherberg was used (results: 4.1.1).

Data collection was partly subjective. Especially the duration of the event was difficult to define. Occasionally, periods with low rainfall amounts (<0.5 mm/hr) were found shortly before or after an event. The decision was made to exclude hours with <0.5 mm/hr precipitation. This influenced mostly the hourly average rainfall estimations. Certain cases remained where it was unclear whether

precipitation should be added to the event or not. For total rainfall estimations and maximum rainfall intensity these decisions were not relevant. Total rainfall and maximum rainfall intensity and were dominated by the values obtained during the strongest phase of an event and adding a few hours of low intensity rainfall did not affect the maximum rainfall intensity or total rainfall estimation.

### 3.2.3. Overview of the 12 past events with additional DOC data

For all events in the event database, the availability of autosampler samples was checked in TEODOOR. Additional samples were taken during 12 events (see table 2 and Appendix A). For all sampled events, the timing of the sampling was compared to the hydrograph to see which part of the hydrograph was covered. Mostly, pre-event conditions were poorly covered. For 5 events, some pre-storm samples were available. Samples close to the hydrological peak were always available. For most events samples were also available from the falling limb of the hydrograph. However, the sampling program stopped often before a new baseflow level was established. In Appendix A more information is provided for each event. In Appendix A discharge is plotted together with DOC for all events showing DOC behavior in relation to discharge.

| Event number | Event date | Hydrological increase | Total Rainfall | Maximum Intensity | Data quality |
|---|---|---|---|---|---|
| 1 | 16 September2015 | 11 | 30 | 5.20 | No data on rising limb |
| 2 | 28 January 2013 | 11.6 | 57 | 1.20 | Good coverage of full event |
| 3 | 23 July 2013 | 22.5 | N.D. | N.D. | No data on rising limb and no meteorological data |
| 4 | 8 September 2013 | 27.5 | 31.4 | 3.92 | No data on rising limb |
| 5 | 9 May 2012 | 3.9 | 3.5 | 0.75 | No data on falling limb |
| 6 | 13 July 2012 | 7 | 35.3 | 1.41 | Only data on falling limb |
| 7 | 3 October 2012 | 64 | 58.9 | 4.51 | No data on rising limb |
| 8 | 6 January 2011[a] | 14.7 | 62.8 | 1.32 | Good coverage of full event |
| 8 | 12 January 2011[a] | 3.8 | 63.1 | 0.82 | Good coverage of full event |
| 9 | 21 July 2011 | 72.4 | 5.2 | 1.97 | No data on rising limb |
| 10 | 14 August 2011 | 5.7 | 23.6 | 2.09 | No data on rising limb |
| 11 | 6 May 2014 | 26.6 | 32 | 4.10 | No data on rising limb |
| 12 | 8 July 2014 | 10 | 20 | 1.21 | No data on falling limb |

*Table 2. Overview of all events where additional DOC samples were available. See Appendix A for more information on event characteristics.*

### 3.2.4. Calculation of DOC exports during events

For all 12 events the additional samples were used to calculate weekly DOC export with and without additional samples. This approach was considered to be better suited than an estimation of the impact of events on an annual basis. Every Monday DOC is quantified on a sample taken during the weekly sampling campaign. With only this information available, weekly DOC export is calculated by interpolating between the two samples. This yields a straight line between the two samples. The interpolated concentrations and then multiplied by discharge and by the time per sample interval (600 seconds). This yields the export per 10 minutes (mg/10 minutes). Summing all exports per 10 minutes gives the export per week (mg/week). When additional samples are available, these samples are used

to replace a part of the DOC concentrations obtained in the previous step. Linear interpolation between the additional samples was used to estimate DOC concentrations per 10 minutes. Again, concentrations are multiplied with discharge and the time interval (600 seconds) and summed over the whole week to estimate DOC export per week. The relative increase in DOC export was calculated to assess the importance of high resolution sampling on DOC export estimations (results: 4.3.1).

Maximum DOC concentrations during events were compared with two potential predictor values (baseflow level and maximum rainfall intensity). For this comparison, data from the event database was combined with DOC concentrations from the autosampler (results: 4.3.2)

## 3.3. New events

### 3.3.1. Sampling of new events

In total, two events were sampled in the first part of 2018. Both events were sampled with the autosampler providing 24 samples (AS1 to AS24) per event. After the event sampling, the samples were refrigerated in the autosampler until transferring to FZJ (maximum 7 days). In total 600 mL of sample is sampled by the autosampler. Samples for OC quantification (TOC V-CPN) were prepared directly after transferring since OC is prone to biodegradation. For other analyses, samples were analyzed as soon as possible. Storage in glassware was avoided for FFF-ICP-MS analyses due to the interference between silica and nanoparticles.

The March event was sampled between the 5$^{th}$ of March and the 12$^{th}$ of March (figure 2, left). A standard 8 hour sample interval was applied during non-event conditions. During the event, a sampling interval of 1 to 3 hours was used. When the water level dropped below the trigger level, the 8 hour sampling interval program was activated again. Samples AS1 to AS9 were sampled during baseflow. Samples AS10 and AS11 cover the rising limb of the hydrograph while AS12, AS13 and AS14 cover the falling limb. Samples AS15 to AS24 cover a second minor event and the establishment of a new, higher baseflow level.

The May event was sampled on the 16$^{th}$ of May and the 17$^{th}$ of May. One sample was sampled manually on the 16$^{th}$ of May 17:00 (AS1, baseflow). By coincidence, TERENO technicians were in the catchment on the 16$^{th}$ of May allowing the trigger level to be set very accurately. The trigger level was surpassed on the 16$^{th}$ March 20:10 and a 30 minute resolution sampling program was activated. The presence of samples AS1 and AS2 is special since samples in the very early stages of hydrological response are rare. AS2, AS3 and AS4 were taken on the rising limb of the hydrograph. AS5 to AS24 were taken on the falling limb of the hydrograph (figure 2, right). temporal resolution of this short but intensive event provides a unique option to study event processes in depth. Yet again, the AS stopped before a new baseflow level was established leaving a part of the hydrograph uncovered.

### 3.3.2. Quantification of Organic Carbon

#### *3.3.2.1. Shimadzu TOC V-CPN*

Organic Carbon is measured as Non-Purgable Organic Carbon (NPOC) which considered to be equal to Total Organic Carbon in the sample. Depending on the filters used, OC measured for a sample can be TOC or DOC. A Shimadzu TOC analyzer (V-series, CPN) was used to quantify OC in samples. This device measures OC by acidifying the sampling using Phosphoric acid and leading a carrier gas through the sample carrying away Inorganic Carbon (IC). The remaining organic carbon is quantified by oxidizing the carbon with persulfate transferring organic carbon in the sample to $CO_2$ (wet oxidation). $CO_2$ is quantified using non-dispersive infrared photometry by determining the infrared light adsorption in

the 2.5 nm – 8 nm wavelength range. The TOC V-CPN is maintained and calibrated by lab technicians from IBG-3 Martina Krause and Andrea Ecker.

#### *3.3.2.2 Organic Carbon Detector (LC-OCD)*

The OCD detector (DOC labor, Karlsruhe, Germany) has been described by Gottselig (2016). This paragraph summarizes the main features of importance for this thesis based upon the description of Gottselig (2016). The OCD applies the Gräntzel thin-film reactor working with the principle of wet oxidation. Like the Shimadzu V-CPN, IC is firstly removed from the sample after sample acidification (2.5 gram of $K_2S_2O_8$ + 20mL 85% $H_3PO_4$ dissolved in Milli-Q water). By constant purging the sample with $N_2$ carrier gas, IC is transferred from the sample. The compartment where this happens is completely shielded from UV-light. After the IC is removed, the sample enters the UV area where the principle of wet oxidation is applied. Sample water is used for the oxidation. OH radicals are formed by exposing the sample water to a wavelength of 185 nm. OH radicals are very strong oxidants allowing a conversion of OC to $CO_2$. The $CO_2$ produced is carried by $N_2$ gas towards the C detector. The detector is based upon non-dispersive infrared photometry and $CO_2$ is quantified by determining the infrared light adsorption in the 2.5 nm – 8 nm wavelength range.

Calibration curves were constructed using dilutions of a TOC standard solution. OC concentrations (mg OC/L) of 0.00 (Milli-Q), 0.05, 0.1, 0.5, 1.0, 3.0, 5.0 and occasionally 10.0 when high OC concentrations were expected were used for the calibration curves. Samples were placed in the FFF autosampler and transferred to the OCD via the FFF channel without the activation of cross-flow. Per sample 0.5 mL was injected for OC quantification and calibration. Peak areas were calculated in EXCEL and linear regression lines were drawn through the relative peak areas.

#### *3.3.2.3 Shimadzu TOC V-CPN versus OCD*

The main advantage of the OCD detector is the direct coupling between the FFF and the OCD which allows a continuous measurement of OC in various particle size classes. The TOC-V-CPN requires a much larger sample volume and cannot cope well with low volumes of sample with a low OC concentration. The TOC V-CPN device only works off-line meaning that samples have to be collected manually from the FFF and injected into TOC V-CPN. The OCD can directly measure OC after FFF by on-line attachment. The quantification efficiency of both systems was tested by Gottselig (2016). On average, the OCD detected 94% of all C detected by the TOC V-CPN. 85% detection of OC detected by TOC V-CPN was reported as a minimum recovery. 85% recovery of OC by OCD is therefore considered to be a conservative estimation of the recovery rate of the OCD. The OCD is therefore considered to be as reliable as TOC V-CPN having a low standard deviation (average 2.2%) and thus a good reproducibility.

Both methods were used in this thesis. For practical purposes some samples were analyzed using the TOC V-CPN while other samples were analyzed using the OCD. Since results should be comparable (max 15% difference), OC data can either come from the OCD or TOC V CPN.

### 3.3.3. Quantification of P, Fe and Al using ICP-MS

Phosphorus (P), Iron (Fe) and Aluminum (Al) were quantified by Inductively Coupled Plasma – Mass Spectrometry (ICP-MS) (Aglient 7400). ICP-MS has the quality to quantify extremely low elemental concentrations of a wide range of elements. The focus in this thesis is on P and its potential binding partners Al and Fe.

The basic principle of ICP-MS is that a sample containing a mixture of compounds is converted to individual ions of atoms by the Inductively Coupled Plasma (ICP). The ICP is a plasma of ionized Argon

ions with reaches a temperate above 6000 Kelvin. At this temperature, all compounds with a lower ionization potential then Argon itself (nearly all elements) are separated into atoms which are ionized in the plasma. The ionized atoms are separated on basis of their mass to charge ratio (m/z ratio) by a quadrupole mass analyzer. By gradually changing the conditions in the quadrupole, elements are separated on basis of their m/z ratio. This separation enables quantification of elemental concentrations using an electron multiplier detector.

Calibration standards were prepared with 1 g/L reference standards of each element (P, Fe, Al, Mn, Ca and Si). For each element, 100 µL of the reference standard was dissolved in 9.4 mL 3% $HNO_3$ solution. This provides a stock solution containing 1000 µg/L of each element. This stock solution was diluted further in acid with an internal standard (Rhodium (Rh) and Yttrium (Y)). Since Rh and Y should only occur in extremely low concentrations in natural samples and laboratory environments these elements serve as an internal standard during the measuring process. All element counts for the elements of interest are corrected for ICP-MS dependent measurement errors revealed by increasing or decreasing Rh and Y concentrations. From the integrated peak areas of the concentrations of each elemental concentrations, calibration lines are constructed with are used for further quantification. For each series of measurements, a new calibration line was prepared. 10 µg/L, 25 µg/L, 100 µg/L, 250 µg/L, 500 µg/L and 1000 µg/L were used for calibration. With the linear regression line, concentrations could be derived from the peak areas of the event samples. Data was handled in EXCEL where a baseline correlation was applied.

Results are provided for Total concentrations in section 5.1 and 5.2. Figures discussing elemental fluxes (µg/s) are provided in Appendix C.

### 3.3.4. Fractionation of samples using AF4

#### *3.3.4.1. Introduction to FFF*

Asymmetric Flow Field Flow Fractionation (AF4) is a separation technique to separate compounds on basis of their particle size. AF4 is a form of Field Flow Fractionation (FFF) with was developed by J. Calvin Giddings. FFF is a unique separation method because the method is non-destructive and can be applied to samples without prior adjustments like acidification or filtration. Phosphorus research often relies on the extraction of various forms of phosphorus which destructs the sample (for example: Reddy et al. 1995). Opposed to chromatography, the FFF does not separate particles by a chemical interaction with stationary phase (HPLC). AF4 has the property that the bottom wall of the channel is permeable. A PES membrane on top of a porous ceramic frit allows compounds with a too low molecular weight (< 1 kDa) to exit the channel. This separates the fraction we define as truly dissolved (<1 kDa particle size) from the fraction that we define as nanoparticulate (>1 kDa, <100 nm) and fine colloidal (>100 nm, <450 nm). Typically, colloids with a diameter of >450 nm are not detected using this method on natural stream water (N. Gottselig, personal communication). In most studies samples are filtered before analysis (Dahlqvist et al. 2004; Hassellöv & Von der Kammer, 2008). Too large particles are observed as a void peak (N. Gottselig, personal communication).

With Field Flow Fractionation, the sample is injected into a channel via the tip flow and is counteracted by the focus flow. The combination of the tip flow and the focus flow leaves particles at a certain position in the channel (focusing). A cross-flow is added to the channel perpendicular to the tip flow direction pushing the cloud of particles to the bottom of the channel (figure 3, left). During the elution step of the fractionation, natural diffusion (Brownian Motion) counteracts the crossflow. Smaller particles are capable of diffusing higher into the flow channel than larger particles. This difference in diffusion height causes the separation of particle sizes because a parabolic flow profile is maintained in the channel. Particles diffusing higher into the channel are therefore eluted faster from the channel compared to particles with a lower diffusion height (see figure 3, left). By coupling AF4 to a detection system, a fractogram can be created with a detector signal on the Y axis and elution time on the X axis (see figure 3, right). By specifying border times the fractogram is split into size classes (fractions). The concentration of elements for each fraction can then be assessed.

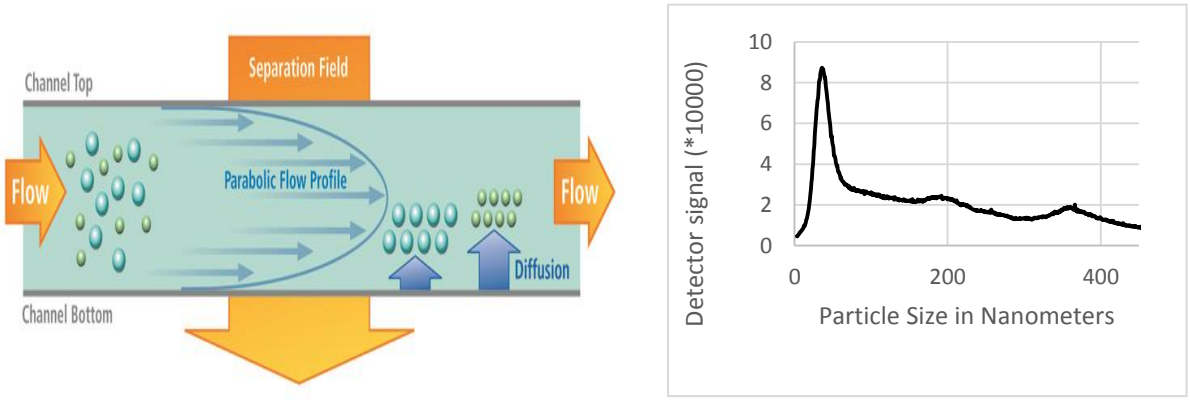


*Figure 3. Left: schematic overview of the FFF principle. Right: theoretical fractogram with a detector signal on the Y axis and elution time (particle size) on the X axis.*

#### *3.3.4.2. FFF instrumentation settings*

The FFF method of Gottselig et al. (2014) was used for this thesis. A short summary of the method will be provided in this chapter. Untreated samples are placed in the refrigerated FFF autosampler compartment. Sample is taken up from the vial and mixed with the carrier solution (25 mmol NaCl solution in Milli-Q water). In total 5 mL of sample is injected into the FFF channel with a tip flow speed of 0.2mL/min. After focusing a cross-flow gradient was applied starting with 3.0 mL/min and dropping to 0 mL/min in 30 minutes. The flow running to the detector is 0.5 mL/min.

### 3.3.5. Fractionation of sampling using a filtration cascade

A series of PES filters was used to separate different particle sizes. PES was chosen as a filter material because the membrane in the FFF is also made from PES. The following sizes were used: 5.00 µm, 1.00 µm, 0.45 µm and 0.10 µm (see table 3). The 5.00 µm filter filters out the largest particles (larger than fine silt). The 1.00 µm filter separates particles from colloids. The 0.45 µm filter separates colloids from fine colloids. The 0.10 µm filter is the smallest syringe mountable filter on the market. This filter separates nanoparticles from fine colloids.

Filtrates were analyzed using ICP-MS to detect total elemental concentrations. In theory, filtering should provide similar concentrations as FFF. Filtering with a 0.10 µm filter overlaps with most of the 1st, 2nd fraction, a part of the 3rd fraction and the truly dissolved fraction. Elements found in the filtrate <0.45 µm and >0.10 µm should more or less correspond with the 3rd fraction of the FFF (for more information on the fractions see 1.3 and 3.3.6).

The OC coming off filters was tested by washing all filters with known amounts of Milli-Q water. The filtrates were analyzed with the OCD in triplicate for OC content (figure 4). An additional experiment was added to test whether OC could be derived from particles trapped in a clogged filter (clogging experiment). Filter washing proved to be highly important, but the effect of washing with larger volumes of water quickly decreased. The decision was made to wash all filters 3 times. During the clogging experiment the filters were clogged with 75 mL of sample rich in suspended sediments. After clogging, a blank sample (Milli-Q) was filtered to determine the amount of OC coming from a clogged filter. This proved to be less than the amount of OC coming from unclogged filters and the amount increased with increasing filter size. These results are discussed further in section 7.1.3.

| **Filter size (µm)** | **Filtrate** | **Scientific relevance** |
|---|---|---|
| 5.00 | Fe, Al, $P_{<5.00}$ | Separation of silt particles and larger from clay |
| 1.00 | Fe, Al, $P_{<1.00}$ | Separation colloids from particles |
| 0.45 | Fe, Al, $P_{<0.45}$ | Separation fine colloids from colloids |
| 0.10 | Fe, Al, $P_{<0.10}$ | Separation of nanoparticles from fine colloids |

*Table 3. Overview of the filters used, the respective sample names of the used filters and their scientific relevance.*

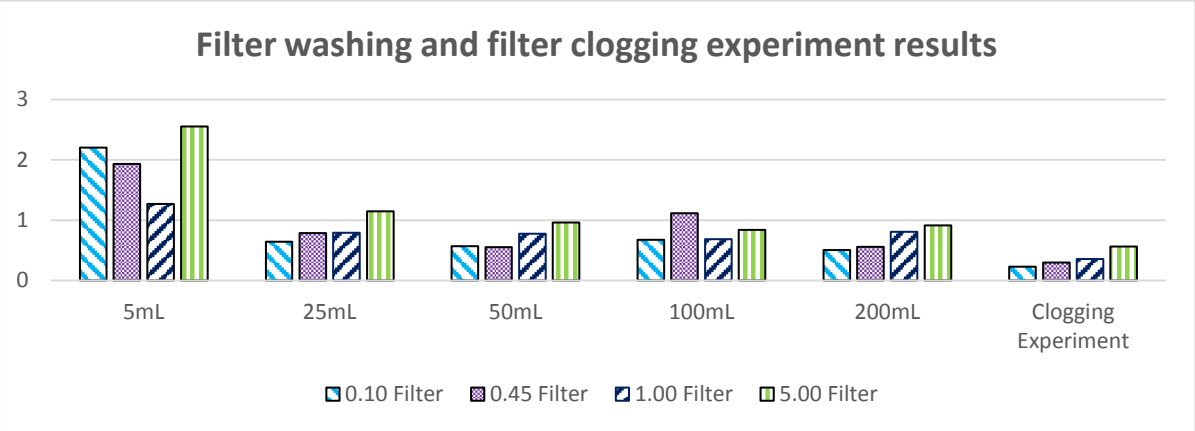


*Figure 4. Results from Filter washing and filter clogging experiment to determine background OC concentrations coming from filters.*

### 3.3.6. Combining FFF with ICP-MS

The combination between FFF and ICP-MS allows the determination of the elemental composition of nanoparticles and fine colloids with a variable size (Mitrano et al. 2011). Since FFF elutes a range of particle size classes over time, the continuous quantification of elements shows the concentrations of elements in various particle size fractions. Elemental concentrations are calculated per time interval.

The elemental concentrations are then summed for specific time periods equaling the size fractions. The 1st fraction elutes from the FFF between 33 min. - 38 min., the 2nd fraction elutes between 38 min. – 54 min. and the 3rd fraction elutes between 54 min. – 90 min. For all elements of interest, elemental concentrations are calculated for each fraction. The method used in this thesis is suited for nanoparticles and fine colloids from 1 kDa (0.66 nm) to 450 nm in diameter. The 1st fraction incorporates particles between 1 kDa (0.66 nm) to 20 nm, the 2nd fraction incorporates particles between 20 nm and 60 nm and the 3rd fraction incorporates particles between 60 nm and 450 nm (although practically all particles are smaller than 300 nm).

In Chapter 5 discusses the importance of colloids with regard to total elemental concentrations. This percentage is calculated as the sum of the 1st, 2nd and 3rd fraction divided by the total concentration (unfiltered). The term colloidal is not entirely suited since colloids range between 1 nm and 1000 nm while the three fractions incorporate colloids between 1 nm and 450 nm. Because all colloids are practically smaller than 300 nm the term colloidal was considered to be appropriate.

# 4. Results: Past events

In this chapter, events occurring between 2010 and 2017 are studied. In paragraph 4.1 the seasonality of events and extreme precipitation is researched. In paragraph 4.2, rainfall intensity and total rainfall amounts are compared with catchment responses to see which factor has the most influence. In paragraph 4.3, DOC data from historical events is used to show the relevance of high resolution sampling for DOC export estimations. Maximum DOC concentrations during events are compared with predicting variables such as baseflow conditions and rainfall intensity.

## 4.1. Seasonality of events

The winter months (November, December, January, February and March) have more extremely wet days (>16.5 mm/day) than the spring months April, May and June. July and September stand out against the other spring, summer and autumn months (figure 5). The highest chance of encountering high maximum rainfall intensities (>2 mm/10 minutes) is in June, followed by July and August. These three months clearly stand out compared to other months. From February to April extreme maximum intensities are rare. Between September and January extreme rainfall intensities are also infrequently observed (figure 5). Most hydrological events (peak flow > 3 times higher than baseflow) were found in the summer period (July, August and September). The higher chance of high maximum rainfall intensities in June did not clearly stand out in figure 5. More hydrological events occur in August than July which may be explainable from the higher chance of extreme rainfall intensities (4.1.2). July has more days with high precipitation amounts than August, but it seems that maximum rainfall intensity is more important for hydrological events. Another explanation is that the catchment might be more responsive to rainfall during the end of the summer due to catchment drying (Rosenbaum et al. 2012).

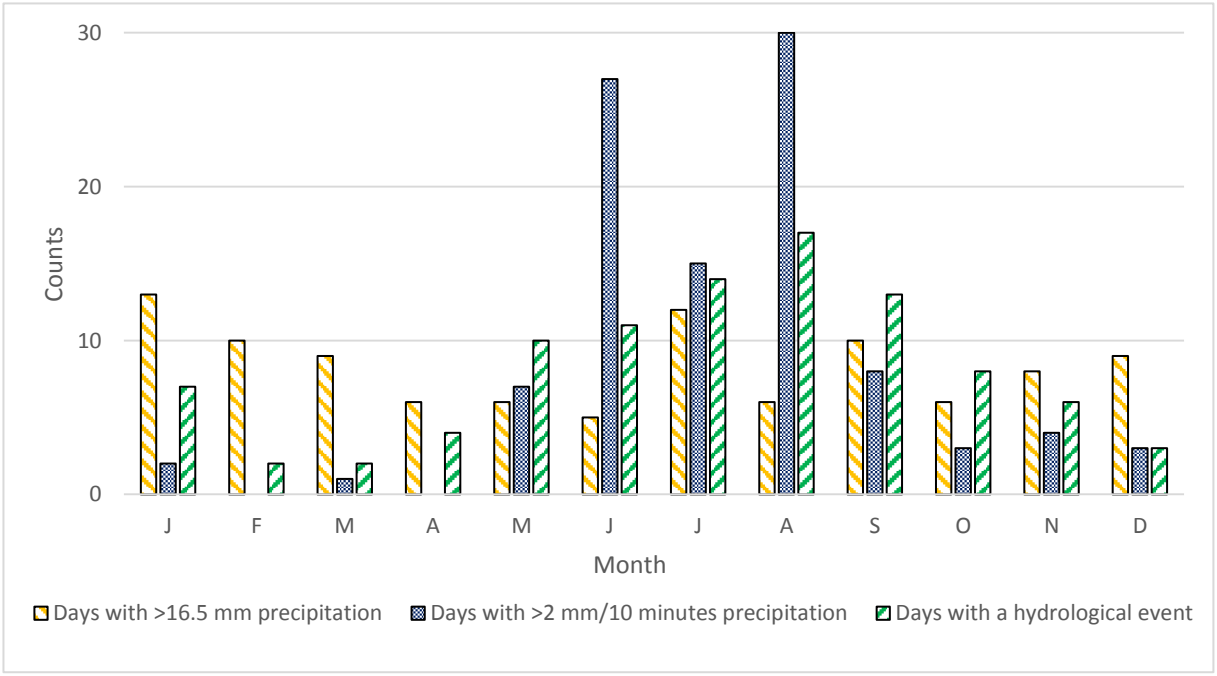


*Figure 5. Seasonality of rainfall and discharge events in the Wüstebach Catchment*

## 4.2. Catchment response to precipitation

Rainfall intensity (figure 6, left) and average rainfall per hour (figure 6, right) were found to be better predictors for catchment response than total rainfall amount (data not shown). These figures are based upon events in the storm database (N=98). Average rainfall intensity proved to be a slightly better

predictor ($R^2$ = 0.46) than peak rainfall intensity ($R^2$ = 0.35) whereas total rainfall amount was a poor predictor ($R^2$ = 0.0075). These results underline that catchment response is linked to rainfall intensity and not to total rainfall amount. However, the figures also indicate that individual catchment responses are very variable even with similar rainfall intensities.

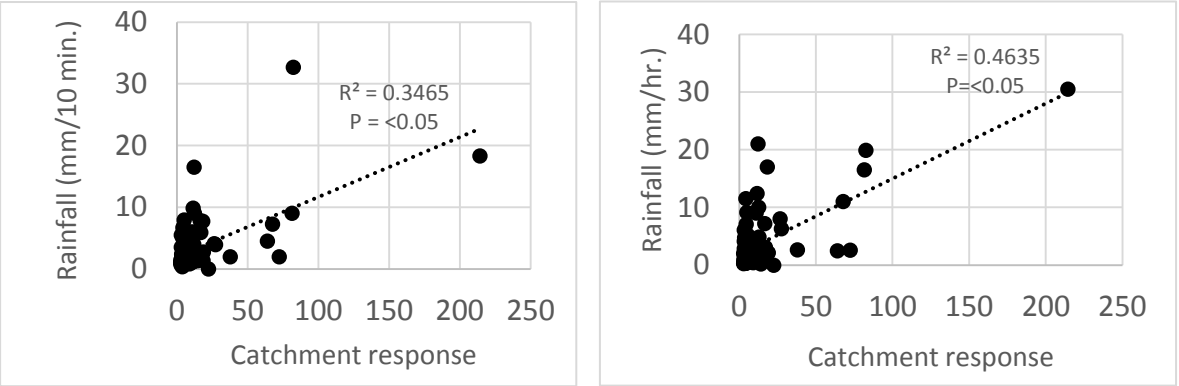


*Figure 6. Relationship between catchment response (peak flow / baseflow) on the X-axis and 10 minute rainfall intensity (left) and average rainfall per hour (right).*

## 4.3. DOC response to high-intensity rainfall events

### 4.3.1. Weekly DOC Export

For all events, the weekly DOC export was calculated with additional event samples and without additional event samples. The weekly DOC export was calculated by multiplying DOC concentrations with discharge (see Methods 3.2.4). The relative export increase was calculated by comparing the weekly DOC export with and without additional samples. Figures for all events and additional descriptions are available in appendix A.

The weekly DOC export increased on average with 32.9% when additional samples were incorporated. A maximum export increase of 85% was found for one summer event. For this event, additional DOC samples were available for the entire hydrological response. In total, 7 events were reasonably well sampled (event 1, 3, 5, 6, 8, 9, 12). For these 7 events, the average relative increase in DOC export was 46%. The average hydrological response was 11.7 for these 7 events. Such strong events occur on average 3.5 times per year. Event 5 however shows that also for small events (4 times hydrological response), the relative increase can be 25%. Events with >4 times hydrological responds however occur 10 times per year on average. For the estimation of the importance of events on a yearly basis, the smaller events (2-4 times baseflow) forms the largest knowledge gap. High resolution continuous measurements as described by Snyder et al. (2018) would lead to much higher DOC export estimations.

### 4.3.2. Maximum DOC concentrations

Maximum DOC concentrations measured during events were compared to two factors: maximum rainfall intensity (mm/10 minutes) and baseflow (figure 7, left and right). High maximum rainfall intensity might create a rapid pressure wave causing a discharge increase (section 2.7). Baseflow is considered to be a predictor value for catchment dryness with low baseflow conditions suggesting prolonged catchment drying (section 1.1).

Maximum rainfall intensity (figure 7, left) proved to be a better predictor for maximum DOC concentrations than baseflow conditions (figure 7, right). Extreme rainfall events (> 2 mm/10 minutes) are more likely to cause high maximum DOC concentrations than weaker rainfall events. The P value

for maximum rainfall intensity was significant (P=0.02) while the P value for baseflow was not significant (P = 0.11). The highest DOC concentration was measured when baseflow was only 0.6 L/s. However, event 1 shows that also for higher baseflow conditions (5 L/s), high maximum DOC concentrations (18.3 mg/L) can be found. With an expansion of this research in the future, it might be possible to obtain a significant correlation between baseflow and maximum DOC concentration as well.

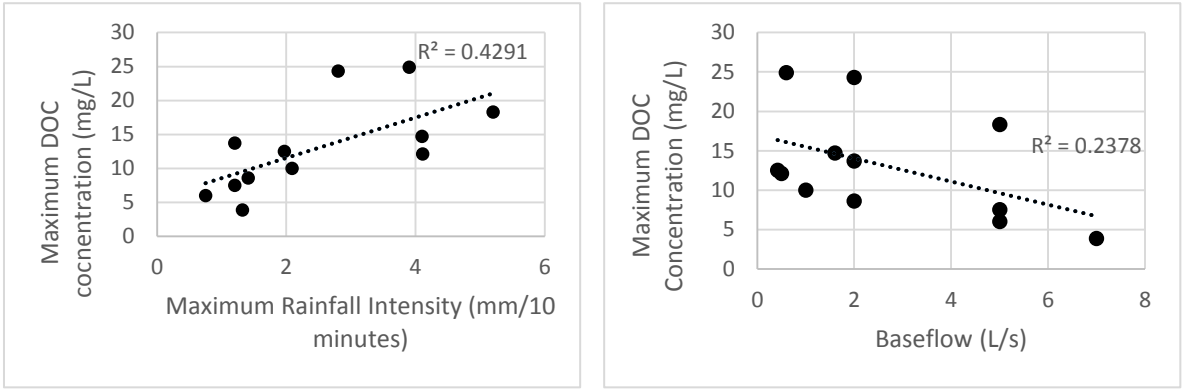


*Figure 7. Relationship between two predictor variables and maximum DOC concentrations measured during events. Left figure shows maximum rainfall intensity (mm/10 minutes), right figure shows baseflow (L/s).*

# 5. Results: New events

## 5.1. March event 05-03-2018-12-03-2018

### 5.1.1. Event description

The March event was preceded by a wet December 2017 (183 mm rain) and a wet January 2018 (176.5 mm rain) while February was dry (39.5 mm rainfall) (Monschau-Kalterherberg). The long-term precipitation average for these months is 148 mm (December), 141 mm (January) and 122 mm (February). December 2017 and January 2018 had elevated average temperature (2.1 and 3.4°C) while February was cooler than normal (-2.9°C) (Sistig-Kall) (Long-term average: 1.3, 0.4 and 0.6 °C). During February snow accumulated in the Wüstebach (20 – 30 cm). On the 6th of March 12:00 (figure 8, bottom left) the entire catchment was still covered with snow while on the 8th of March 15:00 (figure 8, bottom right) the majority of the snow was already melted. The event was caused by a combination between snowmelt and precipitation. In total 17.4 mm rainfall was recorded between the 7th of March and the 12th of March (figure 8, top). On the 7th of March, 2 mm rainfall was recorded. On the 8th of March, 9.5 mm fell while 4.5 mm rainfall was recorded on the 10th of March (Wüstebach Climate Station). A maximum intensity of 1.3 mm/10 minutes was recorded on the 8th of March. Peak discharge followed closely after maximum rainfall intensity. Peak flow (22 L/s) occurred during on the 8th of March. This was 3.6 times higher than baseflow conditions (6 L/s). Before the event on the 8th of March, daily discharge fluctuations were observed on the 5th, 6th and 7th of March. The peaks of these daily fluctuations were all in the late afternoon (between 17:00 and 18:00 o'clock). Since no precipitation was measured on these days the daily fluctuations are likely to be temperature-related and indicate snowmelt during the day. Streamwater pH dropped from 6.0-6.1 during baseflow to 5.85 during peak discharge and seemed to establish on a new level (5.9) on the 10th of March. Maximum Streamwater turbidity (26 NTU) was recorded directly at peak flow.

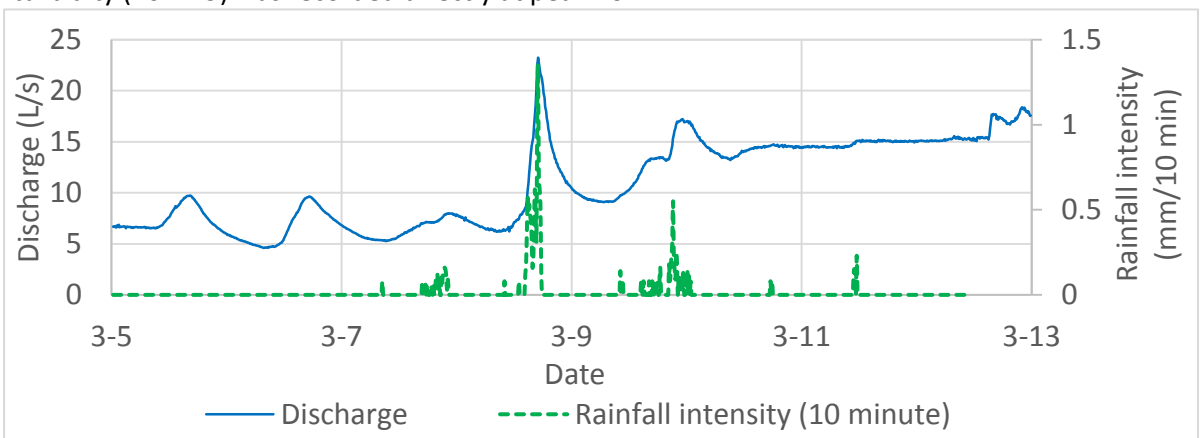


*Figure 8. Rainfall intensity and discharge (top figure) and two pictures of the Wüstebach. Left picture on the 6th of March, right picture on the 8th of March.*

### 5.1.2. Organic Carbon

#### *5.1.2.1. DOC quantification*

DOC was quantified for all samples. DOC concentrations ranged from 2.5 mg/L to 5.8 mg/L (figure 9). The highest DOC concentration (AS13) was measured 2.5 hours after peak flow. For baseflow conditions (AS1 to AS10) the mean DOC concentration was 3.0 mg/L with a standard deviation of 0.5 mg/L. AS12 and AS13 were found to be significantly higher than baseflow average ($\alpha = 0.05$). The average DOC concentration after peak flow (AS15 to AS24) was 3.2 mg/L with a standard deviation of 0.5 mg/L. No significant difference was found between baseflow DOC concentrations and DOC concentrations after peak flow.

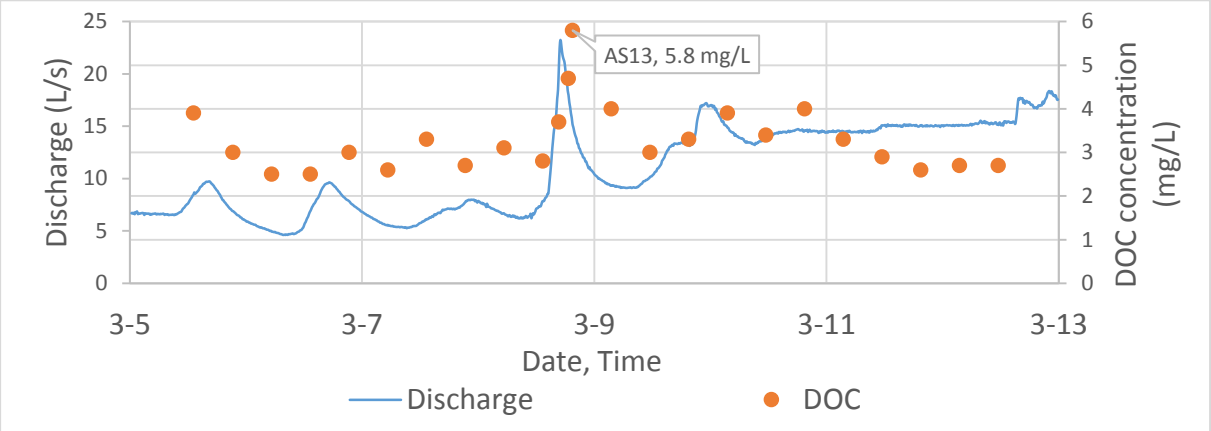


*Figure 9. DOC concentrations during the March event*

#### *5.1.2.2. Organic Carbon quantification of filtered samples (OCD)*

Organic Carbon was quantified in 5.00 µm, 1.00 µm, 0.45 µm and 0.10 µm filtrates using the OCD. The samples AS6, AS8, AS9, AS10, AS11, AS12, AS13, AS14, AS15 and AS20 were analyzed. The expectation was that less OC would be present in the filtrates from smaller filters. This relation was not observed (figure 10). On most occasions $OC_{0.45}$ and $OC_{0.10}$ were similar or slightly higher than $OC_{5.00}$. Especially for AS6, AS8 and event samples AS12 and AS13, $OC_{5.00}$ was considerably lower than $OC_{0.45}$ and $OC_{0.10}$.Replication of this experiment was done on a different day using fresh calibration standards. For the replication, special attention was given to pre-conditioning and washing of filters before filtration. Samples AS8, AS9, AS10, AS11, AS12, AS13 and AS14 were replicated. On average the difference between the two runs was +3% OC. $OC_{5.00}$ results were on average 10% lower in the second run. $OC_{0.45}$ and $OC_{0.10}$ were more consistent (+/- 1% difference). The replication shows that OCD results were reproducible for the 0.45 and 0.10 µm filters while being less reproducible for the 5.00 µm filters.

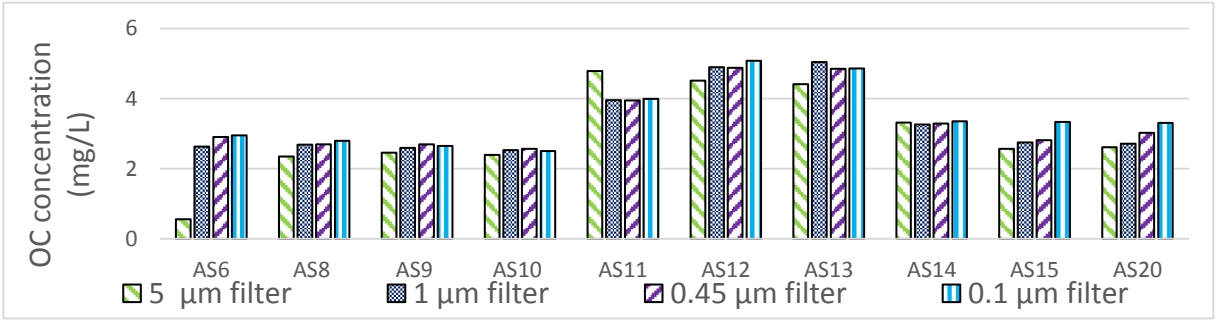


*Figure 10. OC concentrations in different filtrates during the March event*

### 5.1.3. Total Aluminum and Total Iron

For Al pre-event samples (AS1 to AS10) contained an average Al concentration of 61.5 µg/L (standard Deviation: 9 µg/L) (figure 11, left). During the event, the concentration first increased to a maximum at AS11 (267 µg/L) whereafter the concentration dropped to 90 µg/L (AS12). For AS13, a higher concentration was measured again (143 µg/L). For the post-event samples (AS14 to AS24) a mean concentration of 83.7 µg/L (standard deviation 12.2 µg/L) was found. Post-event concentrations were significantly higher than pre-event concentrations ($\alpha = 0.05$). Iron (Fe) behaved similar to Al (figure 11, right). During Pre-event conditions (AS1 to AS10) the average Fe concentration was 225.4 µg/L (standard deviation: 58.4 µg/L). During post-event conditions (AS14 to AS24) the average concentration rose to 309.3 µg/L (standard deviation: 151.2 µg/L). However, the difference between pre-event and post-event samples was not signficant ($P = 0.12$). The highest Fe concentrations were measured during the event. AS11 contained most Fe (2200 µg/L) followed by AS12 (990 µg/L) and AS13 (590 µg/L).

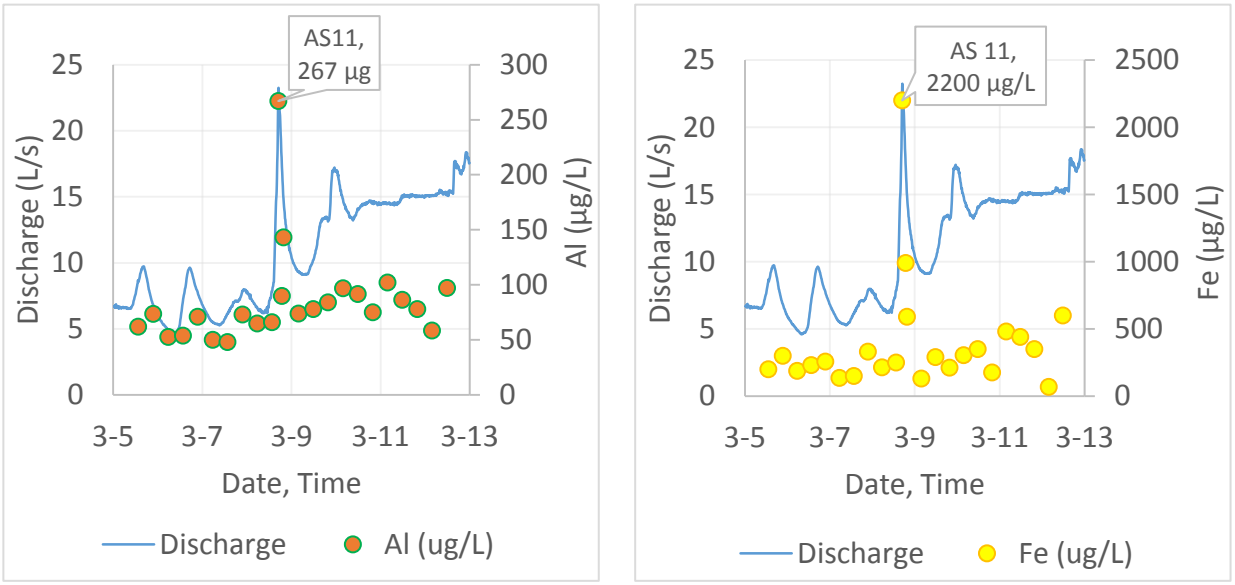


*Figure 11. Total Al (left) and Fe (right) concentrations during the March event plotted against discharge.*

### 5.1.4. Total Phosphorus

P concentrations were highest during peak flow (AS11) (figure 12). During baseflow concentrations between 29 µg/L and 32 µg/L were measured suggesting a low variability in P concentrations. Samples AS12 and AS13 were 1.6 times higher (50 µg/L) than the baseflow average. After the event, P concentrations between 25 µg/L and 29 µg/L were measured. The difference between baseflow samples before and after the event was not significant. Note that not all 24 samples were analyzed for P concentrations. In total 16 samples were measured.

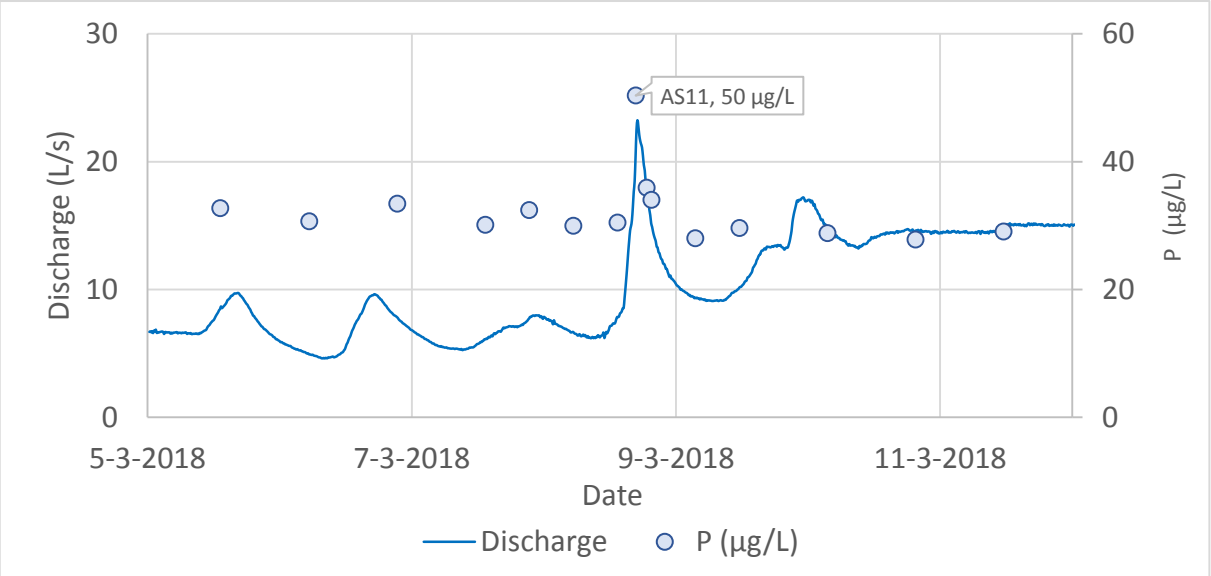


*Figure 12. Total P concentrations during the March event. Note that only 16 samples were analyzed instead of 24.*

### 5.1.5. FFF-ICP-MS Aluminum

During baseflow, 2nd fraction Al was the most abundant fraction (figure 13, top). Least colloidal Al was found in the 1st fraction. On average 0.9 µg/L Al was found in the 1st fraction during baseflow (AS1-AS10). During peak flow this increased to 4.71 µg/L (AS13). After peak flow (AS15-AS24), 1st fraction Al remained elevated compared to baseflow conditions (average 1.8 µg/L). 2nd fraction Al remained highest for all samples. During baseflow, the average concentration in the 2nd fraction was 2.8 µg/L and rose to a maximum of 7.8 µg/L during peak flow (AS13). The average concentration after peak flow was 4.0 µg/L. For the 3rd fraction, baseflow concentrations were on average 1.7 µg/L rising to a maximum of 2.6 µg/L (AS13). After peak flow, the average concentration was 1.8 µg/L. In figure 13 (left bottom) these results are summarized in a table.

Figure 13 (bottom right) shows the percentage of Total Al being transported in a colloidal form (>1 kDa, <450 nm). During baseflow (AS1, AS3, AS5, AS7, AS8, AS9 and AS10) the % Particulate Al ranged between 6% and 12%. For AS11, a sharp drop in % Colloidal Al was measured (4%). For AS12, AS13 and AS14 the % Colloidal Al increased to 15% (AS14). After peak flow (AS15, AS17, AS19, AS21 and AS23) the % Colloidal Al varied much between 8% and 14%.

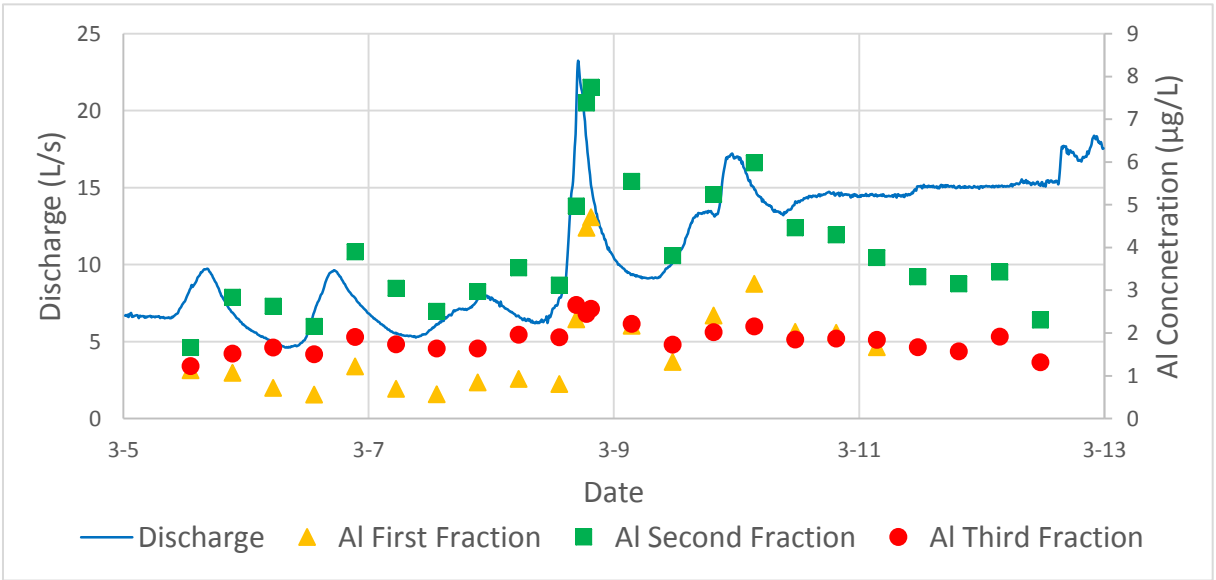

| Fraction | Baseflow (µg/L) | Peakflow (µg/L) | Increase |
|---|---|---|---|
| 1st | 0.9 | 4.7 | 5.2 |
| 2nd | 2.8 | 7.8 | 2.8 |
| 3rd | 1.7 | 2.6 | 1.5 |

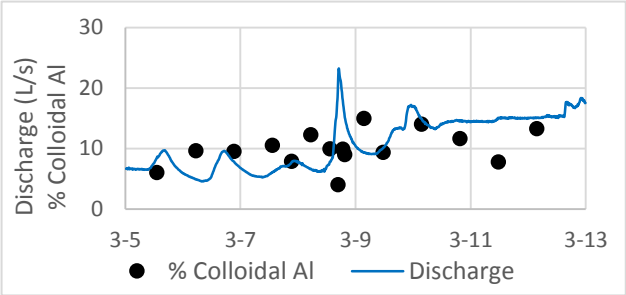


*figure 13. Al fractions during the March event (top figure). Overview of the responses per fraction (bottom left) and the importance of colloidal Al (1 nm – 450 nm) (bottom right).*

### 5.1.6 FFF-ICP-MS Iron

During baseflow, most colloidal Fe was found in the 2nd fraction. Least colloidal Fe was found in the 1st fraction. On average 0.8 µg/L Fe was found in the 1st fraction during baseflow (AS1-AS10). During peak flow the amount of Fe found in the 1st fraction increased to 4.5 µg/L (AS12). After peak flow (AS15-AS24), 1st fraction Fe remained elevated compared to baseflow conditions (average 1.7 µg/L). 2nd fraction Fe remained highest for all samples. During baseflow (AS1-AS10), average concentrations were 7.6 µg/L. Concentrations during peak flow rose to a maximum of 14.5 µg/L (AS12). Average concentrations after peak flow were 9.1 µg/L. For the 3rd fraction, baseflow concentrations were on average 5.7 µg/L rising to a maximum of 11.5 µg/L (AS12). After peak flow, the average concentration was 7.3 µg/L. Concentrations in the 3rd fractions seem to approach concentrations in the 2nd fraction for several samples (AS10, AS20, AS21, AS22, AS23 and AS24. The Fe concentrations in the fractions did not react strongly to the event (table 5). Peak concentrations were 2.6 times higher than baseflow average for the 1st fraction. While being approximately 2 times higher for the 2nd and 3rd fraction. These results are summarized in a table in figure 14 (left bottom).

Figure 14 (right bottom) shows the percentage of Total Fe being transported in a colloidal form. During baseflow (AS1, AS3, AS5, AS7, AS8, AS9 and AS10) the % colloidal Fe ranged between 4% and 11%. For AS11, a sharp drop in % colloidal Fe was measured (1.5%). For AS12, AS13 and AS14 the % colloidal Fe increased to 18% (AS14). After peak flow (AS15, AS17, AS19, AS21 and AS23) the % colloidal varied much between 4% and 11% which is similar to the baseflow range. This shows that the strong increase in Total Fe (figure 21, paragraph 5.2.5.) for AS11 is not colloidal Fe but rather truly dissolved Fe (<1 kDa) or Fe associated to molecules larger than 450 nm.

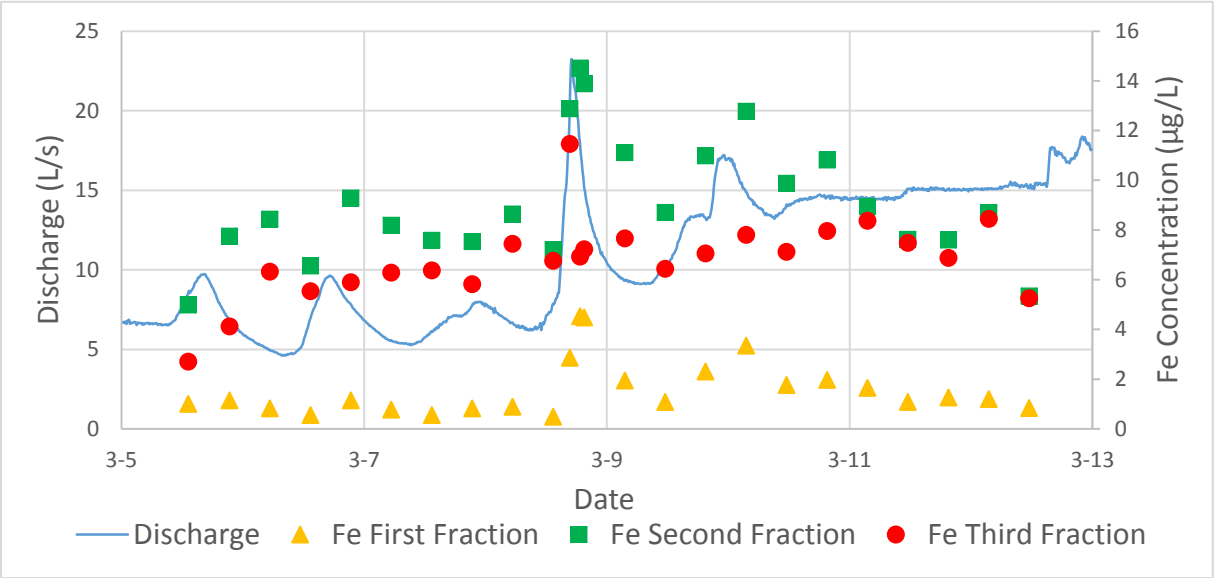


| Fraction | Baseflow (µg/L) | Peakflow (µg/L) | Increase |
|---|---|---|---|
| 1st | 1.7 | 4.5 | 2.6 |
| 2nd | 7.6 | 14.5 | 1.9 |
| 3rd | 5.7 | 11.5 | 2.0 |

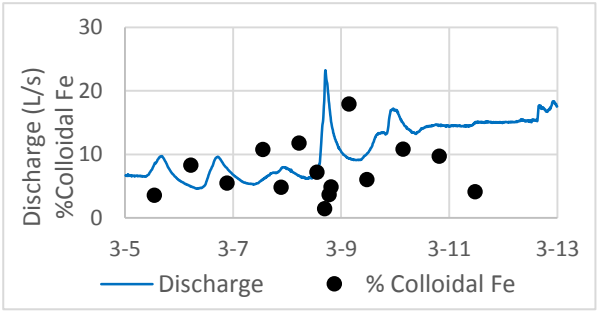


*figure 14. Fe fractions during the March event (top figure). Overview of the responses per fraction (bottom left) and the importance of colloidal Fe (1 nm – 450 nm) (bottom right).*

### 5.1.7. FFF-ICP-MS Phosphorus

During baseflow, most colloidal P was found in the 3rd fraction (figure 15). Least colloidal P was found in the 1st fraction. On average 0.04 µg/L P was found in the 1st fraction during baseflow (AS1-AS10). During peak flow the amount of P found in the 1st fraction increased to 0.19 µg/L (AS12). After peak flow (AS15-AS24), 1st fraction P remained elevated compared to baseflow conditions (average 0.07 µg/L). 2nd fraction P remained highest for all samples. During baseflow (AS1-AS10), average concentrations were 0.4 µg/L. Concentrations during peak flow rose to a maximum of 0.94 µg/L (AS12). Average concentrations after peak flow were 0.5 µg/L. For the 3rd fraction, baseflow concentrations were on average 0.7 µg/L rising to a maximum of 1.0 µg/L (AS12). After peak flow, the average concentration was 0.6 µg/L. The 2nd fraction gains more importance during the event relative to the 3rd fraction. The results are summarized in a table in figure 15 (left bottom).

The most important observation derived from figure 15 is that especially the 2nd fraction reacts mostly during this event. During non-event conditions, there is a +/- 0.2 µg/L difference between the second and the third fraction. For the event samples (AS11, AS12, A13 but also AS17) the concentration of P in the second fraction approaches the concentration in the third fraction. For all fractions, the P concentration is clearly elevated for samples AS11, AS12 and AS13. In terms of relative increase, the 1st fraction reacts strongest to the event, followed by the 2nd fraction.

Figure 15 (bottom right) shows the % colloidal P. Overall contribution of Colloidal P was lower than expected. For most samples, Colloidal P contributed to 3%-4% of Total P. For the event samples AS12 and AS13 the contribution of colloidal P reached 6%. For AS11 the contribution of colloidal is however surprisingly small (3.6%) suggesting that most P during peak discharge is truly dissolved (<1 nm size). For AS17 the contribution of colloidal was higher than expected. This sample was taken on the 'falling limb' of a very small discharge increase. This may suggest a higher contribution of colloidal P on the falling limb in general.

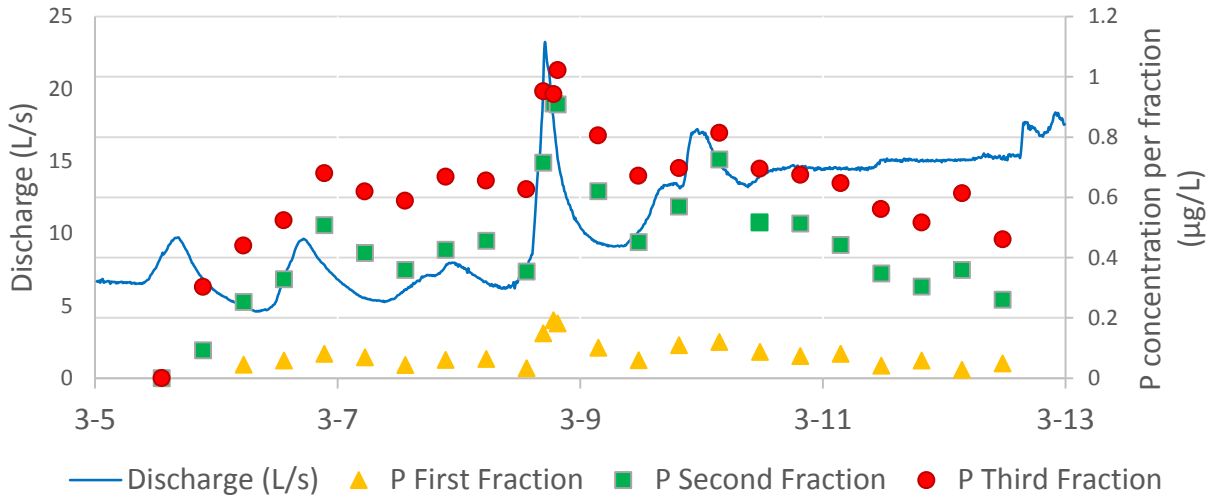


| Fraction | Baseflow (µg/L) | Peakflow (µg/L) | Increase |
|---|---|---|---|
| 1st Fraction | 0.05 | 0.19 | 3.8 |
| 2nd Fraction | 0.40 | 0.94 | 2.4 |
| 3rd Fraction | 0.65 | 1.02 | 1.6 |

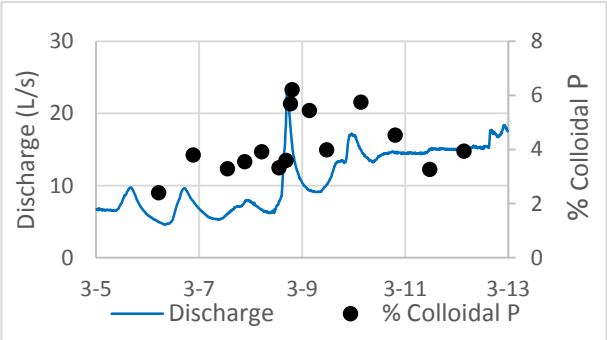


*figure 15. P fractions during the March event (top figure). Overview of the responses per fraction (bottom left) and the importance of colloidal Al (1 nm – 450 nm) (bottom right).*

### 5.1.8. Combined results

Pearsons $R^2$ was calculated for linear regression lines between the predictor variables (fractions of Fe and Al) and response variable (fractions of P) (table 4).

Significant correlations were found for all fractions besides the 3rd fraction of Fe with showed a poor correlation with all forms of P. Very little difference was found between the correlation coefficients of 1st and 2nd fraction Fe and P and the three 1st and 2nd fraction of P. 3rd fraction P was less well predicted by 1st fraction Al and 1st fraction Fe. The interpretation of this table will be discussed in section 7.5.

| | P(1st) | P(2nd) | P (3rd) |
|---|---|---|---|
| **Al (1st)** | **0.70** | **0.71** | **0.59** |
| **Al(2nd)** | **0.75** | **0.80** | **0.69** |
| **Al(3rd)** | **0.67** | **0.73** | **0.76** |
| **Fe(1st)** | **0.74** | **0.73** | **0.60** |
| **Fe(2nd)** | **0.72** | **0.78** | **0.68** |
| **Fe(3rd)** | 0.21 | 0.24 | 0.35 |

*Table 4. Overview of the $R^2$ for several correlations between P fractions and Fe/Al fractions during the March event.*

## 5.2. May event 16-05-2018

### 5.2.1. Event description

The spring of 2018 was exceptionally warm compared to the long-term average. At Sistig-Kall the monthly mean temperatures were 2.5 °C for March, 11.2 °C for April and 14.0 °C for May (long term average 3.7, 6.7 and 11.1°C. The warm weather was accompanied by several heavy thunderstorms in the region and exceptional weather phenomena. At weather station Monschau-Kalterherberg 123.6 mm rainfall was recorded during May 2018 (long-term average 90 mm). Four days with high precipitation amounts (>15 mm/day) were recorded. March and April 2018 which were both circa 20 mm drier than normal.

On the 16th of May the Wüstebach responded to a 14.6 mm rainfall event (Wüstebach Climate Station, 18.3 mm at Monschau-Kalterherberg). The catchment was at baseflow (2 L/s) conditions at the start of the event and rose to 18 L/s during peak flow conditions. The catchment reacted quickly to rainfall. At 19:40 discharge already rose from baseflow 1.9 L/s to 2.1 L/s with only 0.4 mm of rain being reported. Peak rainfall intensity was measured at 20:20 and 20:30 whereas peak discharge was recorded at 21:30 (figure 16). Streamwater pH fluctuated during baseflow conditions (14th of May to 18th of May) between 6.1 and 6.4 following a diurnal pattern and dropped to 5.9 during peak discharge. Baseflow pH conditions were reestablished after 24 hours. Streamwater turbidity peaked 20 minutes before peak discharge (26 NTU, exactly the same value as for the March event, section 5.1.1). The turbidity peak was recorded at 21:00, sample AS3 was sampled at 20:40 and AS4 at 21:10. The turbidity peak was thus missed by the autosampler. At 21:10 turbidity was however still 25.7 NTU falling to 11.3 NTU for AS5 (21:40). The turbidity peak shows evidence for a 'first flush' process occurring before peak discharge as described by Stutter et al. (2008). Since turbidity is measured every 10 minutes, it is not really known how narrow the turbidity peak is and where maximum turbidity is exactly recorded.

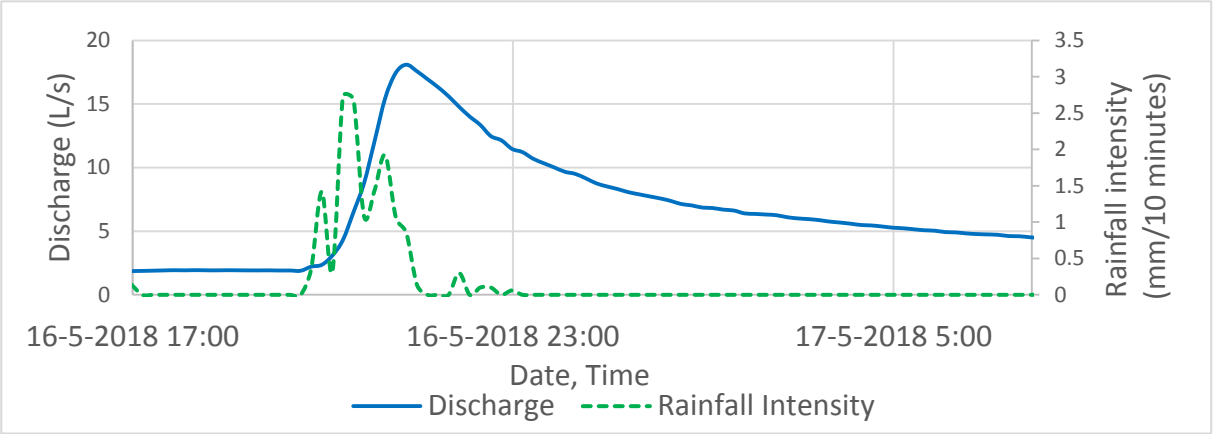


*Figure 16. Overview of rainfall intensity (mm/10 minutes) and discharge during the May event.*

### 5.2.2. Organic Carbon

#### *5.2.2.1. DOC (0.45 µm filtered)*

DOC concentrations were analyzed for all samples (figure 17). For AS1 (baseflow), DOC concentration was 5.9 mg/L, for AS2 (3.0 L/s) DOC concentration was 5.6 mg/L whereas for AS3 (8.8 L/s) DOC concentration was 6.0 mg/L. Thus, during the early stages of hydrological response, DOC concentration did already slightly increase. AS4 (17.4 L/s) had a distinctly higher DOC concentration of 10.0 mg/L. DOC concentrations suggesting that a large jump in DOC concentrations occurred between 20:40 and 21:10. After sample AS4, concentrations remained above 10 mg/L until sample AS12 and showed very little variation. After AS12 concentration declined but remained elevated compared to baseflow for all samples. Peak rainfall intensity was recorded between 20:20 and 20:40 which might have played a role in the rapid increase in DOC concentrations.

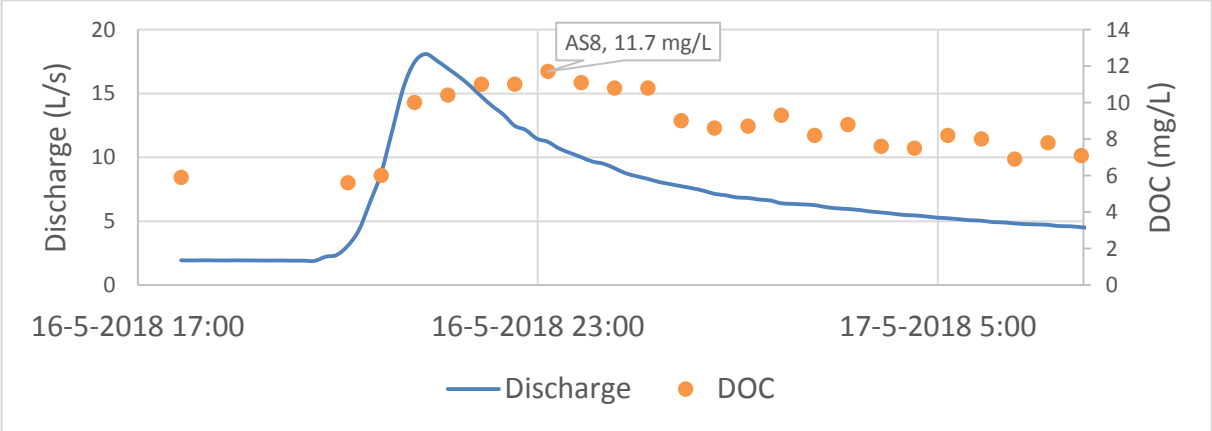


*Figure 17. Overview of DOC concentrations (mg/L) during the March event*

#### *5.2.2.2. OC in filter cascade*

All samples were analyzed unfiltered and filtered with a 5.00, 1.00, 0.45 and 0.10 µm filter to study the amount of OC being particulate or dissolved (figure 18). Despite all samples were analyzed, only the uneven numbers are shown in figure 18 to keep the figure readable. $OC_{0.45}$ and $OC_{0.10}$ were often found to be higher than $OC_{unfiltered}$, $OC_{5.00}$ and $OC_{1.00}$. Despite extensive washing and pre-conditioning, OC concentrations in $OC_{0.45}$ and/or $OC_{0.10}$ were often higher than in unfiltered samples. Because this is theoretically impossible, the filtration experiment was considered to be wrong. In section X.X.X. the potential causes and implications will be discussed further.

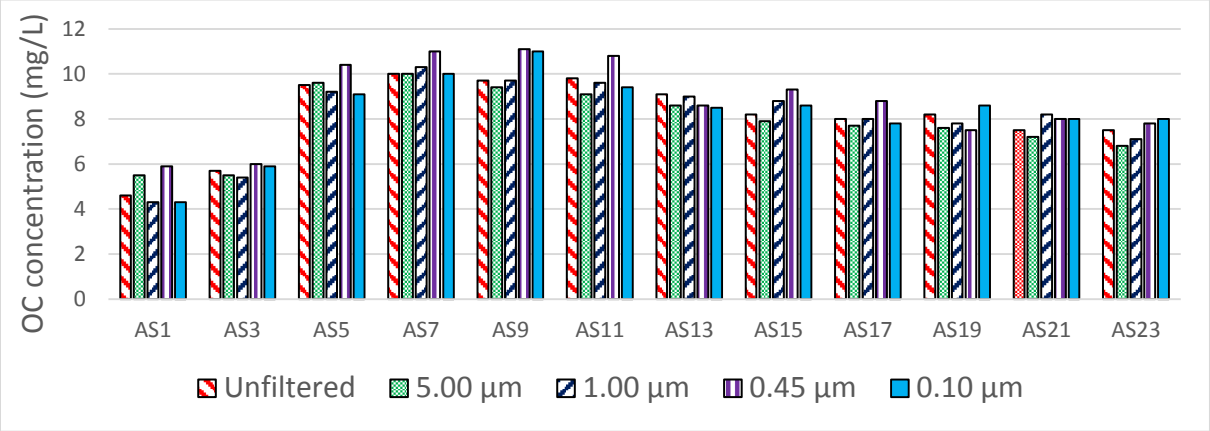


*Figure 18. Overview of OC in filtrates taken from the May event. Only the uneven samples are shown to keep the figure readable.*

### 5.2.3. Total Aluminum and Iron

Aluminum and Iron concentrations were clearly highest during peak flow (AS4) with a concentration of 418 µg/L and 2100 µg/L respectively (figure 19). Two baseflow samples were available showed a concentration below 100 µg/L for Al and 250 µg/L for Fe. After peak flow, Al concentrations remained relatively elevated (150 µg/L) compared to baseflow concentrations. For Fe, concentrations remained as well elevated (300 µg/L) above baseflow conditions during the falling limb of the hydrograph. Significance could not be tested since only 2 baseflow samples were taken. The similarities in terms of response time and behavior after peak flow might suggest similar transportation mechanisms for Al and Fe. For more information see section 7.2 (discussion).

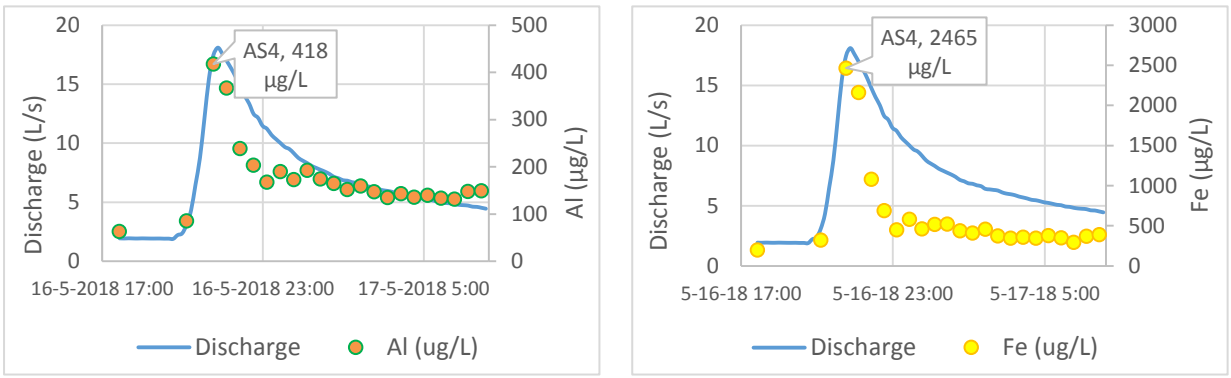


*Figure 19. Al and Fe concentrations during the May event.*

### 5.2.4. Total Phosphorus

Phosphorus (P) showed an interesting development during the May event (figure 20). Unlike Fe and Al, AS4 was however not the sample with the highest P concentration. For AS4, AS5, AS6, AS7 and AS8 P concentrations remained between 12 and 13 µg/L. The highest concentrations were measured for AS9 (19 µg/L) and AS10 (16 µg/L). After AS10, concentrations declined like to baseflow conditions (5 - 10 µg/L). Compared to Al and Fe, P concentrations responded much slower and remained elevated until AS10 (2.5 hours after baseflow).

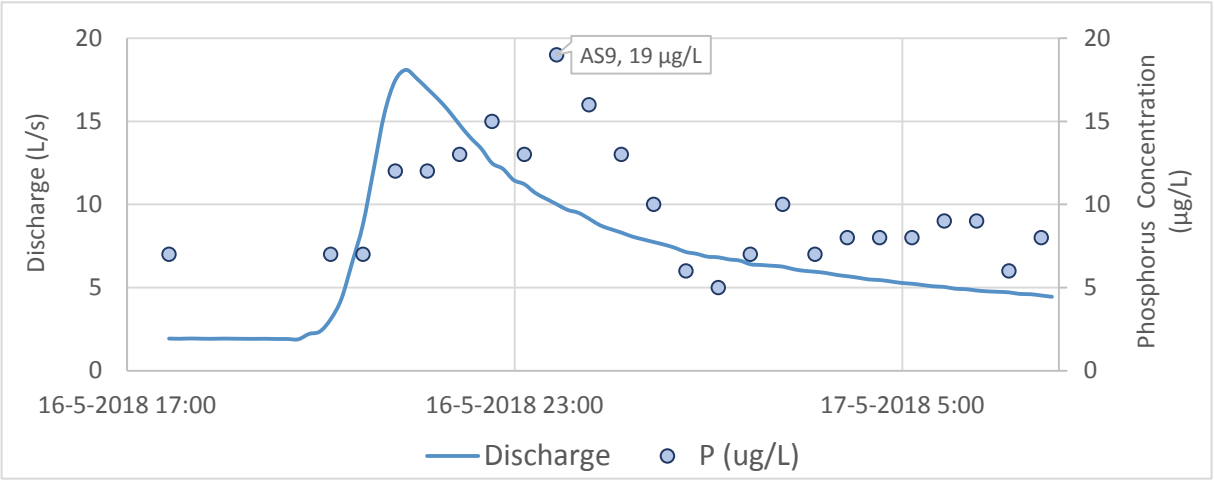


*Figure 20. Total P during the May event*

### 5.2.5. ICP-MS quantifications of filtered samples

Al, Fe and P were quantified for filtered samples using a filtration cascade using a 5, 1, 0.45 and 0.10 µm filter. Total concentrations were also measured for unfiltered samples. Figure 21 summarizes the percentual difference between concentrations in filtrates and Total concentrations (unfiltered). The percentages are provided as the average of all samples (N=24). Figure 21 shows the forms of Fe (left) and Al (right) found by cascade filtration. For Fe, similar concentrations were found in a particulate form and in the nanoparticulate + dissolved form (43 and 44%). For Al, the majority of total Al was found in a nanoparticulate form (77%). For Fe, circa 6% was found in the size ranges >0.10 µm <0.45 µm and <5.00 µm and >0.45 µm. For Al, 2-3% was found in these ranges. Particulate Al contributed 11% of total Al.

For the event samples (AS4 to AS10) the relative importance of the fractions changed compared to baseflow samples (AS11-AS24). During event conditions, 33% of total Fe was nanoparticulate + dissolved while particulate Fe increased to 55%. During baseflow, the nanoparticulate + dissolved fraction made up 55% of total Fe whereas the particulate fraction dropped to 34%. For Al, event conditions also led to a smaller fraction of nanoparticulate + dissolved Al (72%) and a higher fraction of particulate Al (21%). During baseflow, the nanoparticulate + dissolved fraction contained 84% of total Al while the particulate fraction contained 13% of total Al. The other fractions remained relatively small and differences between event conditions and baseflow were less than 3% of these fractions. In theory, the dissolved + nanoparticulate fractions of Fe and Al should partially overlap with the 1st and 2nd fraction obtained by Field Flow Fractionation. This link will be discussed in section X.X.

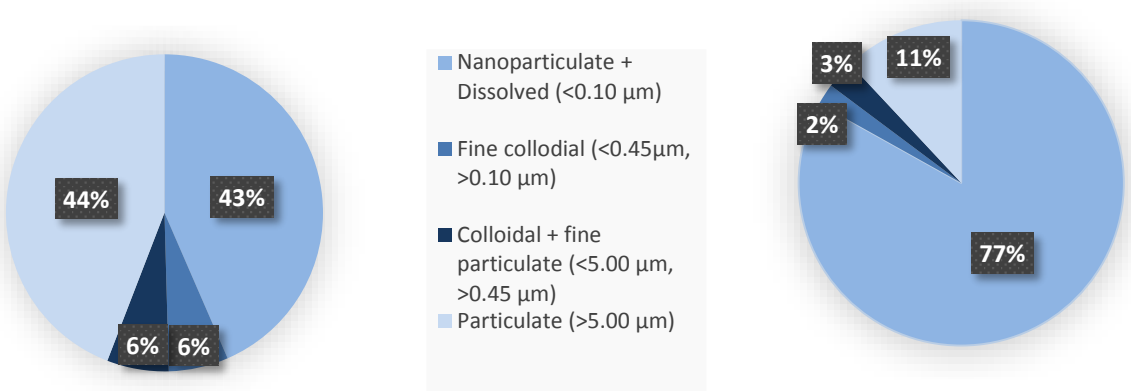


*Figure 21. Overview of the different size fractions obtained by cascade filtration for the May event. For the March event, no filtration cascade was applied.*

### 5.2.7. FFF-ICP-MS Aluminum

AS1 shows that the Al concentrations in the three fractions are very similar during baseflow (figure 22). Concentrations range from 2.9 µg/L to 3.6 µg/L. During the event, Al in the 1st fraction quickly responds rising from 3.1 µg/L (AS1) to 3.9 µg/L (AS2) to 4.3 µg/L (AS3) continuing to peak concentrations of 13.6 µg/L for AS7. 1st fraction Al remained elevated compared to baseflow throughout the event with concentrations of 8.2 µg/L even at AS24. 2nd fraction Al responded much less to the event. For AS1, 2.9 µg/L was found in the 2nd fraction. The concentration increased slowly to peak concentrations at AS9 (4.7 µg/L). 3rd fraction Al hardly increased during the event. From baseflow concentration 3.6 µg/L to maximum concentrations of 5.2 µg/L which were found for AS24 surprisingly. It's clear that the 1st fraction showed to strongest concentration increase while the 2nd and 3rd fraction increased much less (table 8). The 3rd fraction even hardly increased during peak flow but became more important during the final stages of hydrological regression.

For AS4, 4.1% of total Al is colloidal. During baseflow conditions 15.3% of total Al was found to be colloidal. During the regression of the hydrological event, the percentage of Al being found in a colloidal form, gradually increased to 13.5% (AS8). After AS8, the colloidal fraction stabilized around 12%-13%. The relatively high %Al being colloidal for AS8 is primarily caused by the high concentrations of Al in the first fraction (nanoparticulate).

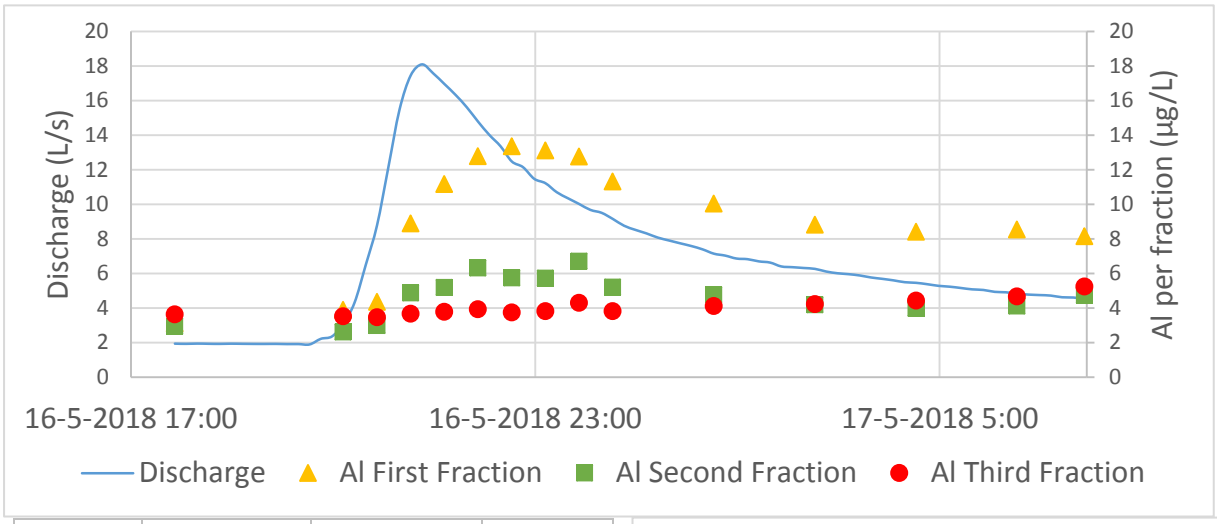


| Fraction | Baseflow (µg/L) | Peakflow (µg/L) | Increase |
|---|---|---|---|
| 1st Fraction | 3.1 | 13.6 | 4.4 |
| 2nd Fraction | 2.9 | 4.7 | 1.6 |
| 3rd Fraction | 3.6 | 5.2 | 1.4 |

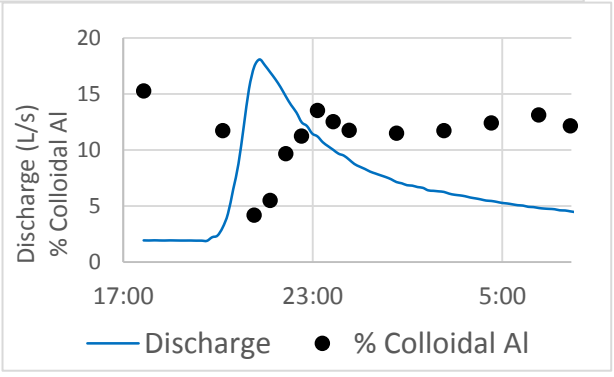


*Figure 22. Al fractions during the May event (top), summarizing table (bottom left) and % colloidal Al (1 nm – 450 nm) (bottom right).*

### 5.2.8. FFF-ICP-MS Iron

During baseflow, 3rd fraction Fe was most abundant (19.7 µg/L) followed by 2nd fraction Fe (10.4 µg/L). Only 3.4 µg Fe/L was transported in the 1st fraction. During the event, this organization was very different. 1st fraction Fe went from least abundant to most abundant for AS7, AS8, AS9 and AS10. Maximum concentrations of 1st fraction Fe were AS1 31 µg/L. 2nd fraction Fe rose to maximum concentrations of 28.6 µg/L for AS6 were it became the most dominant fraction. 3rd fraction Fe did not respond strongly to the event, but became more abundant during the later stages of peak regression (AS20, AS21, AS22, AS23 and AS24) with maximum concentrations of 29.2 µg/L

Table 9 summaries the strength of the responses of each fraction to the event. The 1st fraction responded very strongly with a 9.4 times increase compared to baseflow conditions. The 2nd fraction responded much weaker. The 3rd fraction hardly responded. As for Al, 3rd fraction Fe seemed to be more important in the later stages of hydrological regression. This feature will be discussed in more detail in the discussion section. The % colloidal Fe was around 16.8% during baseflow conditions and dropped rapidly during peakflow (figure 23). For AS4, only 2.4% of Total Fe was found in a colloidal form. After AS4, the importance of colloidal Fe increased quite gradually and showed an increasing trend even until AS22 (22.8%). For the last sample, a lower percentage was found being similar to baseflow conditions. For now it remains unclear whether the percentage stabilized around the % found at AS24 or whether the increasing trend actually continues.

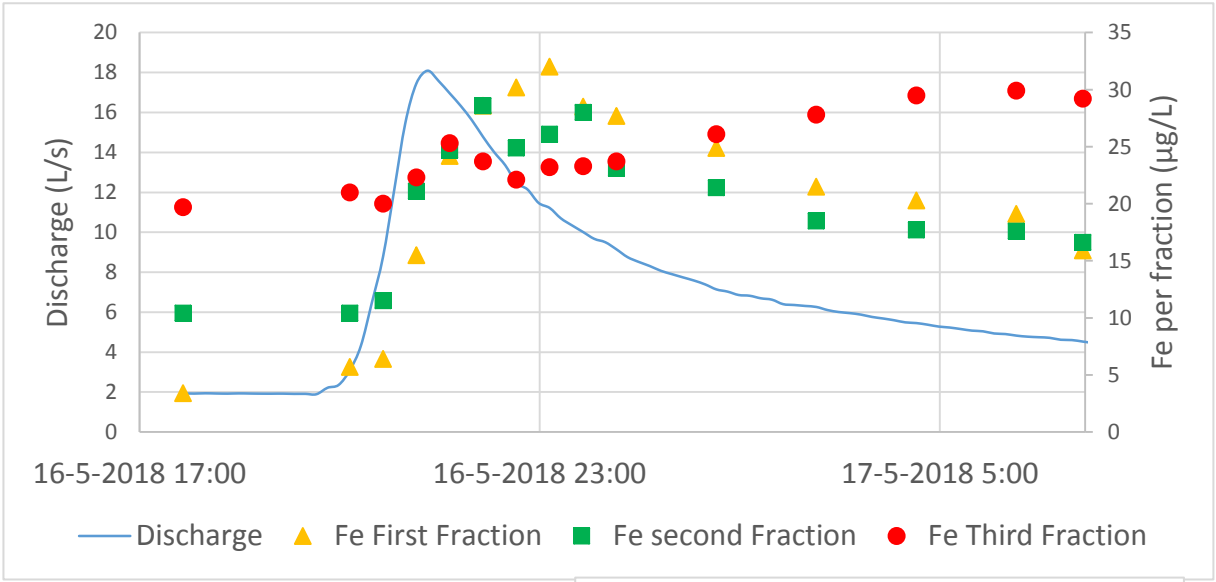


| Fraction | Base flow (µg/L) | Peak flow (µg/L) | Relative increase |
|---|---|---|---|
| 1st fraction | 0.17 | 1.6 | 9.4 |
| 2nd fraction | 0.77 | 3.8 | 4.9 |
| 3rd fraction | 1.1 | 3.6 | 3.2 |

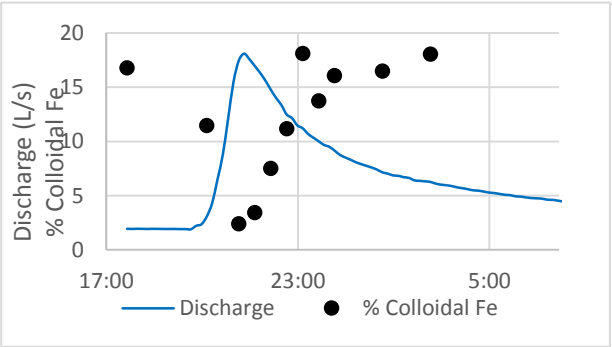


*Figure 23. Fe fractions during the May event (top), summarizing table (bottom left) and % colloidal Fe (1 nm – 450 nm) (bottom right).*

### 5.2.9. FFF-ICP-MS Phosphorus

The FFF-ICP-MS analysis revealed that the nanoparticulate and fine colloidal fractions behaved quite complex during the event (figure 24) During baseflow most P is transported in the 3rd fraction. During the event, the 1st and 2nd fraction become more important. The 1st fraction transported the lowest P concentrations throughout the event, but approached P concentrations transported in the 3rd fraction for samples AS7 and AS8. In terms of relative increase, the 1st fraction responded strongest to the event (table 10, bottom left). The 2nd fraction responded in a similar way as the 1st fraction with maximum concentrations on the falling limb of the hydrograph with maximum concentrations for AS6, AS7 and AS9. The transport of P in the 2nd fraction became more important than P transport in the 3rd fraction from sample AS6 until sample AS22. The reaction of the 3rd fraction was much different compared to the 1st and 2nd fraction. Maximum transport in the 3rd fraction occurred very early (AS2, AS3, AS4 and AS5). After AS5 the importance of the 3rd fraction became much smaller. Compared to the 3rd fractions of Al and Fe, 3rd fraction P did respond reasonably to the event.

The percentage of P being transported in a colloidal form is lowest during peak flow conditions (figure 24, bottom right). For AS4, 4.1% of total Al is particulate. During baseflow conditions 15.3% of total Al was found to be particulate. During the regression of the hydrological event, the percentage of Al being found in a particulate form, gradually increased to 13.5% (AS8). After AS8, the particulate fraction stabilized around 12%-13%. The relatively high %Al being particulate for AS8 is primarily caused by the high concentrations of Al in the first fraction (nanoparticulate).

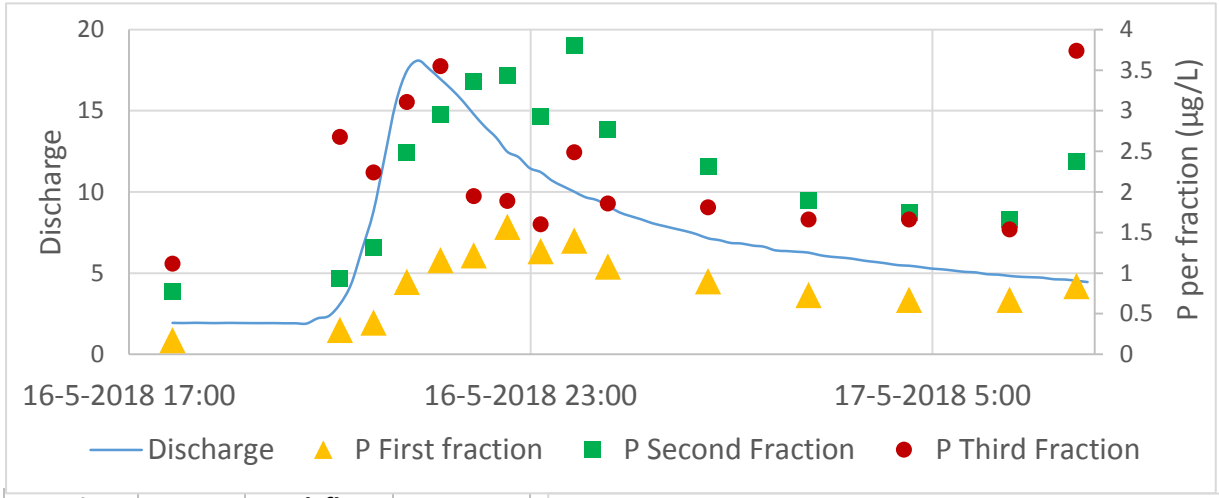


| Fraction | Base flow (µg/L) | Peak flow (µg/L) | Increase |
|---|---|---|---|
| 1st Fraction | 3.4 | 32 | 9.4 |
| 2nd Fraction | 10.4 | 28.6 | 2.75 |
| 3rd Fraction | 19.7 | 29.9 | 1.5 |

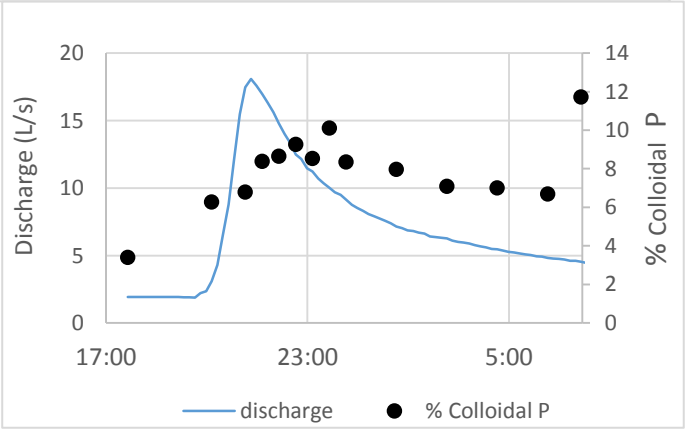


*Figure 24. P fractions during the May event (top), summarizing table (bottom left) and % colloidal P (1 nm – 450 nm) (bottom right).*

### 5.2.10. Combined results FFF-ICP-MS

Pearsons $R^2$ was calculated for linear regression lines between the predictor variables (fractions of Fe and Al) and response variable (fractions of P) (table 11). These results will be discussed further in section 7.5. Correlations during the May event were higher than during the March event for the nanoparticulate fractions (1 kDa - 60 nm) and lower for the fine colloidal fraction (60 nm – 450 nm).

| | **P(1st)** | **P(2nd)** | **P (3rd)** |
|---|---|---|---|
| **Al (1st)** | **0.94** | **0.89** | 0.01 |
| **Al(2nd)** | **0.90** | **0.96** | 0.02 |
| **Al(3rd)** | 0.01 | 0.02 | 0.04 |
| **Fe(1st)** | **0.84** | **0.77** | 0.01 |
| **Fe(2nd)** | **0.89** | **0.91** | 0.00 |
| **Fe(3rd)** | 0.01 | 0.00 | 0.00 |

*Table 5. Correlations between fractions of Al, Fe and P during the May event*

# 6. Discussion Past Events

## 6.1. Precipitation events and catchment responses

### 6.1.1. Precipitation events

It was found that days with more than 16.5 mm precipitation per day (upper 5$^{th}$ percentile) occur in every month of the year with a preference for July and September and the winter period. There are virtually no scientific sources to compare these results with. Mormal & Tricot (2004) looked at the monthly distribution of >1 mm rainfall days in the nearby High Fens and found a dip as well in rainfall days in August compared to July and September and a preference for rainy days in the winter.

For the heaviest maximum rainfall intensities (>2 mm/10 minutes) showed a very clear distribution with virtually no events in spring, a few events in autumn and most events in summer. Relatively many high intensity rainfall events occur in August and June compared to July. August has a lower chance of precipitation days suggesting that if rainfall occurs in August, it is likely to be intensive (Mormal & Tricot, 2004). June showed an unexpected high chance of high-intensity rainfall events as well.

### 6.1.2. Catchment responses

A hydrological event was defined as a catchment response > 3. This boundary was not based upon scientific literature, but on trial and error. A catchment response of >3 yielded 98 hydrological events over the last 7 years which was considered to be a realistic amount. It was found that hydrological events mostly occur during summer (July, August and September). The catchment response is poorly predicted by total rainfall and better predicted by maximum rainfall intensity. However, when separated into summer events and winter events it becomes apparent that summer storms are better predicted by average rainfall (mm/hr) while winter storms are better predicted by total rainfall amount (data not shown). A typical summer event reaches peak flow directly after peak rainfall intensity and drops quickly to baseflow conditions. A typical winter event can last a few days with discharge slowly climbing to a maximum followed by a slow regression (Stockinger et al. 2014). Winter events can be marked by long periods of low-intensity rainfall. Combined with a low evapotranspiration, the catchment becomes waterlogged. During these conditions, the entire catchment responds to rainfall and infiltrated rainfall slowly moves through the soil from distant locations to the stream. During summer events precipitation is typically short-lived and intensive while only the riparian zone is responsive. It is therefore explainable that winter events are predicted better by total rainfall amount (longer timescale) while summer storms are predicted better by rainfall intensity (shorter timescale).

Most hydrological events were observed in August followed by July. This indicates once more that maximum rainfall intensity is a better predictor for catchment response than rainfall amount. September however contradicts this by showing a high chance of hydrological events but a lower chance of high maximum rainfall intensities. Rosenbaum et al. (2012) showed that the Wüstebach average soil moisture content decreases throughout the summer and reaches minima in October. Wiekenkamp et al. (2016a) found that preferential flow is more likely during dry catchment conditions which makes preferential flow more likely in at the end of summer. Catchment dryness has also been associated with soil hydrophobicity and shrinking-swelling behavior of clays both stimulating preferential flow (Wiekenkamp et al. 2016a). The suggestion is therefore that the higher chance of encountering a hydrological event in September is caused by favorable catchment conditions as a result of catchment dryness.

## 6.2. DOC concentrations for past events

The dataset of DOC concentrations during events for the Wüstebach is limited to only 12 events. Because individual event characteristics and catchment responses differ greatly between individual events, discovering general rules on DOC behavior during events is complicated. From the data presented in section 5.2 the following observations were isolated.

Discharge proved to be the controlling factor regarding DOC export. The added value of additional DOC samples for the estimation of weekly DOC export was higher for short and intensive events. This was caused by a lack of samples during longer events. In such cases, a low DOC concentration was multiplied with a high value for discharge giving a high export. In reality however, the high discharge level should be multiplied with a higher DOC concentration. DOC export is therefore often strongly underestimated on a weekly basis for longer events (most clear for event 2, 7 and 14, Appendix A).

The results presented in section 4.3.2 and Appendix A, suggest that peak DOC concentrations are typically found close to or shortly after peak flow making it unlikely that the majority of DOC is transported on the rising limb of the hydrograph (see Raymond & Saiers, 2010). Only the event on 8 September shows highest DOC concentration before peak flow (Appendix A). Inamdar et al. (2011) found similar results when analysis a selection of storm events. Since the sampling resolution was often 10, 20 or 30 minutes, DOC peaks might be actually higher and fall between two samples. Stutter et al. (2008) for instance showed a very narrow peak in suspended solids shortly before peak discharge ('first flush'). In theory such a narrow peak could be missed with a 10 minute sampling resolution. No evidence can however be provided for or against this suggestion.

In section 4.3.3 an attempt was made to study the effect of baseflow conditions and rainfall intensity on maximum DOC concentrations. The trends found in 4.3.2 support the existing ideas on processes inducing high DOC concentrations (Tunaley et al. 2016). A positive correlation ($R^2 = 0.43$, $p = 0.02$) was found between maximum rainfall intensity and maximum DOC concentration. Maximum rainfall intensity thus drives catchment responses and DOC concentrations for summer events. This could be related to the development of a stronger pressure wave when heavy rainfall occurs. No significant regression ($R^2 = 0.24$, $p = 0.11$) was found between catchment response and baseflow. More data would however be welcome to fortify the claims made.

Overall, higher DOC event concentrations were found in summer. This is in line with previous scientific research (Mulholland & Hill, 1997, Dawson et al. 2008; Vidon et al. 2010; Bol et al. 2015; Tunaley et al. 2016). The three events with the highest DOC concentrations (>18 mg DOC/L) were on the 23$^{rd}$ of July, 8$^{th}$ of September and 16$^{th}$ of September. These events were marked by relatively high peak rainfall intensities (2.8 – 5.2 mm/10 minutes). Bol et al. (2015) found for the Wüstebach catchment maximum DOC concentrations of 7.4 mg DOC/L on basis of weekly grab samples. Similar maximum DOC concentrations were reported by Sucker et al. (2011) in a study on streams nearby Wüstebach. The results presented in this thesis show that event DOC concentrations in the region can be much higher when event samples are taken in account.

Winter events (snowmelt) are under sampled so far. Only two winter events were studied, one single event (29 January) and one whole January month. Snowmelt events has been acknowledged as a large contributor to annual DOC losses (up to 49%) (Sebestyen et al. 2009). A large snowmelt event occurred during January 2011 and was intensively sampled. Discharge rose to 160 L/s and remained high for most of the month (Appendix A). During this month, 7.5 kg DOC/m$^2$ was export in one month. During the summer storm with the highest peak DOC concentrations (8 september), only 0.044 kg DOC/m$^2$

was exported in one week. Even though the DOC concentration during the month January never exceeded 3.9 mg DOC/L, the amount of exported DOC during January equaled 170 heavy summer events. On an annual scale, these large winter events with very high discharges can dominate the annual DOC cycle as described by Sebestyen et al. (2009). A single summer event seems to be quite insignificant for the annual cycle compared with a winter storm. However, summer storms can cause short-term problems such as declining stream water quality or problems for drinking water production (Chapelle et al. 2013; Regan et al. 2017). Summer events are thus more likely to have an impact on short-term processes while winter events are more important for longer-scale processes.

### 6.3. Advantages and disadvantages of autosampler data

The autosampler proved to be a very useful tool for event sampling. For most events, the results obtained by the autosampler were useful, but there is certainly room for improvement. Often the trigger value of the autosampler was well chosen. For most events 1 or 2 samples were taken on the rising limb of the hydrograph. For events where discharge builds up slowly over the course of several hours, the rising limb was well covered. The falling limb of the hydrograph was also well-covered for most events, but for nearly all events, the autosampler stopped sampling while DOC concentrations were still elevated. As most events show, DOC concentrations remain relatively elevated compared to baseflow conditions for quite a long time. One way to do improve data collection is to switch from a high sampling resolution during peakflow (10-20 minutes) to a lower sampling resolution on the falling limb of the hydrograph (2-3 hour resolution). No cases where observed where large fluctuations were seen on the falling limb without any additional precipitation. Therefore a lower sampling resolution would cover the demand for more data points on the falling limb of the hydrograph. A second way to improve would be a more frequent visit to the autosampler. It would be recommended to appoint a PhD student for this task since the technicians have too little time available. The samples could be taken from the autosampler immediately after an event to make sure that all positions are free again for sampling the falling limb of the hydrograph.

## 7. Discussion New Events

Compared with the storms being described in the storm database (N=98), the March storm was ranked 81$^{th}$ in terms of hydrological response, 70$^{th}$ in terms of rainfall intensity and 53$^{rd}$ in terms of total rainfall. This makes the March event a relatively small one. What makes the event interesting is that a 20 cm snow cover was present in the catchment which had accumulated over February. During the event, the shallow snow cover completely melted, causing a combined rainfall-snowmelt event. Considering the short period where the snow cover was present, the event cannot be compared to large snowmelt events described in some scientific papers (Sebestyen et al. 2009). The term snowmelt event might therefore be somewhat misleading. The May event ranked 31$^{st}$ in terms of hydrological response, 37$^{th}$ in terms of rainfall intensity and 43$^{rd}$ in terms of total rainfall. The May event can therefore be considered as moderate to strong. One special feature of this event is the high maximum rainfall intensity which is not often observed in May.

### 7.1. POC and DOC

#### 7.1.1. March Event

The March event showed a clear delayed DOC peak. The delay between peak flow and maximum DOC concentration was 2 hours and 40 minutes. However, the actual DOC peak could also be higher falling between sample AS12 and AS13. Another option is that the actual DOC peak falls between AS13 and

AS14. Since AS14 is taken 8 hours later than AS13, there is a large period with unknown DOC behavior. This suggests that for this specific experiment, the high-resolution sampling program was stopped too early to study peak DOC dynamics. What however is certain, is that DOC did not respond directly to the discharge event. Considering the season and the catchment conditions (snow cover, early spring) the catchment was likely to be water-logged. The hypothesis is that water moved slowly from the hillslopes to the stream transporting DOC along the way (Stockinger et al. 2014; Tunaley et al. 2016). Water with a longer travel time had more time to take up DOC from the soil and might therefore be more enriched in DOC. When all available DOC was washed away or when the pressure wave in subsoil ceased, the DOC concentrations dropped again as a new stream baseflow level established. During baseflow several small fluctuations in DOC and discharge were recorded. Potentially there is a relation between small discharge variations and small DOC variations, but the DOC variation might also be explained by a diurnal pattern (lower DOC production during night). These DOC concentration differences were too minor to conduct statistical analysis.

### 7.1.2. May Event

DOC concentrations again showed a clearly delayed response to peak flow. Peak flow was reached at 21:20 whereas peak DOC concentration (11.7 mg DOC/L) was reached at 23:10. An interesting observation is that high DOC concentrations (10.0 mg DOC/L) were already reached at AS4 (21:10) shortly before peak flow. During the early stages of hydrological regression, DOC concentrations remained elevated. The only other event that showed this feature clearly is the event on 21 July 2011 (Appendix A). Sample AS4 (21:10) shows that DOC concentrations initially responded rapidly to precipitation. Sample AS3 (20:40) shows a DOC concentration of 6.0 mg/L. DOC concentration thus rose from 6.0 mg/L to 10 mg/L in 30 minutes. It cannot be ruled out that DOC concentrations were higher somewhere between 20:40 and 21:10. Stutter et al. (2008) reported a strong increase in Suspended Particulate Matter before peak discharge during an event. Such processes could have occurred between two samples (AS3 and AS4), but no evidence for or against this hypothesis can be provided. Stutter et al. (2008) also found maximum concentrations of dissolved components (<0.45) were found close to or after peak discharge. This observation is in line with our results. The reason why the DOC response was relatively elongated might be that the catchment is generally rather wet during May and dries out during summer (Rosenbaum et al. 2012). Because of this, the event may show both summer elements (high peak rainfall intensity) and winter elements (relatively saturated soils). The summer elements caused a rapid and strong DOC response shortly after precipitation while the winter element caused an elongated DOC response with water draining in the Wüstebach from relatively distant sources such as hillslopes.

### 7.1.3 DOC versus POC

$OC_{5.00}$ and $OC_{1.00}$ (POC) were found to be considerably lower than $OC_{0.45}$ and $OC_{0.10}$ (DOC) for most samples. According to Laudon et al. (2011) POC and DOC normally differ only around 0.6%. The importance of POC can increase compared to DOC during events (Stutter et al. 2008; Dhillon & Inamdar, 2014). This relation was not found in both the March and May event. In fact, $OC_{0.45}$ and $OC_{0.10}$ proved to be consistently higher than $OC_{5.00}$ and $OC_{1.00}$ which is theoretically impossible. These results were found for both the OCD and the TOC V-CPN which suggests that the difference was found regardless of the measurement device. Filter washing proved to be important for flushing out OC from new filters (figure 4). Surprisingly, more OC was washed from 5.00 µm filters than filters with a smaller pore size. If a correction for OC originating from the filter was considered, the difference between POC and DOC became even larger.

The results are therefore considered to be unreliable and the importance of POC could not be assessed. The reason why OC concentrations in 0.45 and 0.10 filtrates were higher than in 1.00 or 5.00 filtrates remains unknown. Any follow-up research should take a closer look at the filter problem. Inspiration for hypotheses concerning filtration problems might be obtained from reading Zirkler et al. (2012). In this paper, the effect of filter clogging was studied for various types of filters (not for PES). Since we did not take a new filter for each sample, it could be that particles which were stuck within the filters ('lost' sensu Zirkler et al. 2012) were washed out the filters by the next sample (figure 4, clogging experiment). In the clogging experiment it was found that 5.00 µm filters yielded more OC after clogging. Another hypothesis could be that OC comes of the filter if not washed adequately. This hypothesis was tested and it became clear that washing is important to decrease the amount of OC coming from filters. However, this effect decreased quickly, so washing with 75 mL water or 150 mL water only has a marginal effect. This question of the OC filtrates therefore remains open.

## 7.2. ICP-MS Total concentrations

### 7.2.1. Aluminum

For both events, Al concentrations were highest during peak flow. A remarkable feature was that for the March and the May event the relative increase compared to baseflow conditions was similar. The expectation was that more Al would be transported during the May event, which was more severe. However, Muscutt et al. (1993) showed that Al concentrations during peak flow are independent of discharge. Al concentrations in stream water are more dependent on pH with increasing Al concentrations at lower pH (Hendriksen et al. 1984; Jansen et al. 2003). pH often decreases during snowmelt due the dilution of Calcium and Magnesium (Henriksen et al. 1984). During the March event pH dropped to 5.85 during peak flow compared to 6.0-6.1 during baseflow. Although the pH drop was clear, the contribution of the pH drop to actual Al transport cannot be assessed.

### 7.2.2. Iron

Fe concentrations were highest during peak flow for both events. Like for Al, Fe concentrations seemed to respond in a very similar way for both events. For the March event, peak Fe concentrations were 9.8 times higher than at baseflow while for the May event, peak Fe concentrations were 9.9 times higher. Fe concentrations typically show a seasonal pattern with low concentrations during winter and high concentrations during summer (Bol et al. 2015). This pattern has been attributed to a rise in groundwater tables during winter causing reducing conditions around the stream allowing Iron Sulphate (FeS) to form which is insoluble (Muller & Tankere-Muller, 2012). When groundwater tables decrease, Fe is remobilized into soluble forms such as Fe-Humic complexes (Muller & Tankere-Muller, 2012). For summer events it seems therefore more likely that high Fe concentrations are measured during peak flow as mobile colloids are likely to be exported through subsurface flow processes (see section 7.4 for more information). For the March snowmelt-precipitation event the high response in total Fe concentrations is harder to explain. So far no other research was found suggesting high Fe concentrations during snowmelt events. Most likely a change in redox conditions occurred after snowmelt. Perhaps the removal of snow induced oxidation of anoxic FeS compounds. In section 7.4. Fe dynamics are described in detail by looking at Fe concentrations in different particle size fractions.

### 7.2.3. Phosphorus

Contrary to results obtained by Verheyen et al. (2015), P concentrations increased for both events. Phosphorus concentrations increased more during the May event (2.7) than during the March event

(1.7). In absolute values, concentrations between 30 µg/L and 50 µg/L were measured for the March event. For the May event concentrations ranged between 7 µg/L and 19 µg/L. The low concentrations were derived from automatic data evaluation while the high concentrations were found by manual evaluation. The automatic data evaluation for the March event yielded mostly concentrations below limit of detection (4 µg/L). The manual evaluation showed that a relatively small P peak occurred during peak flow conditions. The absolute values are however likely to be overestimated considering previous measurements in the Wüstebach catchment. The May event provided a maximum P concentration of 19 µg/L. This maximum concentrations in both events were quite low compared to results obtained by Julich et al. (2017) who found maxima between 61 and 203 µg/L for 3 events (forest). Stutter et al. (2008) found for 9 events maxima between 52 µg/L and 1026 µg/L (agriculture). The difference with the May and March events could be related to environmental variability (forest type, soil type, geology, hydrology etc.) but potentially a difference in methodology (wet oxidation and digestion with persulfate followed by photometrical detection in other papers) could play a role as well.

## 7.3. Transportation forms of Al

Filtration cascades for the May event showed that the amount of Al >0.45 µm forms on average 14% of total Al. On average, 77% of total Al was found to be smaller than 0.10 µm. The sum of the 1$^{st}$, 2$^{nd}$ and 3$^{rd}$ fraction (1 kDa – 0.45 µm) ranged between 4% and 13% of Total Al. According to the filtration cascade, 2% of total Al was found between 0.10 µm and 0.45 µm leaving around 2% to 11% of total Al between 1 kDa and 0.10 µm. Truly dissolved Al (<1 kDa) forms therefore the majority of total Al (66% - 75%) during the May event. The event sample (AS11) shows the largest contribution of truly dissolved Al (<1 kDa). Cory et al. (2007) suggest that Al is dissolved by the infiltration of acid precipitation and moves towards to stream via subsurface flow pathways. The fact that most truly dissolved Al is found during peak flow would suggest that fresh precipitation reaches the stream quickly (acidification front) or that a pressure wave induced by fresh precipitation reaches the stream quickly. If a pressure wave would travel through the riparian zone as described by Stockinger et al. (2014) it is likely that dissolved Al reaches the stream earlier than larger nanoparticles or fine colloids. For the March event a filtration cascade was not applied, but a drop in the contribution of the colloidal fraction (1 kDa – 300 nm) was seen as well (figure 12). This could either suggest a higher contribution of larger Al colloids (>300 nm) or a higher contribution of truly dissolved Al. The second hypothesis is considered to be more likely.

During the March event, most colloidal Al was transported in the 2$^{nd}$ fraction (20nm – 60nm), but the strongest reaction was seen in the 1$^{st}$ fraction (1 kDa – 20 nm). For the May event, most Al was transported in the 1$^{st}$ fraction and the strongest reaction was also seen for the 1$^{st}$ fraction. During the May event, the 2$^{nd}$ and the 3$^{rd}$ fraction hardly reacted to the event (1.6 and 1.4 times baseflow). The strongest reaction in the 1$^{st}$ fraction is explainable because this fraction is assumed to be the most mobile fraction due to the small size. However, the 2$^{nd}$ fraction is also within the nanoparticle range and would be expected to be mobile as well. The question is whether the distribution of colloidal sizes reflect a seasonal pattern (different colloids in summer than during the winter) or a transportation process (mobility of colloids). Muscutt et al. (1993) showed that a strong relationship ($R^2$ = 0.95) existed between DOC and Al during a summer storm and a poor relation between DOC and Al during a winter storms. In the next paragraph (7.4.) the distribution between the 1$^{st}$ and the 2$^{nd}$ fraction is discussed for Fe as more scientific literature was found on the interaction between colloidal sizes and organic matter for Fe than for Al. Many processes explaining the interaction between colloids and organic matter are however expected to be similar for Fe and Al (Phillipe &

Schaumann, 2014). The hypothesis is that the factors interacting the Fe colloidal size fractions (7.4) also explain Al colloidal size fractions.

## 7.4. Transportation forms of Fe

Filtration cascades for the May event revealed that the amount of particulate Fe is considerable with 44% of total Fe being associated to silt particles and larger (>5.00 µm). 12% of total Fe was found on particles between 0.10 µm and 5.00 µm leaving 45% (rounded) of total Fe being <0.10 µm. The sum of the 1st, 2nd and 3rd fraction (1 kDa – 450 nm) ranged between 1.5% and 18% of total Fe. Considering that 6% of total Fe was found between 0.10 µm and 0.45 µm (filtration), the estimated importance of nanoparticulate Fe is around 12% of total Fe on average leaving 32% of total Fe being truly dissolved. For the Fe cycle, suspended sediments >5.00 µm form a considerable component of the Fe cycle. FFF Fe fractions showed similarities to Al in terms of the distribution of the various fractions. For both events, the 1st fraction responded strongest. For the March event the response of the 1st fraction was much weaker than for the May event (2.6 verus 9.4). During the March event, the first fraction played an insignificant role in terms of total Fe concentrations and the 2nd fraction dominated. During the May event, the 1st fraction and the 2nd fraction were of equal importance with the 1st fraction even being the most important fraction for some samples on the falling limb of the hydrograph. It is known that nanoparticles size distributions are influenced by stream water chemistry (Hassellov & von der Krammer, 2008; Philliphe & Schaumann, 2014; Baken et al. 2016). Philliphe & Schaumann (2014) for instance describe that humic and fluvic acids stabilize nanoparticles while bacterial exudates (polysaccharides) induce flocculation of colloids (both Fe and Al). The absence of humic and fluvic acids would be expected in winter suggesting a potentially a relative increase in bacterial exudates (Inamdar et al. 2011). Bol et al. (2015) showed that low SUVA values (bacterial origin) were occasionally (but not always) found during the winter and high SUVA values (terrestrial origin) during summer.

Stolpe et al. (2013) however came with different explanation. Their study detected larger particle sizes (> 8 nm) during a snowmelt event in Alaska while these larger particles being absent in summer. During summer, 0.5 nm – 3 nm nanoparticles dominated (fluvic acids + Fe). In fact, their observation is similar to ours. Stolpe et al. (2013) explained this switch from larger nanoparticles to smaller nanoparticles by pointing out that the larger nanoparticles were removed from organic soil horizons during snowmelt (erosion) whereas during summer humic-rich groundwater dominated stream water causing the smallest particle sizes to dominate. In several ways, their findings to not match our observations. Our spring melt event was incomparable in terms of discharge and fierceness compared to the spring melt described by Stolpe et al. (2013). Yet, also in the Wüstebach larger nanoparticles were transported while we did not expect that significant overland flow occurred. Also did we observe that the 2nd fraction was 8-9 times more abundant than the 1st fraction before the snowmelt event (baseflow) while the 2nd fraction was only 3 times more abundant during baseflow in the summer event. A second important observation is that during the summer event, the 1st fraction of Fe reacted very strong to event conditions compared to the 2nd fraction suggesting that the 1st fraction is not likely to be related to groundwater. Our hypothesis is that the 1st fraction Fe comes from surficial sources as soil water is transported laterally through the riparian zone. The exact mechanisms of the switch from Fe (but also Al) from 2nd fraction particle sizes (20 nm to 60 nm) to 1st fraction particle sizes (1 kDa – 20 nm) can't be determined in this study. Our hypothesis is that this shift is induced by a. more bacterial OM in winter and more terrestrial OM in summer, b. difference in pH and redox conditions due to permanent high groundwater levels in winter. DOM properties

rather than event characteristics could explain the shift from 2nd fraction Fe in winter to 1st fraction Fe in summer. The hypothesis of Stolpe et al. (2013) pointing to topsoil erosion as the responsible processes for the domination of 2nd fraction Fe during winter is considered to be unlikely for our events.

## 7.5. Transportation forms of P

Like 1st fraction Fe and Al, 1st fraction P responded strongest the event conditions. For the May event the response of the 1st fraction was much stronger (9.4 versus 3.8). Nanoparticulate Fe, Al and P thus show similarities. During the May event, the 1st and 2nd P fractions also showed similarities to DOC, Al and Fe with respect to the response time. The 3rd fractions showed a different behavior. During baseflow, most P is transported in the 3rd fraction. During the March event, 3rd fraction P remained the main carrier of P even though the 3rd fraction hardly responded to discharge. For the March event, the strong increase in 1st fraction P is interesting from a scientific point of view, but less relevant for the P export as concentrations in this fraction remain low. The May event however shows that the 1st fraction can become a fundamental component of P export during summer storms. During the May event, the 1st fraction approached the 3rd fraction while the 2nd fraction dominated the P export. As for both events, the 3rd fraction was most abundant during baseflow, the difference between the March and May event is likely to be caused by a difference in event severity rather than potential seasonal differences as explained in sections 7.3 and 7.4. Missong et al. (2018) show by irrigating soil mesocosms that P-carrying nanoparticles and fine colloids are leached from the topsoil (first 20 cm). During rainfall events, nanoparticles and fine colloids might leach from the topsoil to subsurface water to be transported to the stream. Nanoparticles and fine colloids can thus either stem directly from the topsoil after precipitation events or it can be that nanoparticles and fine colloids accumulate in soil water ('old water') which is flushed out during events (see theory on DOC, section 1.1).

Figure 25 (Left March, Right May) show combined graphs with the sum of the 1st and 2nd fraction Al and Fe (nanoparticulate, 1 kDa – 60 nm) on the X-axis and the sum of the 1st and 2nd fraction P on the Y-axis. Nanoparticulate Al and Fe both correlated strongly with nanoparticulate P for both events. Correlations for the May event were in general higher than for the March event. When the axes of both graphs are compared it becomes clear that all March samples would plot in the left bottom corner of the May graph. The data spreading in March is much smaller than in May. By comparing the slope angle, it seems that the slope angle for Fe is similar in the March event and the May event (0.06-0.08). For Al, a clear difference is found between the slope angles during the May event (0.28) and the March event (0.08). This might suggest that for Fe, the transported amounts are higher during the May event while the transport mechanism involved in Fe-P transport could be similar. For Al however, P-Al transport mechanisms seem to be much stronger during the May event than during the March event. The reason for this difference is unknown and could be a topic for future research. There is a large body of scientific literature on the adsorption kinetics of P (phosphates) and Al/Fe under influence of ionic strength, temperature, pH and the presence of anion substances (for instance Chen et al. 1973 or Tanada et al. 2003). Such research might hold clues to explain observed differences, but incorporating this field of science in this MSc Thesis would be too complicated for the time available.

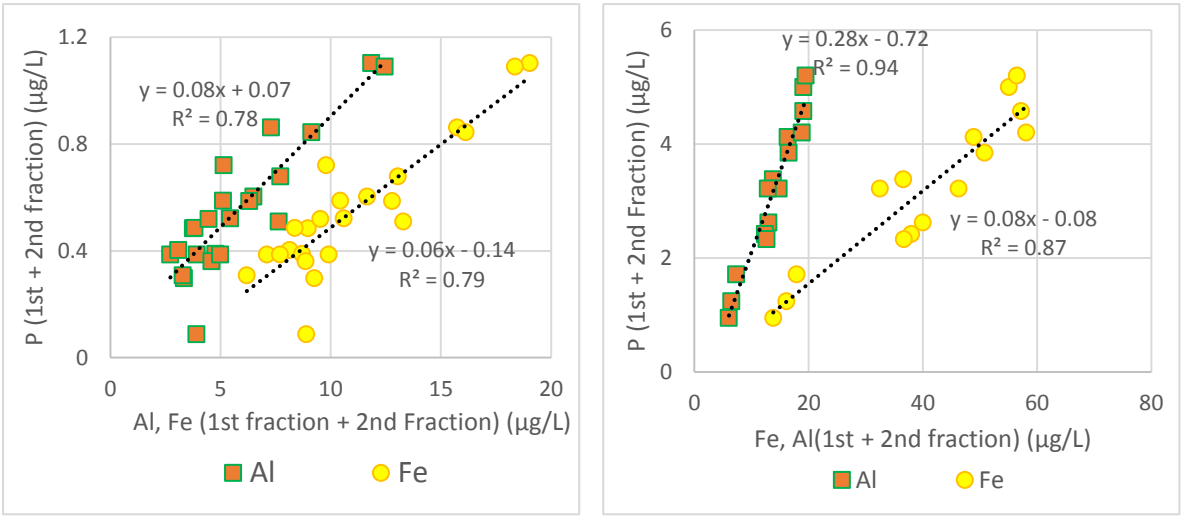


*Figure 25. Correlation between nanoparticulate Al and Fe (1 nm – 60 nm) and nanoparticulate P (1 nm – 60 nm). Left figure shows results from the March event, right figure shows results from the May event.*

Unexpected correlations such a correlation between 1st fraction Al and 3rd fraction P (figure 26, left) were found. The high $R^2$ for the March event seemed to be influenced by the fact that most samples were taken during non-event conditions and only 2 real event samples (AS11 and AS12) were available (figure 26, left). Without these two samples, a much lower $R^2$ was found. Figure 26 (right) shows another misleading correlation between 3rd fraction Al and 3rd fraction P during the May event. A very low $R^2$ (<0.05) was found for these two fractions. Closer observation showed that event samples AS2, AS3, AS4 and AS5 were actually different from other samples. So, although a poor correlation was found, event samples still stood out against baseflow samples. The four event samples are marked by relatively high 3rd fraction P concentration and low 3rd fraction Al concentrations. The non-event samples are characterized by higher Al concentrations and low P concentrations. What exactly causes this difference is unknown. One hypothesis is that AS2, AS3, AS4 and AS5 identify actual Clay transport. This would imply that other Al-rich compounds in the size range 60 nm – 450 nm with no associated P should be more abundant after peak flow. Why the 3rd fraction P is elevated during the event remains unknown and whether clay transport is related to this observation remains open for scientific debate.

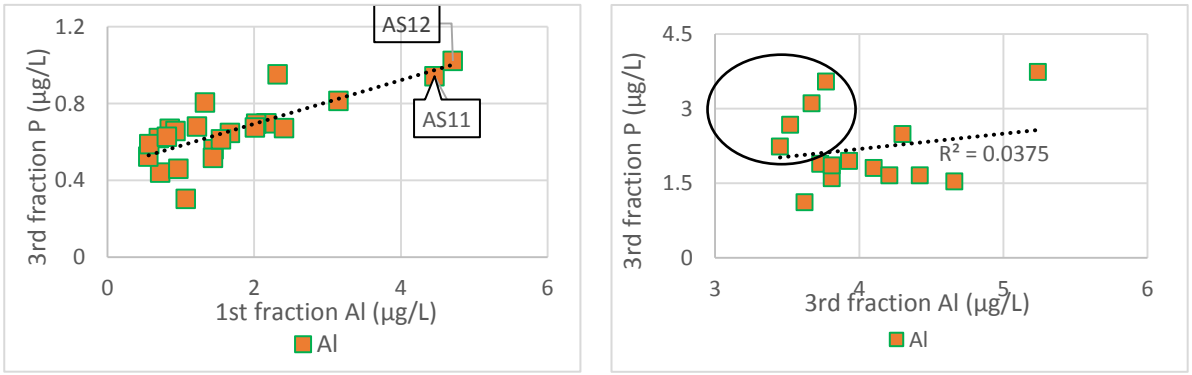


*Figure 26. Unexpected relationships between 1st fraction Al and 3rd fraction P (March) and 3rd fraction Al and 3rd fraction P (May).*

Figure 27 shows yet again that results from the May event (right) provided much more details than the March event (left). For the May event, the transport of nanoparticles can be traced during the rising and the falling limb of the hydrograph. Figure 47 (right) clearly shows that nanoparticles (and DOC) need some time to respond to rainfall and their concentration is highest after peak flow (2.5 hours). This feature is explained as the water entering the Wüstebach through subsurface flow becomes less but more concentrated in nanoparticles.

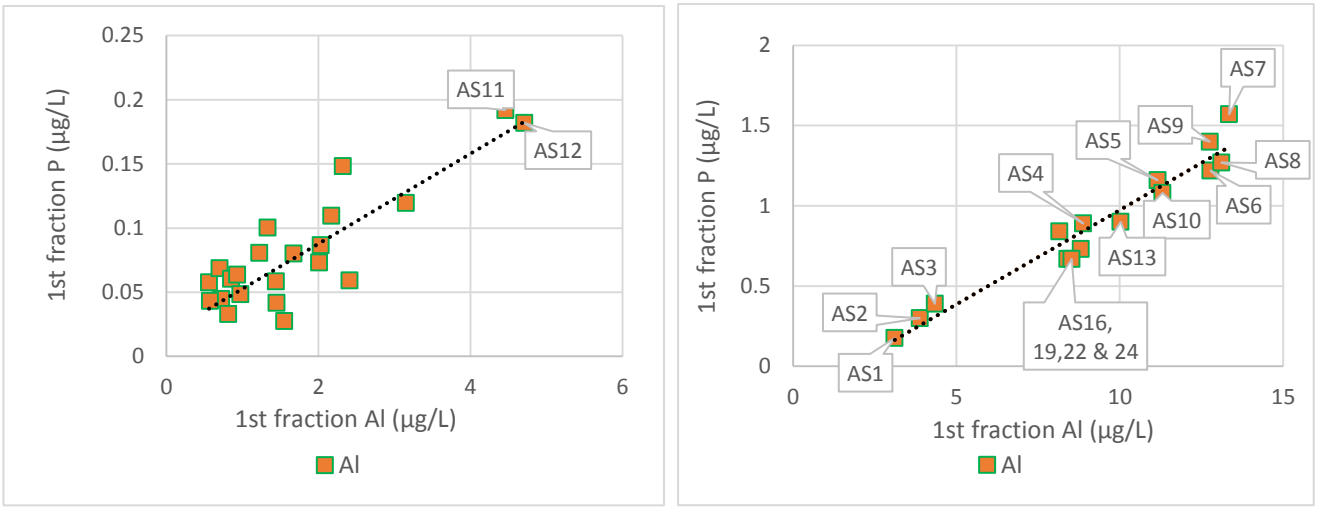


*Figure 27. Nanoparticulate (1 nm – 20 nm) transport during the March event (left) and the May event (right) showing the dynamics of nanoparticulate transport during the events. Especially the May event shows clearly a relation between discharge and the nanoparticulate fractions.*

# 8. Conclusions and recommendations

## 8.1. Hydrological responses in the Wüstebach

It was hypothesized that rainfall intensity (hourly or 10 minute) could predict hydrological responses better than total rainfall amount and that winter and summer events showed fundamental differences. Data from 98 historical events was collected. It was found that for summer events, catchment response was predicted better by rainfall intensity. For winter events however, total rainfall amounts could predict catchment response better than summer events. Summer and winter storms were often clearly different with elongated discharge responses during the winter and flashy, short discharge responses during the summer. Hydrological responses proved however to be complex and depend on various factors making the predictability of the catchment response solely on basis of precipitation impossible. The main achievement of this thesis regarding this research question is that an event database was created containing meteorological data and hydrological data. This could be beneficial as a template for follow-up research.

## 8.2. DOC export during events

For 12 past events high-resolution DOC data was obtained from the open data portal of TERENO. Weekly DOC export was calculated with a without additional DOC data. It became clear that additional samples provide a much more concise insight in DOC losses. Several severe summer storms were sampled with DOC concentrations rising above 15 mg/L. However, when the export was compared to a severe winter event (snowmelt), the impact of summer storms on the annual DOC cycle is only very small. For most events, a large part of the falling limb of the hydrograph was not sampled causing to some extent an underestimation of DOC export. Suggestions to improve event sampling includes more frequent visits to the catchment to empty the autosampler directly after an event and continue an 8-hour sampling program to obtain how the catchment returns to baseflow conditions.

For the first time, all hydrological events where additional autosampler data is available are put together in a table. Although the data quality varies between events, the data is unique for the Wüstebach Catchment. In this thesis no attention was given to several chemical parameters which might be highly interesting for future research. Elemental concentrations of several element including Fe and Al are available for these samples. Looking further at the behavior of other elements could be an interesting follow-up question. Electrical Conductivity, Redox Potential, water temperature, pH and soil moisture status are other parameters which are available could be linked to biogeochemical processes in future research. Linking DOC dynamics with soil moisture status could be interesting to study the effect of catchment dryness on DOC concentrations. It might be possible to combine the work of Wiekenkamp et al. (2016a) on preferential flow with DOC data to see whether DOC is transported along preferential flow paths.

## 8.3. Difference between POC and DOC during events

The expectation was to find more POC relative to DOC during events. Due to a consequent underestimation of POC or an overestimation of DOC, POC was generally lower than DOC. In theory it is not possible that more DOC than POC is present. This feature was attributed to a problem with the usage of our filters. For instance, the leaching of OC from filters or the transferring of OC from a sample to another sample by washing out OC stuck in within the filter.

## 8.4. Aluminum and Iron concentrations and fractions

Fe and Al showed very similar behavior for both events in terms of response (peak concentration/baseflow concentration). Al concentrations increase during the March event was explained by a pH drop during snowmelt (release of 2nd fraction Al, Al-DOM complexes) although it is unclear whether a pH drop of 0.25 can induce significant Al release. During the May event, Al concentrations increase was mainly related to mobilization of nanoparticles (1st fraction) and truly dissolved Al. For Fe, the high winter response might also be induced by a lower pH and changing redox conditions. No scientific reference work was found explaining a link between Fe export and snowmelt. It was found that Fe was mostly carried in the 2nd fraction during winter and in the 1st fraction during summer. This difference was explained as a seasonal difference in Fe colloidal forms due to a difference in DOM properties. This explanation is very different from scientific literature on Fe colloids during snowmelt events (Stolpe et al. 2013). However, our results did not seem to match with the hypotheses provided by Stolpe et al. (2013).

## 8.5. Total Phosphorus concentrations and fractions

We pinpointed that Fe, Al and organic C are important carriers of P during event conditions. Although organic C was not quantified using FFF-OCD, OC is assumed to form an important component of the smallest nanoparticle fractions (Stolpe et al. 2010; Stolpe et al. 2013; Gottselig et al. 2014, 2017a; Baken et al. 2016). Using a combination between FFF and ICP-MS we visualized how Fe and Al interact with P without applying chemical extraction methods (for instance Reddy et al. 1995; Stutter et al. 2008). It was shown that Al and Fe nanoparticles are main carriers of P during events and that they respond quickly to precipitation events. However, the highest concentration of nanoparticles are measured on the falling limb of the hydrograph. Small nanoparticles (1 kDa – 20 nm) react stronger and faster to events (within 20 minutes lasting until 2.5 hours after peak flow). Larger nanoparticles (20 nm – 60 nm) respond slightly slower and the highest fluxes were observed 2 to 3 hours after peak flow. Indications were found that the 3rd fraction (60 nm – 450 nm) responded even slower, but this process was not very clear. The losses of nanoparticulate P seem to be governed by hydrological processes such as hydrological connectivity and stream water transit time. The response time of different particle size classes might show a size-based fractionation which reminds of a Field Flow Fractionation itself with truly dissolved elements (<1 kDa) responding fastest followed by the 1st fraction, 2nd fraction and finally the 3rd fraction. This process was clearer for the May event than for the March event. The March event was less severe and also sampled with a lower resolution. However, on basis of only two events, no general rules can be derived. More events are needed to pinpoint whether these observations are consistent during storms or not.

## 8.6. Main limitations and recommendations for future research

The use of FFF-OCD would be a good way to assess the OC transport in nanoparticulate fractions. For now, it was assumed that OC makes up an important component of the 1st and 2nd fractions as this was shown in previous research. Unfortunately the FFF-OCD combination did not work out. The results from the filtration cascade regarding OC concentrations in different size fractions were unsatisfying as well and were left out of consideration.

There are many more parameters which could be used to get a more robust understanding of catchment processes during heavy rainfall events. For instance, soil moisture data from SOILNET could be very useful to gain more understanding on hydrological processes. Soil moisture status can be used as evidence for the occurrence of preferential flow pathways (Wiekenkamp et al. 2016a) and as an

indicator for hydrological connectivity (Stockinger et al. 2014). For historical events (2011-2015), Fe and Al data is available as well. Considering the high correlation between Al and Fe, evaluation of Al and Fe export during events could be a useful first step to create more understanding regarding P exports during events. It might be possible as well to use Al as a tracer for P transport. When it would be possible to separate the Al fraction between 1 kDa and 100 nm (1$^{st}$ and 2$^{nd}$ fraction) by filtration, it could be that the FFF-ICP-MS combination can be avoided while obtaining a good proxy for nanoparticulate P. A comparison between FFF-ICP-MS results and other techniques (filtration or centrifugation) could be a next step of research.

The value of FFF-ICP-MS was shown in this research and a continuation of this method is recommended to see whether observations are consistent for storm events. This can improve our understanding of the P cycle in forest ecosystems and natural background P fluxes. Since this research approach is new and innovative, results need to be cross-verified by the analysis of more events in various catchments. For agricultural fields the research on event conditions for nanoparticle and fine colloidal P losses could help to answer some important knowledge gaps (Bol et al. 2018).

# Appendix A. DOC during past events and event characteristics

| Event date | Maximum Rainfall Intensity (mm/10 min) | Total Rainfall (mm) | Baseflow (L/s) | Hydrological increase (x) | DOC increase (%per week) | Sampling resolution (minutes) |
|---|---|---|---|---|---|---|
| 16 September | 5.2 | 30 | 5.00 | 11 | 15.7 | 10 or 20 |
| 29 January | 1.2 | 57 | 5 | 11.6 | 7.2 | 20 |
| 23 July[a] | 2.8 | 10 | 2.0 | 22.5 | 42.3 | 30 |
| 8 September | 3.9 | 31 | 0.6 | 27.5 | 85 | 30 |
| 9 May | 0.8 | 3.5 | 5 | 3.9 | 25.9 | 60 |
| 13 July | 1.4 | 35 | 2 | 7 | 35.2 | 60 |
| 3 October | 4.1 | 58.9 | 0.5 | 64 | 26.1 | 20 |
| January | 1.3 | 125.9 | 7 | 14.7 | 40.2 | 240 |
| 21 July | 2.0<br>10.4[a] | 5.2 | 0.42 | 12.4 | 70.1 | 30 |
| 14 August | 2.1 | 23.6 | 1.00 | 5.7 | 13.7 | 60 |
| 8 July | 4.1 | 32 | 1.6 | 26.6 | 30.3 | 20 |
| 6 May | 1.2 | 35 | 2 | 10 | 23.4 | 10 |

*Table 6. All events where additional DOC samples were available and the main properties of each event. [a] TERENO Schöneseiffen*

The figures in this appendix presented below show DOC (mg/L) in red and discharge (L/s) in blue for each event described in table 12. For each figure besides the January event, the time window is 7 days. DOC concentrations and discharge levels on the axes vary for individual events. For all events, discharge is shown on the left axis and DOC is shown on the right axis. All data is derived from the TEODOOR open data portal.

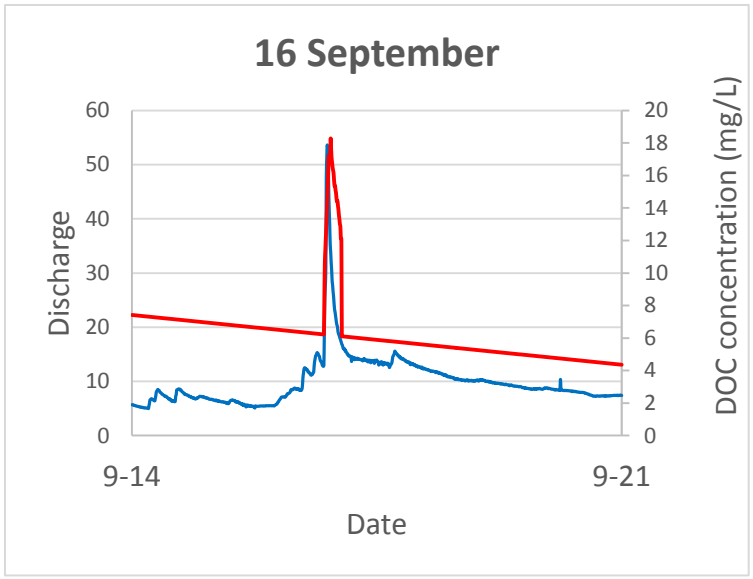
16 September
Discharge
DOC concentration (mg/L)
60
50
40
30
20
10
0
20
18
16
14
12
10
8
6
4
2
0
9-14
9-21
Date

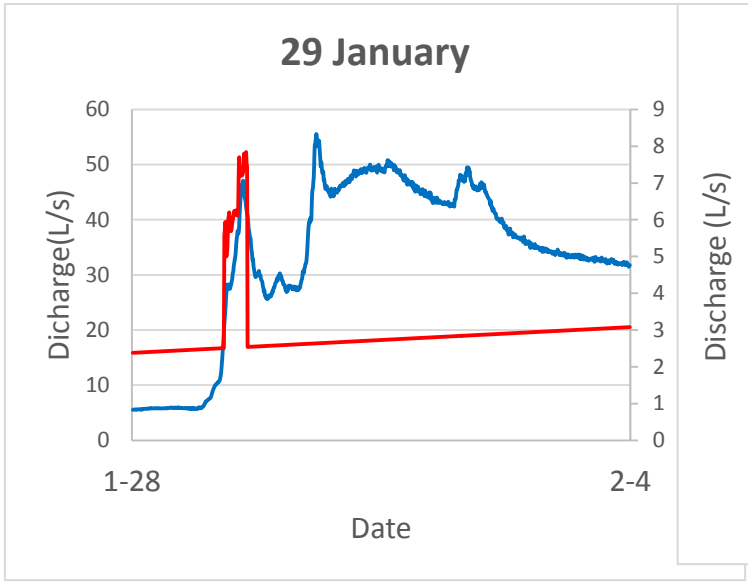
29 January
Dicharge(L/s)
60
50
40
30
20
10
0
9
8
7
6
5
4
3
2
1
0
1-28
2-4
Date

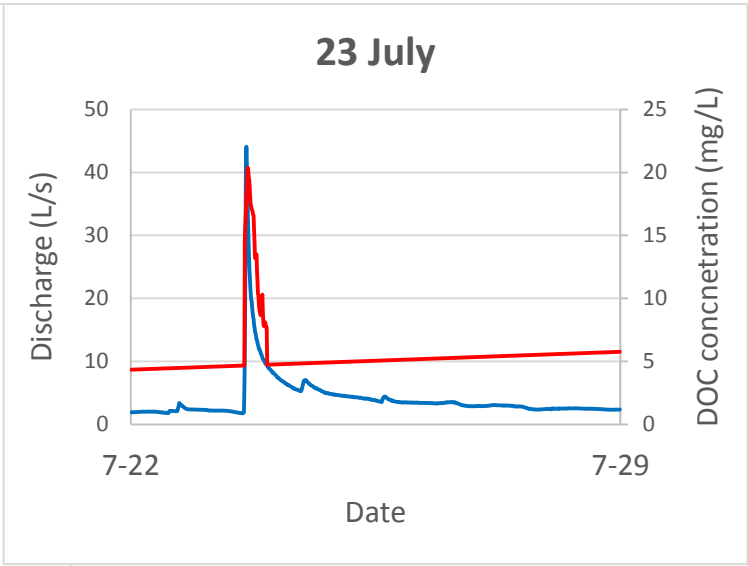
23 July
Discharge (L/s)
DOC concnetration (mg/L)
50
40
30
20
10
0
25
20
15
10
5
0
7-22
7-29
Date

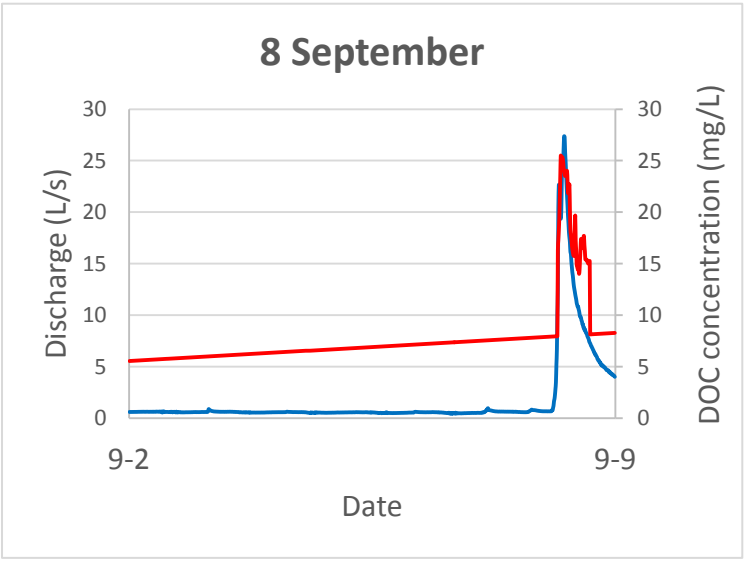
8 September
Discharge (L/s)
DOC concentration (mg/L)
30
25
20
15
10
5
0
9-2
9-9
Date

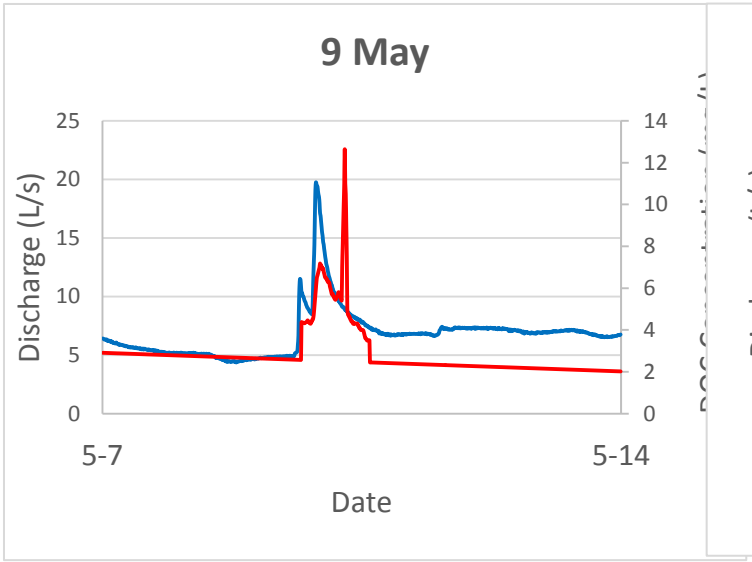
9 May
Discharge (L/s)
25
20
15
10
5
0
14
12
10
8
6
4
2
0
5-7
5-14
Date

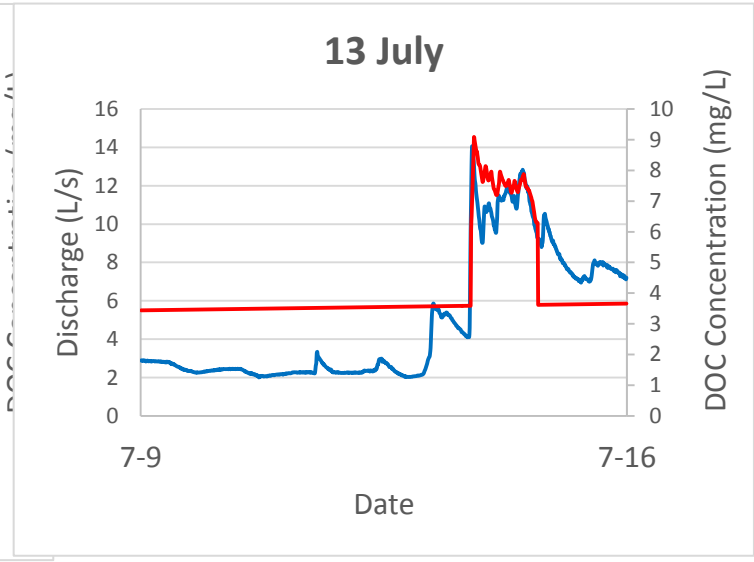
13 July
Discharge (L/s)
DOC Concentration (mg/L)
16
14
12
10
8
6
4
2
0
10
9
8
7
6
5
4
3
2
1
0
7-9
7-16
Date

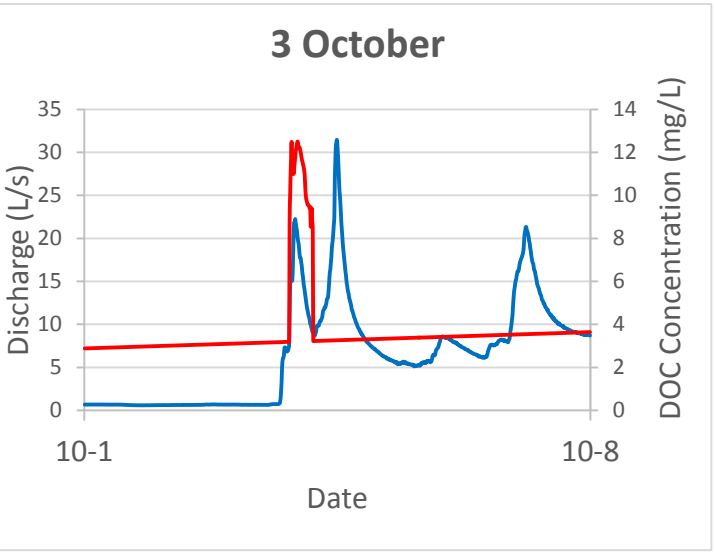
3 October
Discharge (L/s)
DOC Concentration (mg/L)
35
30
25
20
15
10
5
0
14
12
10
8
6
4
2
0
10-1
10-8
Date

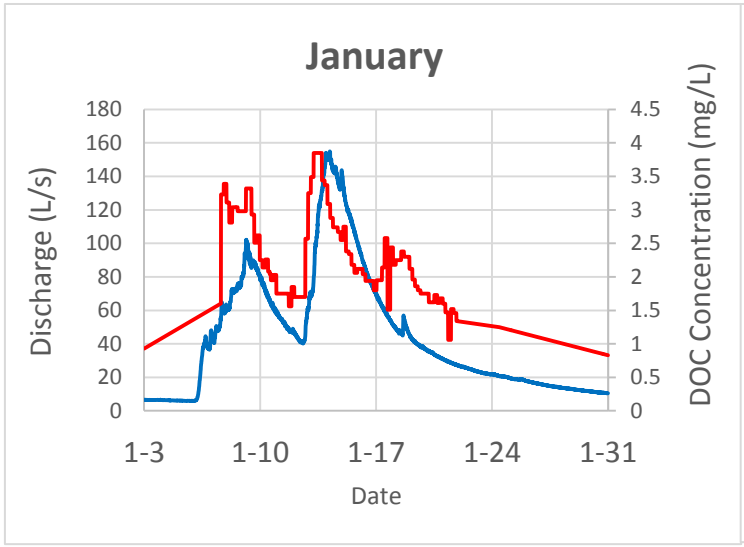
January
Discharge (L/s)
DOC Concentration (mg/L)
180
160
140
120
100
80
60
40
20
0
4.5
4
3.5
3
2.5
2
1.5
1
0.5
0
1-3
1-10
1-17
1-24
1-31
Date

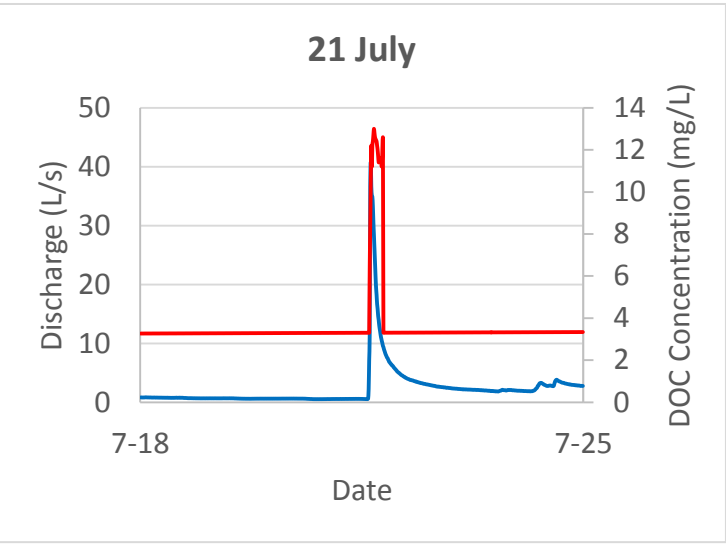
21 July
Discharge (L/s)
DOC Concentration (mg/L)
50
40
30
20
10
0
14
12
10
8
6
4
2
0
7-18
7-25
Date

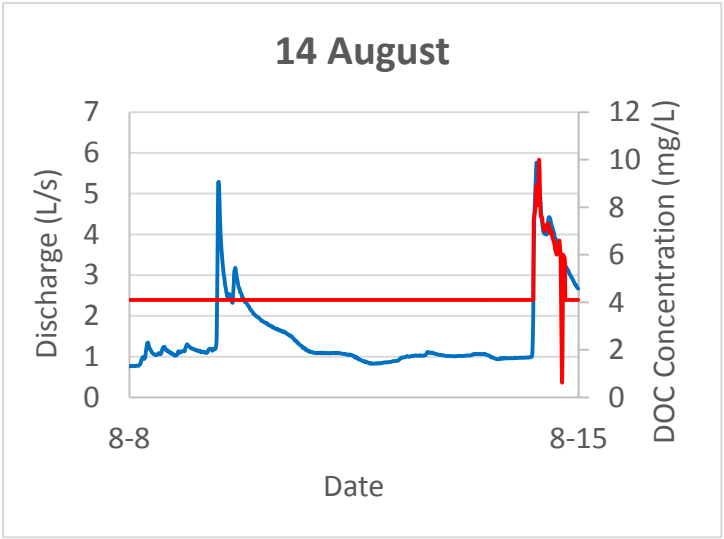
14 August
Discharge (L/s)
DOC Concentration (mg/L)
7
6
5
4
3
2
1
0
12
10
8
6
4
2
0
8-8
8-15
Date

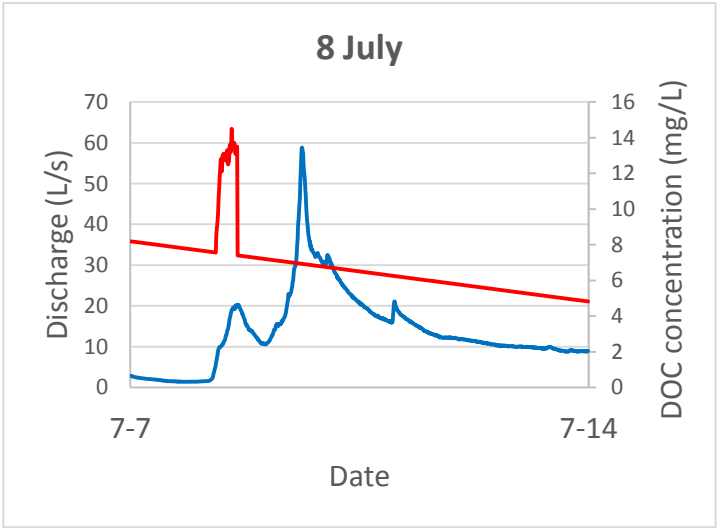
8 July
Discharge (L/s)
DOC concentration (mg/L)
70
60
50
40
30
20
10
0
16
14
12
10
8
6
4
2
0
7-7
7-14
Date

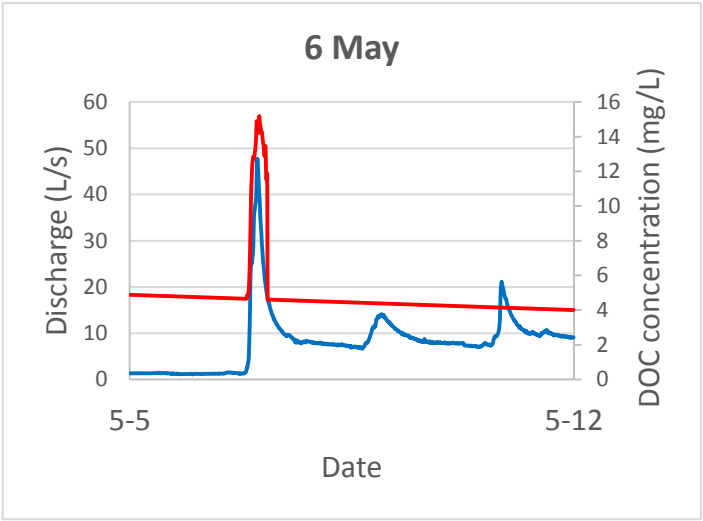
6 May
Discharge (L/s)
DOC concentration (mg/L)
60
50
40
30
20
10
0
16
14
12
10
8
6
4
2
0
5-5
5-12
Date

# Appendix B. Comparing Wüstebach climate station with Monschau-Kalterherberg

The aim of this paragraph is to compare precipitation data obtained by the German Weather Service and the TERENO project. The German Weather Service station is Monschau-Kalterherberg and the TERENO station is Wüstebach. The goal of this paragraph is to check how well these datasets match on a yearly and monthly resolution and finer time scales (daily and 10 minute).

One important difference between data from the German Weather Service and TERENO, is that the German Weather Service corrects their data using the formulas of Richter et al. (1995). According to Graf et al. (2014) the effect of this correction can account for 7% to 15% of the yearly precipitation sum. Table X shows the monthly precipitation data obtained at Monschau-Kalterherberg. Table Y shows monthly precipitation data obtained in the Wüstebach. Yellow fields in the tables are values which were missing for the Wüstebach. These values are replaced with observations from TERENO Schöneseiffen.

| Year | J | F | M | A | M | J | J | A | S | O | N | D | Yearly SUM |
|---|---|---|---|---|---|---|---|---|---|---|---|---|---|
| **2014** | 95 | 80 | 21 | 23 | 86 | 84 | 150 | 193 | 61 | 97 | 55 | 170 | 1116 |
| **2015** | 164 | 66 | 102 | 53 | 55 | 68 | 118 | 90 | 126 | 32 | 203 | 106 | 1184 |
| **2016** | 156 | 147 | 122 | 92 | 76 | 201 | 86 | 78 | 15 | 63 | 95 | 30 | 1163 |
| **2017** | 80 | 107 | 121 | 26 | 73 | 49 | 122 | 123 | 128 | 110 | 123 | 183 | 1245 |

| Year | J | F | M | A | M | J | J | A | S | O | N | D | Yearly SUM |
|---|---|---|---|---|---|---|---|---|---|---|---|---|---|
| 2014 | 83 | 71 | 20 | 27 | 106 | 66 | 217 | 200 | 63 | 89 | 56 | 179 | 1177 |
| 2015 | 146 | 47 | 114 | 60 | 39 | 55 | 113 | 75 | 122 | 39 | 161 | 108 | 1079 |
| 2016 | 130 | 152 | 111 | 70 | 94 | 181 | 137 | 57 | 18 | 74 | 90 | 30 | 1144 |
| 2017 | 69 | 88 | 113 | 23 | 54 | 48 | 124 | 111 | 122 | 84 | 110 | 147 | 1095 |

*Table 7. Comparison of 4 year precipitation data from Monschau-Kalterherberg (upper table) and TERENO Wüstebach (lower table).*

Usually, less precipitation was measured in the Wüstebach than at Monschau-Kalterherberg. The expected cause for this difference is the correction formulas applied at Monschau-Kalterherberg. In general, there is a good agreement between the two data sources. Mostly, both stations measure similar monthly values. Differences due to a difference in geographical position are expected and might be as large as one or two storms per month. On a yearly basis, the underestimation of rainfall at Wüstebach is clearly visible. The annual difference however doesn't exceed 15% which is the expected maximumeffect of the correction formula. In order to correctly compare data from the Wüstebach with data from Monschau-Kalterherberg, data from the Wüstebach should be corrected.

For the year 2014, rainfall measured at Monschau-Kalterherberg was compared with rainfall measured at Wüstebach during storm events. For this question, the storm database (see section 3.1.) was used. The storm database is a collection of large (>3 times) hydrological responses in the Wüstebach. All these responses were termed 'events' in the storm database. For the year 2014, the labor-intensive task was fulfilled to gather the rainfall amount and maximum rainfall intensity during the events in the storm database. The total rainfall amount during each event was summed up for both meteorological stations. Maximum rainfall intensity was also compared (data not shown).The results are expressed as a percental difference.

In total 16 hydrological events occurred during 2014. 6 storms had a relatively comparable rainfall amount (<20% difference). 10 storms however differed more than 20%. When rainfall intensity was considered, only 2 out of 16 storms differed less than 20% (data not shown).

This results show that storms are extremely local and that large differences can be expected during events. Relying on Monschau-Kalterherberg for the analysis of hydrological responses to rainfall events is therefore very tricky. Unfortunately, the TERENO Wüstebach station has been operational since 2014. Older events can therefore only be analyzed using data from Monschau-Kalterherberg.

In paragraph 2.3.3.1 it was shown that Monschau-Kalterherberg and TERENO Wüstebach meteorological data might be comparable, but the data from TERENO must be corrected in order to be able to compare the two data sources on a monthly or yearly scale. However, because the dataset at Monschau-Kalterherberg contains both historical data and recent data, Monschau-Kalterherberg is favored for analysis of long-term climate statistics. On shorter timescales, the advantage of local climate data is shown in 2.3.3.2 as daily and hourly precipitation shows large differences between the two stations.

| **% difference** | **Counts (total = 16)** |
|---|---|
| 0% - 20% | 6 |
| 20% - 40% | 3 |
| 40% - 60% | 5 |
| 60% - 80% | 1 |
| >80% | 1 |

*Table 8. % difference between Monschau-Kalterherberg and TERENO Wüstebach per event for total rainfall.*

# Appendix C. Elemental Fluxes

## March Event

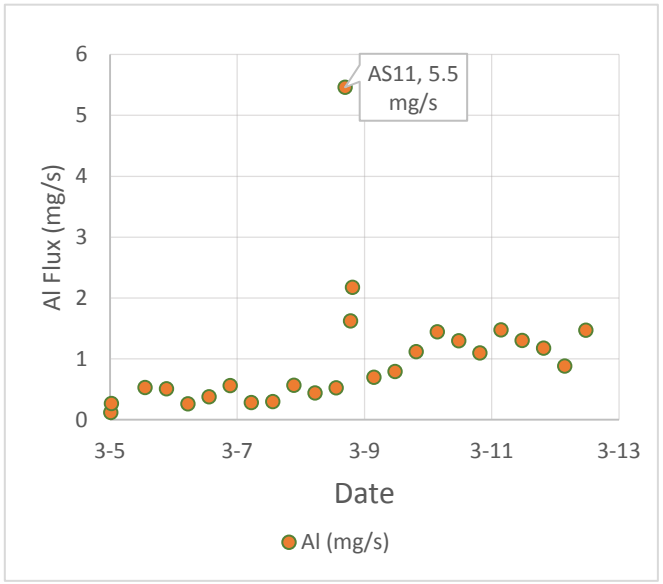


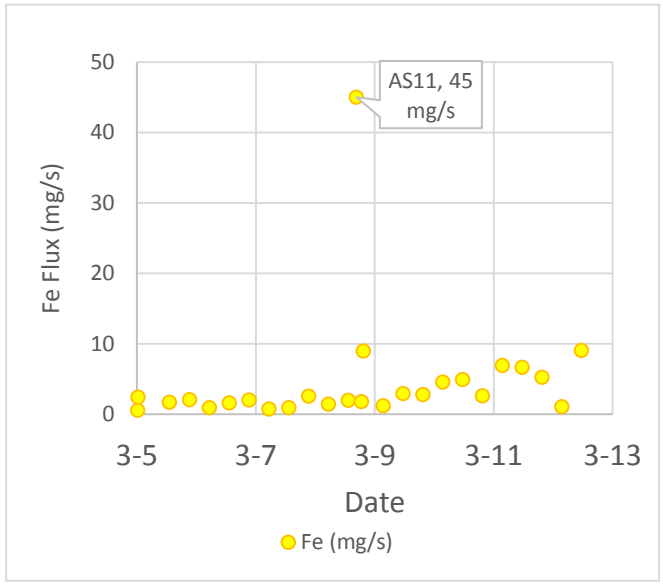


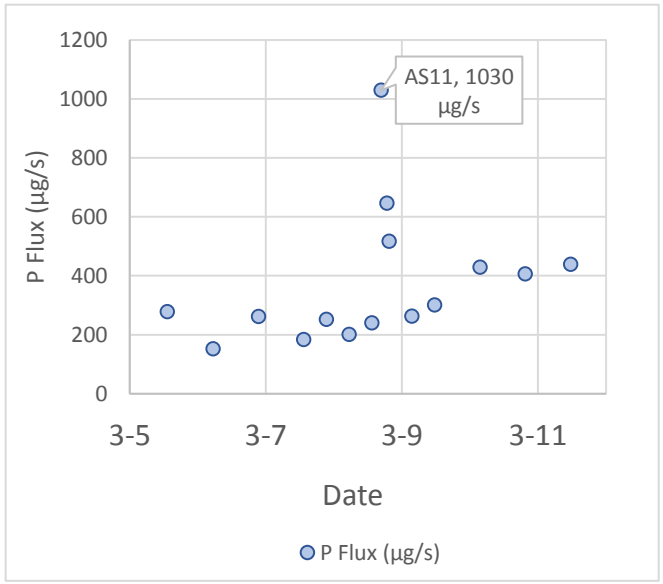


The Al Flux (mg/s) (Left), Fe Flux (mg/s) (Middle) and P flux (ug/s) (Right) show a very similar pattern with high peak levels at AS11, AS12 and AS13. Fluxes are also consistently higher after the event (9$^{th}$ of March to 13$^{th}$ of March) than before the event (5$^{th}$ of March to 9$^{th}$ of March). For Al and P the difference was significant (P = <0.05) for Fe, the difference was not significant (P=0.12).

## May event

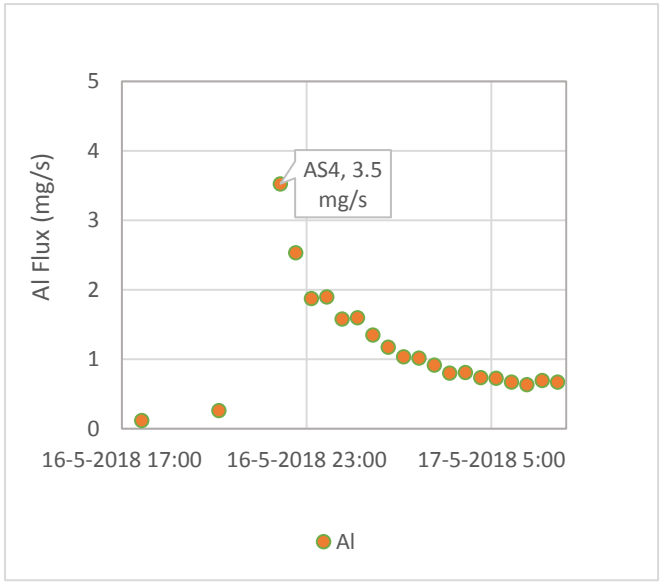


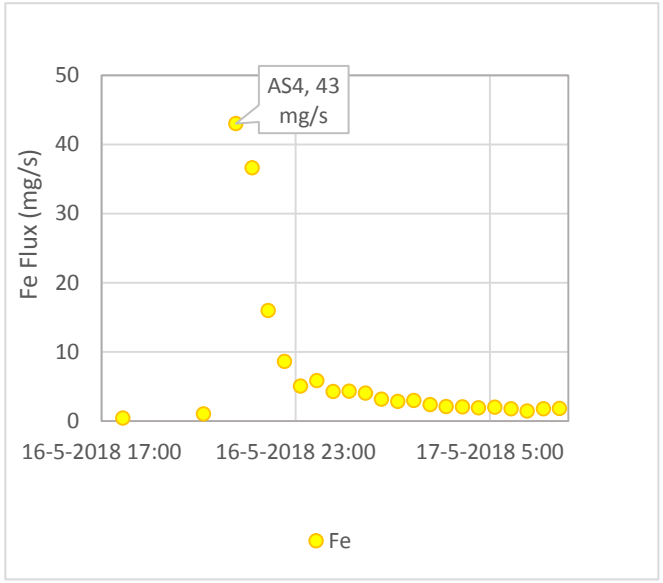


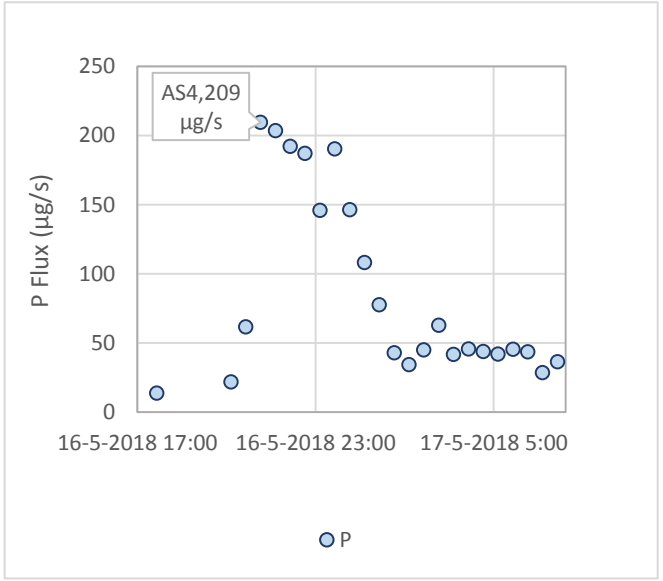


The Al Flux (mg/s) (Left), Fe Flux (mg/s) (Middle) show a very similar pattern with high peak levels at AS4 and AS5. Fluxes are also consistently higher after the event compared to baseflow. Fe and Al followed discharge closely. P (ug/s) (Right) shows a difference in behavior. The P flux remained elevated for several samples and dropped later to a new baseflow condition. This late response is potentially caused by a lower importance of truly dissolved P. 1$^{st}$ and 2$^{nd}$ fraction P also show a delayed response.

# References


Baken, S., Regelink, I. C., Comans, R. N., Smolders, E., & Koopmans, G. F. (2016). Iron-rich colloids as carriers of phosphorus in streams: A field-flow fractionation study. *Water Research, (99)*, 83-90. https://doi.org/10.1016/j.watres.2016.04.060

Bogena, H. R., Huisman, J.A., Baatz, R., Hendricks Franssen, H.J., & Vereecken, H. (2013). Accuracy of the cosmic-ray soil water content probe in humid forest ecosystems: The worst case scenario, *Water Resour. Res., 49*, 5778–5791, DOI: 10.1002/wrcr.20463

Bogena, H. R., Bol, R., Borchard, N., Brüggemann, N., Diekkrüger, B., Drüe, C., ... & Missong, A. (2015). A terrestrial observatory approach to the integrated investigation of the effects of deforestation on water, energy, and matter fluxes. *Science China Earth Sciences, 58(1)*, 61-75. https://doi.org/10.1007/s11430-014-4911-7.

Bol, R., Lücke, A., Tappe, W., Kummer, S., Krause, M., Weigand, S., Pütz, T., Vereecken, H. (2015). Spatio-temporal variations of Dissolved Organic Matter in a German forested mountainous headwater catchment. *Vadose Zone Journal, 14 (4)*. https://doi.org/10.2136/vzj2015.01.0005

Bol, R., Julich, D., Brödlin, D., Siemens, J., Kaiser, K.,…. & Hagedorn, F. (2016), Dissolved and colloidal phosphorus fluxes in forest ecosystems—an almost blind spot in ecosystem research. *J. Plant Nutr. Soil Sci., 179*, 425-438. DOI:10.1002/jpln.201600079

Bol, R., Gruau, G., Mellander, P. E., Dupas, R., Bechmann, M., Skarbøvik, E., ... & VanderGrift, B. (2018). Challenges of reducing phosphorus based water eutrophication in the agricultural landscapes of Northwest Europe. *Frontiers in Marine Science, 5, 276*. DOI: 10.3389/fmars.2018.00276

Bolan, N. S., Adriano, D. C., Kunhikrishnan, A., James, T., McDowell, R., & Senesi, N. (2011). Dissolved organic matter: biogeochemistry, dynamics, and environmental significance in soils. In Advances in agronomy (Vol. 110, pp. 1-75). Academic Press. ISSN: 0065-2113

Borchardt, H. (2012), Einfluss periglazialer Deckschichten auf Abflusssteuerung am Beispiel des anthropogen überprägten Wüstebaches (Nationalpark Eifel), PhD diss., Lehrstuhl für Physische Geogr. und Geoökologie, Fak. für Georessourcen und Materialtechnik, Rheinisch-Westfälische Tech. Hochsch. Aachen, Aaachen, Germany.

Boyer, E. W., Hornberger, G. M., Bencala, K. E. and McKnight, D. M. (1997), Response characteristics of DOC flushing in an alpine catchment. *Hydrol. Process., 11*, 1635-1647. DOI:10.1002/(SICI)1099-1085(19971015)11:12<1635::AID-HYP494>3.0.CO;2-H

Chapelle, F. H., Bradley, P. M., Journey, C. A. and McMahon, P. B. (2013), Assessing the Relative Bioavailability of DOC in Regional Groundwater Systems. *Groundwater, 51*, 363-372. doi:10.1111/j.1745-6584.2012.00987.x

Chen, Y. S., Butler, J. N., & Stumm, W. (1973). Kinetic study of phosphate reaction with aluminum oxide and kaolinite. Environmental Science & Technology, 7(4), 327-332.

Cole, J. J., Prairie, Y. T., Caraco, N. F., McDowell, W. H., Tranvik, L. J., Striegl, R. G., ... & Melack, J. (2007). Plumbing the global carbon cycle: integrating inland waters into the terrestrial carbon budget. *Ecosystems*, *10*(1), 172-185. https://doi.org/10.1007/s10021-006-9013-8

Cory, N., Laudon, H., Köhler, S., Seibert, J. & Bishop, K. (2007). Evolution of soil solution aluminum during transport along a forested boreal hillslope, *J. Geophys. Res., 112, G03014*, doi: 10.1029/2006JG000387.

Crews, T. E., Kitayama, D., Fownes, J.H., Riley R,H., Herbert, D.A., Muellerdombois, D., & Vitousek, P.M. (1995), Changes in soil phosphorus fractions and ecosystem dynamics across a long chronosequence in Hawaii, *Ecology, 76(5)*, 1407–1424. DOI: 10.2307/1938144

Dahlqvist, R., Benedetti, M. F., Andersson, K., Turner, D., Larsson, T., Stolpe, B., & Ingri, J. (2004). Association of calcium with colloidal particles and speciation of calcium in the Kalix and Amazon rivers. *Geochimica et Cosmochimica Acta, 68(20),* 4059-4075. https://doi.org/10.1016/j.gca.2004.04.007

Dawson, J. J. C., Soulsby, C., Tetzlaff, D., Hrachowitz, M., Dunn, S. M., & Malcolm, I. A. (2008). Influence of hydrology and seasonality on DOC exports from three contrasting upland catchments. *Biogeochemistry, 90(1),* 93-113.

Delay, M., & Frimmel, F. H. (2012). Nanoparticles in aquatic systems. *Analytical and Bioanalytical Chemistry, 402(2),* 583-592. DOI: 10.1007/s00216-011-5443-z

Dhillon, G.S. & Inamdar, S. (2014). Storm event patterns of particulate organic carbon (POC) for large storms and differences with dissolved organic carbon (DOC). *Biogeochemistry, 118*, 61-81. https://doi.org/10.1007/s10533-013-9905-6

Domagalski, J. L., & Johnson, H. M. (2011). Subsurface transport of orthophosphate in five agricultural watersheds, USA. *Journal of Hydrology, 409(1-2),* 157-171. https://doi.org/10.1016/j.jhydrol.2011.08.014

Evans, D. J., & Johnes, P. J. (2004). Physico-chemical controls on phosphorus cycling in two lowland streams. Part 1–the water column. Science of the Total Environment, 329(1-3), 145-163. https://doi.org/10.1016/j.scitotenv.2004.02.018

Gottselig, N., Bol, R., Nischwitz, V., Vereecken, H., Amelung, W., & Klumpp, E. (2014). Distribution of phosphorus-containing fine colloids and nanoparticles in stream water of a forest catchment. *Vadose zone journal, 13(7).* doi:10.2136/vzj2014.01.0005

Gottselig, N., Nischwitz, V., Meyn, T., Amelung, W., Bol, R., Halle, C., ... & Klumpp, E. (2017a). Phosphorus binding to nanoparticles and colloids in Forest stream waters. Vadose Zone Journal, 16(3). DOI: 10.2136/vzj2016.07.0064

Gottselig, N., Wiekenkamp, I., Weihermüller, L., Brüggemann, N., Berns, A. E., Bogena, H. R., ... & Pütz, T. (2017b). A three-dimensional view on soil biogeochemistry: A dataset for a forested headwater catchment. *Journal of Environmental Quality, 46(1),* 210-218. DOI:10.2134/jeq2016.07.0276

Grabs, T., Bishop, K., Laudon, H., Lyon, S. W., & Seibert, J. (2012). Riparian zone hydrology and soil water total organic carbon (TOC): implications for spatial variability and upscaling of lateral riparian TOC exports. *Biogeosciences, 9(10)*, 3901-3916. https://doi.org/10.5194/bg-9-3901-2012

Graf, A., Bogena, H.R., Drüe, C., Hardelauf, H, Pütz, T., Heinemann, G. & Vereecken, H. (2014). Spatiotemporal relations between water budget components and soil water content in a forested tributary catchment, *Water Resour. Res., 50,* 4837–4857, doi: 10.1002/2013WR014516.

Hassellov, M., & von der Kammer, F. (2008). Iron oxides as geochemical nanovectors for metal transport in soil-river systems. *Elements, 4(6)*, 401-406. https://doi.org/10.2113/gselements.4.6.401

Haygarth, P. M., Heathwaite, A. L., Jarvis, S. C., & Harrod, T. R. (2000). Transfer of Phosphorus from Agricultural Soil. *Advances in agronomy*. *66*, 195-249. https://doi.org/10.1016/S0065-2113(08)60428-9

Heathwaite, A., Dils, R. (2000): Characterising phosphorus loss insurface and subsurface hydrological pathways. *Sci. Total Environ. 251*, 523–538. https://doi.org/10.1016/S0048-9697(00)00393-4

Hedin, L. O., Vitousek, P. M., & Matson, P. A. (2003). Nutrient losses over four million years of tropical forest development. *Ecology, 84(9)*, 2231-2255. https://doi.org/10.1890/02-4066

Henriksen, A., Skogheim, O. K., & Rosseland, B. O. (1984). Episodic changes in pH and aluminium-speciation kill fish in a Norwegian salmon river. Vatten, 40, 255-260.

Hornberger, G. M., Bencala, K. E., & McKnight, D. M. (1994). Hydrological controls on dissolved organic carbon during snowmelt in the Snake River near Montezuma, Colorado. *Biogeochemistry, 25(3)*, 147-165.

Inamdar, S., S. Singh, S. Dutta, D. Levia, M. Mitchell, D. Scott, H. Bais, and P. McHale (2011), Fluorescence characteristics and sources of dissolved organic matter for stream water during storm events in a forested mid-Atlantic watershed, *J. Geophys. Res., 116*. https://doi.org/ 10.1029/2011JG001735

Jansen, B., Nierop, K. G., & Verstraten, J. M. (2003). Mobility of Fe (II), Fe (III) and Al in acidic forest soils mediated by dissolved organic matter: influence of solution pH and metal/organic carbon ratios. *Geoderma, 113(3-4),* 323-340. https://doi.org/10.1016/S0016-7061(02)00368-3

Jansson, M., Persson, L., De Roos, A. M., Jones, R. I., & Tranvik, L. J. (2007). Terrestrial carbon and intraspecific size-variation shape lake ecosystems. Trends in Ecology & Evolution, 22(6), 316-322. https://doi.org/10.1016/j.tree.2007.02.015

Jones, R.I. (1992). The influence of humic substances on lacustrine planktonic food chains *Hydrobiologia, 229*. 73-91. https://doi.org/10.1007/BF00006992

Julich, S., Benning, R., Julich, D., & Feger, K. H. (2017). Quantification of Phosphorus Exports from a Small Forested Headwater-Catchment in the Eastern Ore Mountains, Germany. *Forests, 8(6*), 206.

Kalbitz, K., & Kaiser, K. (2003). Ecological aspects of dissolved organic matter in soils. *Geoderma, 113(3-4)*, 177-178. https://doi.org/10.1016/S0016-7061(02)00359-2

Kirchner, J. W. (2003), A double paradox in catchment hydrology and geochemistry. Hydrol. Process., 17: 871-874. DOI: 10.1002/hyp.5108

Klapproth, J. C., & Johnson, J. E. (2009). Understanding the science behind riparian forest buffers: effects on water quality. Virigina Cooperative Extension, Blacksburg (Virigina).

Kruse, J., Abraham, M., Amelung, W., Baum, C., Bol, R., Kühn, O., ... & Santner, J. (2015). Innovative methods in soil phosphorus research: A review. *Journal of plant nutrition and soil science, 178(1)*, 43-88. https://doi.org/10.1002/jpln.201400327

Laudon H., Berggren M., Ågren A., Buffam I., Bishop K., Grabs T., Jansson M., Köhler S. (2011). Patterns and dynamics of Dissolved Organic Carbon (DOC) in boreal streams: The role of processes, connectivity, and scaling. *Ecosystems. 14*. 880–893. DOI: 10.1007/s10021-011-9452-8

Lead, J. R., & Wilkinson, K. J. (2006). Aquatic colloids and nanoparticles: current knowledge and future trends. *Environmental Chemistry, 3(3),* 159-171. https://doi.org/10.1071/EN06025

Lennartz, G., & Röös, M. (2006). Nationalpark Eifel: Wald in Entwicklung. Bericht zur Fachtagung, 4(5).

Leipe, T., Tauber, F., Vallius, H., Virtasalo, J., Uścinowicz, S., Kowalski, N., ... & Myllyvirta, T. (2011). Particulate organic carbon (POC) in surface sediments of the Baltic Sea. *Geo-Marine Letters, 31(3),* 175-188. https://doi.org/10.1007/s00367-010-0223-x

Lowinski, L. M. (2014). Belgium's record rainfall event: a look back at the Eupen flash flood of 1953. *Weather, 69(6)*, 147-153. https://doi.org/10.1002/wea.2261

Martin, J. M., Dai, M. H., & Cauwet, G. (1995). Significance of colloids in the biogeochemical cycling of organic carbon and trace metals in the Venice Lagoon (Italy). *Limnology and Oceanography, 40(1),* 119-131. https://doi.org/10.4319/lo.1995.40.1.0119

Mayer, T. D., & Jarrell, W. M. (1995). Assessing colloidal forms of phosphorus and iron in the Tualatin River Basin. *Journal of Environmental quality, 24(6),* 1117-1124. doi:10.2134/jeq1995.00472425002400060010x

McMillan, S.K., Wilson, H.F., Tague, C.L., Hanes, D.M., Inamdar, S., … & Vidon, P. (2018) Before the storm: antecedent conditions as regulators of hydrologic and biogeochemical response to extreme climate events. *Biogeochemistry*, 1-15, https://doi.org/10.1007/s10533-018-0482-6

Meyer W., Stets J. (2007) Quaternary Uplift in the Eifel Area. In: Ritter J.R.R., Christensen U.R. (eds) Mantle Plumes. Springer, Berlin, Heidelberg

Meersmans J., Van Weverberg K., De Baets S., De Ridder F., Palmer S., van Wesemael B., & Quine T. (2016). Mapping mean total annual precipitation in Belgium, by investigating the scale of topographic control at the regional scale, *Journal of Hydrology, 540,* 96-105. https://doi.org/10.1016/j.jhydrol.2016.06.013

Morgan, R. P. C. (2009). Soil erosion and conservation. John Wiley & Sons. ISBN: 978-1-405-14467-4

Mormal, P., & Tricot, C. (2004). Aperçu climatique des Hautes-Fagnes. *Koninklijk Meteorologisch Instituut van België* or *Institut Royal Météorologique de Belgique.*

Muller, F. L., & Tankéré-Muller, S. P. (2012). Seasonal variations in surface water chemistry at disturbed and pristine peatland sites in the Flow Country of northern Scotland. *Science of the Total Environment, 435*, 351-362. https://doi.org/10.1016/j.scitotenv.2012.06.048

Mulholland, P. J., & Hill, W. R. (1997). Seasonal patterns in streamwater nutrient and dissolved organic carbon concentrations: Separating catchment flow path and in-stream effects. *Water Resources Research, 33(6),* 1297-1306. https://doi.org/10.1029/97WR00490

Muscutt, A. D., Reynolds, B., & Wheater, H. S. (1993). Sources and controls of aluminium in storm runoff from a headwater catchment in Mid-Wales. Journal of hydrology, 142(1-4), 409-425. https://doi.org/10.1016/0022-1694(93)90021-Z

Philippe, A., & Schaumann, G. E. (2014). Interactions of dissolved organic matter with natural and engineered inorganic colloids: a review. Environmental Science & Technology, 48(16), 8946-8962. DOI: 10.1021/es502342r

Phillips & Pitt (2015). Comparison of European Freshwater Nutrient Boundaries Used for the Water Framework Directive: A Report to ECOSTATP. 1–176

Preedy, N., McTiernan, K., Matthews, R., Heathwaite, L., & Haygarth, P. (2001). Rapid incidental phosphorus transfers from grassland. *Journal of Environmental Quality, 30(6)*, 2105-2112.

Raymond, P. A., & Saiers, J. E. (2010). Event controlled DOC export from forested watersheds. *Biogeochemistry, 100*, 197-209. https://doi.org/10.1007/s10533-010-9416-7

Reddy, K. R., Diaz, O. A., Scinto, L. J., & Agami, M. (1995). Phosphorus dynamics in selected wetlands and streams of the Lake Okeechobee Basin. *Ecological Engineering, 5(2-3)*, 183-207. https://doi.org/10.1016/0925-8574(95)00024-0

Regan, S., Hynds, P., & Flynn, R. (2017). An overview of dissolved organic carbon in groundwater and implications for drinking water safety. *Hydrogeology Journal, 25(4),* 959-967. https://doi.org/10.1007/s10040-017-1583-3

Regelink, I.C., G.F. Koopmans, C. van der Salm, L. Weng, and W.H. van Riemsdijk. 2013. Characterization of colloidal phosphorus species in drainage waters from a clay soil using asymmetric flow field-flow fractionation. J. Environ. Qual. 42:464–473. DOI:10.2134/jeq2012.0322

Richter, D. (1995), Ergebnisse methodischer Untersuchungen zur Korrektur des systematische Meßfehlers des Hellmann-Niederschlagmessers, in Berichte des Deutschen Wetterdienstes, vol. 194, 93 pp, LRG (Lysimeter Research Group), Selbstverlag des Deutschen Wetterdienstes, Offenbach am Main, Germany.

Rockström, J., Steffen, W., Noone, K., Persson, Å., Chapin III, F. S., Lambin, E., ... & Nykvist, B. (2009). Planetary boundaries: exploring the safe operating space for humanity. *Ecology and society, 14(2)*.

Röös, M., & Mauerhof, J. (2014). Nationalpark Eifel: Aktive Waldentwicklung bei Fichte und Douglasie. *Natur in NRW, 4*, 11-15.

Rosenbaum, U., Bogena H.R., Herbst, M., Huisman, J.A., Peterson, T.J., Weuthen, A., Western, A.W., & Vereecken, H. (2012). Seasonal and event dynamics of spatial soil moisture patterns at the small catchment scale, *Water Resour. Res., 48*, W10544, DOI: 10.1029/2011WR011518.

Sebestyen, S. D., E. W. Boyer, and J. B. Shanley (2009), Responses of stream nitrate and DOC loadings to hydrological forcing and climate change in an upland forest of the northeastern United States, *J. Geophys. Res., 114, G02002*, DOI: 10.1029/2008JG000778.

Sharpley, A., H. P. Jarvie, A. Buda, L. May, B. Spears, and P. Kleinman. 2013. Phosphorus Legacy: Overcoming the Effects of Past Management Practices to Mitigate Future Water Quality Impairment. *J. Environ. Qual. 42*, 1308-1326. doi:10.2134/jeq2013.03.0098

Snyder, L., Potter, J. D., & McDowell, W. H. (2018). An evaluation of nitrate, fDOM, and turbidity sensors in New Hampshire Streams. *Water Resources Research, 54*. https://doi.org/10.1002/2017WR020678

Stacy, E. M., Hart, S. C., Hunsaker, C. T., Johnson, D. W., & Berhe, A. A. (2015). Soil carbon and nitrogen erosion in forested catchments: implications for erosion-induced terrestrial carbon sequestration. *Biogeosciences, 12 (16),* 4861-4874, DOI: 10.5194/bg-12-4861-2015

Stallard, R. F. (1998), Terrestrial sedimentation and the carbon cycle: Coupling weathering and erosion to carbon burial, Global Biogeochem. Cycles, 12(2), 231–257, doi: 10.1029/98GB00741.

Stockinger, M. P., Bogena, H.R.,Lücke, A., Diekkrüger, B., Weiler, M., Vereecken, H. (2014). Seasonal soil moisture patterns: Controlling transit time distributions in a forested headwater catchment, *Water Resour. Res., 50,* 5270–5289, DOI: 10.1002/2013WR014815.

Stolpe, B., Guo, L., Shiller, A.M., Hassellöv, M. (2010). Size and composition of colloidal organic matter and trace elements in the Mississippi River, Pearl River and the northern Gulf of Mexico, as characterized by flow field-flow fractionation. Marine Chemistry, 118(3-4), 119-128, https://doi.org/10.1016/j.marchem.2009.11.007.

Stutter, M. I., Langan, S. J., & Cooper, R. J. (2008). Spatial contributions of diffuse inputs and within-channel processes to the form of stream water phosphorus over storm events. *Journal of Hydrology, 350(3-4)*, 203-214. https://doi.org/10.1016/j.jhydrol.2007.10.045

Sucker, C., Von Wilpert, K., & Puhlmann, H. (2011). Acidification reversal in low mountain range streams of Germany. *Environmental monitoring and assessment, 174(1-4)*, 65-89. https://doi.org/10.1007/s10661-010-1758-z

Tanada, S., Kabayama, M., Kawasaki, N., Sakiyama, T., Nakamura, T., Araki, M., & Tamura, T. (2003). Removal of phosphate by aluminum oxide hydroxide. Journal of colloid and interface science, 257(1), 135-140. https://doi.org/10.1016/S0021-9797(02)00008-5

Trostle, K. D., Runyon, R. J., Pohlmann, M. A., Redfield, S. E., Pelletier, J., McIntosh, J., & Chorover, J. (2016). Colloids and organic matter complexation control trace metal concentration-discharge relationships in Marshall Gulch stream waters. *Water Resources Research, 52(10),* 7931-7944. DOI: 10.1002/2016WR019072.

Tunaley, C., D. Tetzlaff, J. Lessels, and C. Soulsby (2016), Linking high-frequency DOC dynamics to the age of connected water sources, *Water Resour. Res., 52*, 5232–5247, DOI: 10.1002/2015WR018419

Verheyen, D., Van Gaelen, N., Ronchi, B., Batelaan, O., Struyf, E., Govers, G., ... & Diels, J. (2015). Dissolved phosphorus transport from soil to surface water in catchments with different land use. *Ambio, 44(2)*, 228-240. DOI: 10.1007/s13280-014-0617-5

Vidon, P., Allan, C., Burns, D., Duval, T. P., Gurwick, N., Inamdar, S., Lowrance, R., Okay, J., Scott, D. & Sebestyen, S. (2010), Hot Spots and Hot Moments in Riparian Zones: Potential for Improved Water Quality Management. *JAWRA Journal of the American Water Resources Association, 46*: 278-298. doi:10.1111/j.1752-1688.2010.00420.x

Walker, T. W., & Syers, J. K. (1976). The fate of phosphorus during pedogenesis. *Geoderma, 15(1),* 1-19. https://doi.org/10.1016/0016-7061(76)90066-5

Weigand, S., Bol, R., Reichert, B., Graf, A., Wiekenkamp, I., Stockinger, M., ... & Amelung, W. (2017). Spatiotemporal analysis of dissolved organic carbon and nitrate in waters of a forested catchment using wavelet analysis. *Vadose Zone Journal, 16(3).* DOI:10.2136/vzj2016.09.0077

Wiekenkamp, I., Huisman, J. A., Bogena, H. R., Lin, H. S., & Vereecken, H. (2016a). Spatial and temporal occurrence of preferential flow in a forested headwater catchment. *Journal of Hydrology, 534*, 139-149. https://doi.org/10.1016/j.jhydrol.2015.12.050

Wiekenkamp, I., Huisman, J. A., Bogena, H. R., Graf, A., Lin, H. S., Drüe, C., & Vereecken, H. (2016). Changes in measured spatiotemporal patterns of hydrological response after partial deforestation in a headwater catchment. Journal of hydrology, 542, 648-661. https://doi.org/10.1016/j.jhydrol.2016.09.037

Wigginton, N. S., Haus, K. L., & Hochella Jr, M. F. (2007). Aquatic environmental nanoparticles. *Journal of Environmental Monitoring, 9(12)*, 1306-1316. DOI: 10.1039/B712709J

Withers, P. J., Ulén, B., Stamm, C., & Bechmann, M. (2003). Incidental phosphorus losses–are they significant and can they be predicted? *Journal of Plant Nutrition and Soil Science, 166(4),* 459-468. doi:10.1002/jpln.200321165

Zirkler, D., Lang, F., & Kaupenjohann, M. (2012). "Lost in filtration"—The separation of soil colloids from larger particles. *Colloids and Surfaces A: Physicochemical and Engineering Aspects*, 399, 35-40. https://doi.org/10.1016/j.colsurfa.2012.02.021